IAEA-TECDOC-1604

# Neutron Imaging: A Non-Destructive Tool for Materials Testing

*Report of a coordinated research project*
*2003–2006*

IAEA
International Atomic Energy Agency

September 2008

IAEA-TECDOC-1604

# *Neutron Imaging: A Non-Destructive Tool for Materials Testing*

*Report of a coordinated research project*
*2003–2006*

IAEA
International Atomic Energy Agency

September 2008

The originating Section of this publication in the IAEA was:

Physics Section
International Atomic Energy Agency
Wagramer Strasse 5
P.O. Box 100
A-1400 Vienna, Austria

NEUTRON IMAGING: A NON-DESTRUCTIVE TOOL FOR MATERIALS TESTING
IAEA, VIENNA, 2008
IAEA-TECDOC-1604
ISBN 978–92–0–110308–6
ISSN 1011–4289



Printed by the IAEA in Austria
September 2008

# FOREWORD

Neutron radiography is a powerful tool for non-destructive testing of materials for industrial applications and research. The neutron beams from research reactors and spallation neutron sources have been extensively and successfully used for neutron radiography over the last few decades. The special features of neutron interaction with matter make it possible to inspect bulk of specimen and to produce images of components containing light elements such as hydrogen beneath a matrix of metallic elements, like lead or bismuth. The technique is complementary to X ray and gamma ray radiography and finds applications in diverse areas such as the examination of nuclear fuels and the detection of explosives.

The neutron source properties, the collimator design and the fast and efficient detection system decide the performance of a neutron radiography facility. Research and development in these areas becomes essential for improving the output. Detection systems have taken a big jump from conventional photographic film to digital real-time imaging. The use of fast and epithermal neutrons as sources and the exploitation of more specialized neutron interactions, like resonance absorption and phase shifts, has further opened up the field of neutron imaging for research and development. Application of new types of radiation detectors and improved signal processing techniques with an increase in the efficiency and resolution will be beneficial for low intensity neutron sources.

Although neutron radiography is used in many research reactor centres, only a few are well developed and have state-of-the-art facilities, while the remainder still continue to use low end technology such as the film based detection system.

With the aim of bringing together experts from advanced facilities having well developed instruments with operators of less efficiently used installations, a Coordinated Research Project (CRP) on "Development of Improved Sources and Imaging Systems for Neutron Radiography" was launched in 2003. The development of detection systems for fast neutron radiography, software for correction to radiographs and microtron based neutron source are some of the outputs of the CRP, which was completed in 2006. This publication presents the summary of the results of the findings of the CRP and includes the contributions by the participants.

The IAEA is grateful to E. H. Lehmann, Paul Scherrer Institute, Switzerland, for his support in the preparation of the report including the summary.

The IAEA officer responsible for this publication is S. K. Paranjpe of the Division of Physical and Chemical Sciences.

## *EDITORIAL NOTE*

*The papers in these Proceedings (including the figures, tables and references) have undergone only the minimum copy editing considered necessary for the reader's assistance. The views expressed remain, however, the responsibility of the named authors or participants. In addition, the views are not necessarily those of the governments of the nominating Member States or of the nominating organizations.*

*Although great care has been taken to maintain the accuracy of information contained in this publication, neither the IAEA nor its Member States assume any responsibility for consequences which may arise from its use.*

*The use of particular designations of countries or territories does not imply any judgement by the publisher, the IAEA, as to the legal status of such countries or territories, of their authorities and institutions or of the delimitation of their boundaries.*

*The mention of names of specific companies or products (whether or not indicated as registered) does not imply any intention to infringe proprietary rights, nor should it be construed as an endorsement or recommendation on the part of the IAEA.*

*The authors are responsible for having obtained the necessary permission for the IAEA to reproduce, translate or use material from sources already protected by copyrights.*

*Material prepared by authors who are in contractual relation with governments is copyrighted by the IAEA, as publisher, only to the extent permitted by the appropriate national regulations.*

**CONTENTS**

SUMMARY

## 1. BACKGROUND OF THE CRP

Neutron radiography is a powerful tool for non-destructive testing of materials and finds numerous applications in industry and in material research as well. The basic principle is similar to that of X ray radiography. A beam of neutrons falls on the sample and after passing through the sample, leaves the sample image on a photographic plate or on a detector. The neutrons interact with the nuclei of the atoms that compose the sample and the absorption and scattering properties of the contained elements make it possible to produce images of components containing light elements, like hydrogen beneath a matrix of metallic elements, (lead or bismuth), which cannot be easily done with conventional X ray radiography. Exploiting this property, neutron radiography has been used in applications requiring the identification of (light) materials inside solid samples.

Because state-of-the-art neutron detection methods are digital ones, both the performance and the diversity of neutron imaging methods have been improved. Whereas traditional transmission radiography still plays an important role, more sophisticated techniques like tomography, dynamic imaging or energy selective inspection — all based on digital image data — are available nowadays. Therefore, it is fair to replace neutron radiography by the more global term neutron imaging.

Strong neutron sources like research reactors and accelerator-based spallation neutron sources can provide intense neutron beams, required for efficient and practical neutron imaging. Such beams have been successfully used for neutron radiography during the last two decades and neutron radiography has found its greatest applications in the examination of nuclear fuels, explosives, electronic components and engine turbines blades. Recently, neutron imaging has been used in new branches: fuel cell research, the study of objects from cultural heritage, geo-science and soil physics. The extension of applications into new domains depends very much on the performance of the beam lines, the research infrastructure and the access conditions for external users.

Progress in furthering applications has led to the development of three dimensional imaging methods (tomography), the exploitation of different neutron energies in the impinging beam to gain additional information and the real-time analysis of systems including fluid flow and/or moving components. With the advent of portable neutron sources, neutron radiography can also be employed away from reactors, opening up applications, like checking for drugs and explosives concealed in luggage and cargo containers.

The outcome from the application of the neutron imaging depends strongly on the neutron source properties and the detection system used. This has, in turn, generated much demand for research and development in these areas. Detection systems have taken a big jump from conventional photographic film to digital real-time imaging. The use of fast and epithermal neutrons as sources and the exploitation of more specialized neutron interactions, like resonance absorption and phase shifts, has further opened up the field of neutron imaging for research and development. Although neutron radiography is used to some extent in some research reactor centres in addition to the neutron scattering applications, there are only a few which are well developed and have advanced facilities (termed as type A) while the remainder employ standard technology requiring optimization and upgradation (termed as type B).

In addition to beam modifications and neutron source development, much improvement in neutron imaging may also be obtainable from the application of new types of radiation detectors and improved signal processing techniques. An increase in the efficiency and resolution over those of the detectors in existing systems may make it practical to employ neutron sources with lower intensities, thereby opening the neutron imaging application to additional research reactors. The following methods for improving neutron imaging are either recently available or are under development:

- The photographic film technique is an old method, but the resulting images can now be digitized using a variety of scanners. This however, may be done at the cost of dynamic range.
- Electronic camera based systems using a neutron sensitive scintillator screen. There is still a potential for improvements for the camera itself, the optical systems, the scintillators and by light intensifying systems. Further options are triggering, stacking of image sequences and fast time series.
- Imaging plates, commonly used in medical imaging, have been made neutron sensitive and have demonstrated excellent results with respect to sensitivity, resolution and dynamic range.
- Amorphous silicon flat panel detectors are under development for medical applications. It was shown recently that they can be converted for neutron imaging too. The advantages are high sensitivity, high frame rates, large field-of-view and a reasonable spatial resolution.
- Track-etch foils in close contact with a converter can be used. The digitization of the tracks can subsequently be done with an optical camera. The method is useful for activated sample or high gamma-background. The performance is limited due to long exposure, development and scanning time. It is not very useful for quantitative investigations due to a small dynamic range and non-linearity.

Type A facilities (defined for convenience only) are the ones having the following characteristics:

- Well developed instruments and techniques – cold source, optimised collimators, energy selecting devices, research infrastructure.
- Imaging techniques like electronic cameras, imaging plates or well developed other detecting systems, including know-how in image processing.
- Capability of fabricating and maintaining advanced equipments.
- Expert knowledge in digital imaging and availability of suitable trained manpower.
- Willingness to collaborate with and act as mentor to a type B facility.

Type B facilities (called so for convenience only) have following characteristics:

- Non optimised instruments, including the beam line design.
- Under utilised facilities.
- Lack of trained manpower and infrastructure for maintenance of equipments.
- Desire to work and improve the existing system in cooperation with other facilities.

The aim of the present CRP was to bring these two facilities (and the involved operators) together to develop a good neutron imaging system, bring in young workers in this field who can maintain the facilities and are desirous of improving the existing set ups or building new

facilities. Development of cost efficient, fast imaging systems for an optimized utilization of the available neutron beam conditions is another field of interest.

### 1.1. Overall Objective

The enhancement of utilization of research reactors is one of the major objectives of the IAEA's project on "Effective Utilization of Research Reactors". In particular, the improvement of existing installations for neutron imaging and the effective utilization of such facilities are intended.

From the experience of Type A facilities, it is obvious that some investment is required to come from simple neutron imaging methods (film, track-etch foils) to the more enhanced ones. Related to the installation and operation of the whole reactor system, the volume of the investment for an imaging device is minor. Also compared to the installations for neutron scattering research, neutron imaging systems are relatively cheap, but very efficient in the use of the neutrons.

Therefore, one of the aims of the CRP was to look for adapted solutions for the individual reactor installation and beam line.

### 1.2. Specific Research Objectives

- To optimize the neutron beams for imaging purpose using modern simulation techniques.
- To enhance the beam intensity using modern layout principles, neutron optics, like focusing and beam guides and filters.
- To develop a standardized, low cost, neutron image grabber and analyzer for efficient data collection that can be used with low intensity sources.
- To improve signal processing techniques used in neutron imaging applications.

### 1.3. Expected Research Outputs

- Neutron radiography is used at research reactor centres in many Member States, but the facilities are not optimized for attractive potential applications. This fact has been brought out at various discussion meetings. The CRP is aimed at improving the design of beam lines in terms of neutron collimation and intensity.
- Improvements in resolution are normally achieved at a cost in intensity. For an instrument exhibiting good resolution, one needs to employ a fast counting system. It is proposed to work along these lines to develop an optimised detection system. Many facilities, at present, have small CCD systems, but they are not optimised. The experience of advanced facilities will be used to optimise their operation. Optimisation should result in additional applications and/or increased utilization of neutron radiography.
- This CRP will help to expand the knowledge and understanding of various neutron radiography imaging techniques and their applications among the research reactor community in developing Member States and will be helpful in training qualified neutron radiography specialists who, in addition to operating existing facilities, will be able to take up developmental work in future.
- The programme will help in building long term relationships between scientists from developing and developed countries. This will help in encouraging further bilateral

and/or multilateral collaborations among institutions/reactor facilities in various Member States.

## 1.4. Results and Outcome of the CRP

The details of the research and development activities of the participants under the project are given in the presentations following the summary report. Only a short summary with the highlights and common statements made during the final research coordination meeting are given here.

### *1.4.1. Azali Muhammed, Malaysian Institute for Nuclear Technology Research (MINT), Malaysia*

The digital radiography system is planned to be installed at Tangential Beam port in TRIGA mark II research reactor. The development of the new radiography facility (NUR-3) will be divided into two main parts, namely design and fabrication of a neutron collimator, and the utilization of the CCD camera imaging system.

The Monte Carlo N-Particle Transport Code (MCNP) was used for the design of the neutron collimator. Six major collimator components were optimized namely --beam port medium, neutron moderator, collimator aperture, collimator geometry and gamma filter. Variance reduction technique was used for optimization in all the simulation cases. The estimated thermal neutron flux after the optimization at the end of the beam port was around $1\times10^{6}$ neutron $cm^{-2}$ $s^{-1}$, whereas, the calculated L/D ratio was around 100. The neutron to gamma ratio for the design will meet the recommended value ($\geq10^{6}$ n $cm^{-2}$ $mR^{-1}$).

In order to familiarize with the operation the system is set up and tested at existing radiography facility, NUR-2. The arrangement includes CCD camera, lead shutter, collimator, beam shutter, beam trap, motorized sample holder and trolley. Since the testing will be carried out at the set up on radial beam port, calculation and design of additional shielding required to protect the electronic components in the CCD camera is in progress.

### *1.4.2. Amar Sinha, Bhabha Atomic Research Centre (BARC), India*

The processes and systems developed under this CRP include the design of collimator at CIRUS reactor, design of cooled CCD based detector for neutron, real time neutron imaging detector using intensified CCD for two phase flow, design of a radiography assembly using a microtron and the development of simulation tools for phase imaging.

Design calculations have been done for the collimator assembly for both the 12-inch and the 4-inch diameter beam-holes. Monte Carlo Code, MCNP, has been used for these designs. Neutron flux > $10^{6}$ n/$cm^{2}$ /s can be expected from both 4-inch and 12-inch tube diameter at L/D of 90. For phase contrast radiography, it is proposed to put a Cd slit with hole of 200-300 micron on the output face of the 12-inch collimator. The object to source distance will be about 2 meters and detector to object distance will be variable in order to maximize phase effect. In parallel with the design of collimator, design of the shielding of the experimental hutch has been carried out. The shielding wall consists of 9-inch thick lead bricks followed by about 15 inches of borated paraffin.

The major work has been on the development of an in house visualization software using VTK as 3D tomography requires specialized software which can depict 3D volume data to highlight various aspects of the object. Such a software is required to use both volume and

surface rendering technique to assign opacity values, to do shading correction to depict three dimensional image.

Two phase flow studies have become important in many fields of applied and industrial research. The work on real time radiography and two-phase flow studies have been done and is being applied for thermal hydraulics studies for Advanced Heavy Water Reactor (AHWR). We have made an attempt to improve the software and hardware for these studies.

A microtron based neutron source for Microtron Centre at Mangalore University has been designed using EGS and MCNP. A comparative study between the simulated and experimentally measured neutron yield using CR-39 film has been done.

### *1.4.3. Nurul Islam, Bangladesh Atomic Energy Commission (BAEC), Bangladesh*

The jobs completed to develop the real time neutron radiography at the 3 MW TRIGA MK-II research reactor are:

(1) Design and fabrication of a beam stopper using shielding materials for neutrons and gamma radiation.
(2) The existing fixed beam catcher has been changed to a moving system.
(3) A rotation sample holder has been fabricated.
(4) Dose measurements have been done.

In addition, a study of wood and wood plastic composites with and without additive and, of jute reinforced polymer composites has been done using film neutron radiography.

Film neutron radiography method has been adopted for comparative study of water absorption behavior in wood and wood plastic composites (WPC) of Simul using the thermal neutron radiography facility. Variations of optical density due to water absorption of these samples are measured from neutron radiographic images. WPC samples were prepared by impregnating monomer methylmethacrylate (MMA) under gamma radiation to study their water absorption behavior. The water absorption nature of Simul wood (*Salmalia mamabrarica)* and its composites with and without urea as additive was monitored by optical density measurements.

### *1.4.4. Marin Dinca, Institute of Nuclear Research (INR), Romania*

The actions initiated to install a neutron imaging system based on CCD camera for real time and tomography investigations include:

- Calculations to estimate necessity of an image intensifier.
- Calculations of optical parameters and spatial resolution of imaging system.
- Gathering of necessary components namely the scintillator, aluminised mirror, lenses, image intensifier and CCD camera.
- Design and construction of a light tight box for components of the detector.
- A contract with PROOPTICA Bucharest to deliver an assembly of the components: lenses, image intensifier, CCD camera and a PC for image acquisition.
- Design and construction of a special holder for fresh nuclear fuel pins investigations.

### *1.4.5. Vitaly Mikerov, All-Russian Research Institue of Atomatics. Russian Federation*

- The efficient imaging detector for fast neutron radiography and tomography with a cone beam has been developed. The operational ability of the designed CCD-detector has been experimentally proved.
- Major characteristics of the radiographic system have been measured. A spatial resolution of the system amounts to about 2 mm and is appropriate for fast neutron radiography and tomography with a cone fast neutron beam. A relative standard deviation of the image intensity over the detector view field amounts to about 1%. This restricts the dynamic range of the detector. It has been shown that systematic spatial deviations in image intensity interfere also in the measurements of detective quantum efficiency (DQE).
- The contribution of gamma radiation background was estimated using measured gamma spectra, detector response to 661 keV gamma and fast neutrons, results of simulations as well. This contribution is acceptable and amounts to about 2%.

### *1.4.6. Reynaldo Pugliesi, Institute. de Pesquisas Energeticas e Nucleares (IPEN), Brazil*

Three radiography methods were proposed for the CRP project:

(1) to inspect thin samples;
(2) A digital system to improve images registered in track etch foils and
(3) A Dy-TV based system to inspect radioactive samples.

The parameters for the irradiation conditions to obtain the best contrast in the image, the sensitivity to discern thickness and the spatial resolution were presented. A new radiography method using triton from a LiF screen as penetrating radiation is still in development.

### *1.4.7. Nikolay Kardjilov, Hahm Meitner Institut (HMI), Germany*

(1) The results of the radiography experiments on stainless steel and aluminum cubic samples with cold neutrons were presented.
(2) Explanation about the absence of strong scattering component in case of steel was given.
(3) The Bragg cut-off phenomenon in the attenuation spectrum of iron based on the elastic coherent scattering was discussed and its importance for the scattering properties of polycrystalline materials was shown.
(4) Comparative measurements with monochromatic neutrons for better illustration of the Bragg-edge effects were presented.
(5) Since the MCNP code does not describe properly the elastic coherent scattering, it was concluded that MCNP is not appropriate for scattering correction for neutron radiography of polycrystalline samples.

### *1.4.8. Frikkie de Beer, NECSA, South Africa (SA), Nikolay Kardjlov, HMI, Germeny and Eberhard Lehmann, Paul Scherrer Institute, Switzerland, (Collaboration)*

- During the project, different approaches were taken to solve the problem of scattering artefacts, which affect the precise quantification of neutron transmission data.
- Transmission experiments were performed at the facilities SANRAD (SAFARI-1 reactor, NECSA, SA), NEUTRA (SINQ, PSI, Switzerland) and CONRAD (BER-2

reactor, HMI, Germany) using well defined sample geometries (Al containers for water sample, plates of Cu, Al, steel). These beam lines have different parameters and require different treatment to the radiography data in respect to the spectra.

- The Point-Scattered-Functions were derived with the help of the particle transport code MCNPX based on initial considerations about the scattering in the samples.
- In a final step, these functions were approximated with analytical functions and superimposed on the resulting scattering background signal. The obtained data fit well to the experimental results and enable a correction of the data on high quantitative level.
- The software tool for a general correction algorithm of radiography and tomography data (QNI) is prepared by PSI. It is based on the IDL programming language and was made available by the end of 2006. It is the main output of the PhD work of Mr. R. Hassanein (Paul Scherrer Institute, Switzerland).

### *1.4.9. Richard Lanza, Massachusetts Institute of Technology (MIT), United States of America*

- Work on fast Neutron Resonance Radiography (NRR) was reported. In this technique fast neutrons in the 2 to 6 MeV range are used to take high resolution transmission images of objects. The absorption for a particular element varies with energy in a manner unique to a given element; NRR utilizes element specific resonances in energy to enhance the contrast and is especially effective for imaging light elements such as carbon, oxygen and nitrogen, but can be extended to others. This enhancement mechanism is then used to produce elementally resolved images of objects under inspection and is of particular usefulness for security inspection of containers. The problems of this technique have much in common with thermal neutron radiography: source intensity, detector efficiency and reconstruction and processing of data.
- The source is an accelerator-based neutron source which produces neutrons through the reaction $d(d,n)^3He$. The target gas is 4 atm of deuterium with a 6-micrometer thick tungsten front window. The window is held by a thicker structure, also made of tungsten. It was emphasized that for such imaging applications it is necessary to reduce production of gammas by correct choice of target structural materials. In particular, the use of tungsten windows and lining of the target with tungsten foil reduces gamma contamination.

Two detectors have been used in the system. The first was the rather conventional one of using a thick plastic scintillator imaged by a cooled CCD camera. The major limitation of this is the limited amount of light produced in the plastic by fast neutrons ($\sim 10^3$ per 2 MeV neutron) as compared to normal thermal neutron screens ($\sim 10^5$ photons/neutron). The alternative approach is to use $2.5 \times 2.5$ cm$^2$ plastic scintillators in counting mode. With this approach, high efficiency can be combined with the ability to reject gammas through pulse height selection but the spatial resolution is reduced to ~ 1cm in the system. For several applications, this resolution is satisfactory but the cost/pixel is high.

## 1.5. Discussion

### *1.5.1. General aspects of neutron radiography*

A brainstorming discussion took place on the results of the work done, the details of various components for neutron radiography namely the source, sample holders and imaging systems. The source part focused on the improvement of neutron flux at the sample position with

research reactor beam lines and the non- reactor sources namely the accelerator based ones, which were used by participants under the project work. The discussion included the selection criteria for various components based on the problems to be undertaken, the optimization of beam lines, shielding and collimators and detection systems. These sessions were found to be very useful, sharing and exchange of information, especially for the developing facilities.

### *1.5.2. Source development and improvement*

**Reactor Based**

*Design of collimator, simulations*

Monte Carlo simulation is useful technique to optimize the design and fabrication of a best possible collimator assembly. Parameters such as neutron flux, gamma dose, neutron /gamma ratio, epithermal to thermal component can be simulated using Monte Carlo techniques. Besides MCNP type codes based on first principle considerations, MACSTAS as ray tracing option becomes also common in the past years.

Following factors need special attention in the design of a neutron radiography facility:

- Gamma Reduction: Filtering of gamma radiations is necessary especially for radial beam ports; bismuth or lead are good candidates. Consideration of neutron absorption makes bismuth a better choice and a single crystal helps in avoiding Brag cut off edges in the transmitted neutron spectrum. The optimum size, and neutron vs. gamma flux need to be resolved using simulation for the given reactor parameters. Typically single crystal of bismuth with 10 cm in length is used.
- Shielding: The shielding has to take care of both neutron and gamma radiations. It could be a sandwich of borated polyethylene and lead. Concrete is also used depending on the availability of space. The use of materials, which can give capture gamma radiation should be avoided.
- Beam catcher: The beam catcher should be designed in a manner that it absorbs the beam transmitted through the sample without back scattering. Boron carbide in a sealed aluminum box works well.

### *1.5.3. Cold neutron radiography*

To extract an intense neutron beam for radiography purposes a large scale facility like a research reactor or a spallation source is needed. In research reactors neutrons are produced by fission of Uranium. The energy of the neutrons as produced is of the order of a few MeV. These high energy neutrons are not well suitable for conventional experimental purposes. Therefore, they are moderated to energies of a few meV using a moderator like light or heavy water. The advantage of a steady source like a fission reactor for neutron imaging is the stable and continuous neutron flux which enables tomographic measurements with extended exposure times.

An important characteristic of a neutron source is the mean energy of the neutron beam provided for experiments. As mentioned above, the neutrons are moderated to thermal energies, corresponding to a few meV. Additional moderation by a “cold source”, i.e. a moderator at low temperature (e.g. liquid hydrogen or deuterium at 25-30K) is used to obtain cold neutrons.

*1.5.3.1.Specifics of the imaging with cold neutrons*

Due to their low energy the attenuation coefficients of penetrated materials are higher for cold neutrons than for thermal neutrons for many materials. For some others, the relation is inversely. A more complicated energy dependency of the scattering cross-sections can be found in crystalline materials due to the Bragg edges at grid planes. Using cold neutrons some non-conventional imaging techniques are possible due to the following reasons:

- The Bragg cut-offs for many crystal materials are in this energy range that allows radiography contrast variations by applying of energy-selective imaging techniques.
- The wavelength range and the beam intensity are optimal for various neutron optic components like super-mirror-devices, refraction lenses, polarizer which can be successfully used for a spatial (producing convergent or divergent beams) or spectral beam modulations. Beams suitable for micro-tomography, phase-contrast radiography and neutron polarizing imaging experiments can be obtained.

### *1.5.4. Use of neutron guides*

*1.5.4.1.Curved neutron guide*

Curved neutron guide provides a high cold neutron flux directly at the end of the guide with a negligible background of γ-radiation and fast neutrons. The absence of fast neutrons allows relatively light and flexible shielding which gives the possibility to change the beam components and geometry any time. Furthermore, the low background is a good circumcise for conducting time consuming experiments like phase-contrast imaging and energy-selective radiography at high Signal/Noise ratio.

*1.5.4.2.Focusing neutron guide*

Nowadays in many neutron radiography facilities common pinhole geometry is usually used where the beam collimation is performed by the combination of a small aperture with a diameter *D* close to the source and a long distance *L* from the aperture to the sample position. This way, the quality of the radiography image depends on the ratio L/D-ratio which is the main parameter to characterize the performance of the facility. The increase of the aperture diameter *D* leads to a gain in the neutron flux while reducing the image resolution and vice versa. Depending on the experimental requirements – high flux or high resolution, - an optimal *L*/*D* ratio can be chosen. A considerable improvement may be achieved using a focusing neutron guide instead of a conventional guide. This way a flux gain can be achieved in combination with an increase of the L/D ratio if the beam size in the focal point is made as small as possible. The first results are promising showing that using parabolic or elliptic focusing guide the neutron beam of several square centimeters can be focused on a spot of a size of 1 $mm^2$ with a considerable gain of flux. The state-of-the-art neutron radiography set up at Paul Scherrer Institute is shown in fig. 1.

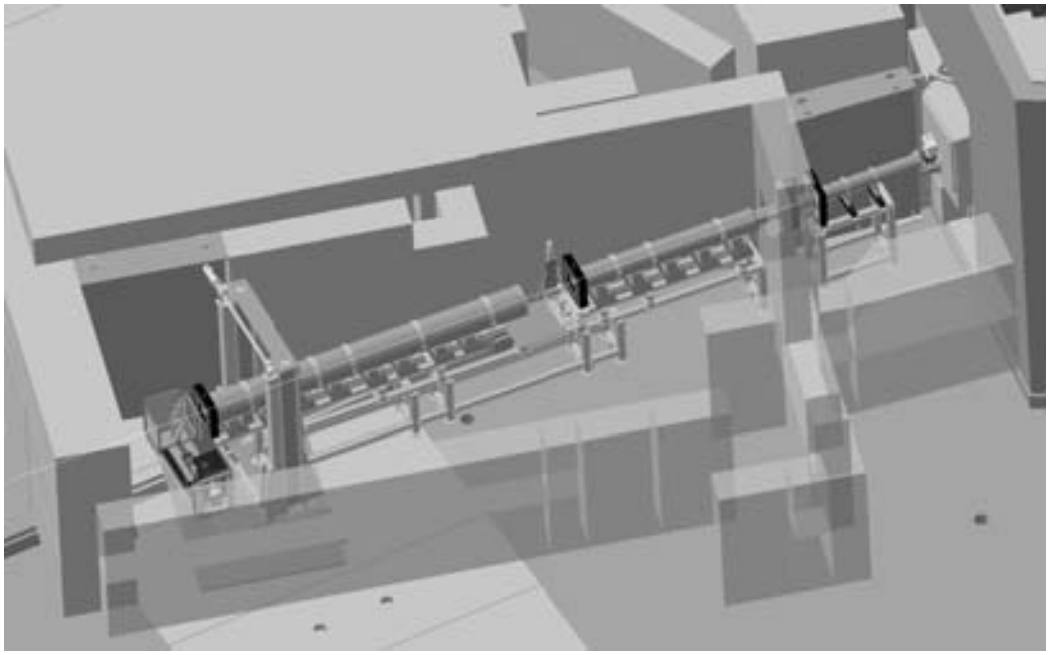

*Fig. 1. ICON installation at the Paul Scherrer Institute (PSI), Switzerland completed in 2005. It is in use for imaging with cold neutrons and has two beam ports: one for micro-tomography in the middle and another for the inspection of large objects at the end position.*

### *1.5.5. Advanced neutron imaging techniques*

*1.5.5.1.Phase-contrast imaging*

The phase-contrast radiography is an edge-enhancement technique that allows visualizing objects, which provide very low contrast with the standard absorption radiography technique. In this method a neutron beam with a high spatial transversal coherence is used for the visualization of phase shifts produced by the sample under investigation.

To provide appropriate conditions for a phase contrast imaging a small pinhole with a large distance between the pinhole and the sample is necessary. A measure for the achieved spatial coherence is the coherence length $l_c=L\lambda/D$, where $L$ is the distance between the sample and the pinhole, $D$ is the diameter of the pinhole and $\lambda$ is the neutron wavelength. In the case of cold neutrons with a spectrum having a maximum at 4.5 Å and setup parameters $D$ = 0.5 mm and $L$ = 5 m, the obtained coherence length is 4.5 μm which is two times higher than that achieved in case of thermal neutrons.

Recently, it was shown that the phase information of the neutron beam interacting with a sample can be obtained directly. This technique is based on grating interferometry principles and might be useful for the direct visualization of magnetic domains in special materials.

*1.5.5.2.Energy selective radiography*

The position of the Bragg cut off for the most metals is around 4 Å in the cold spectrum and depends on the crystal cell parameters and provides the possibility to change the contrast in radiography images just by using monochromatic neutrons with energies in the neighbourhood of the Bragg edge. Textures in the materials will be directly visible.

### *1.5.6. Detectors/Imaging systems*

*1.5.6.1.Parameters and Definitions*

The following parameters are used to describe image, imaging system or its part:

(1) Spatial resolution.
(2) Contrast sensitivity (figure of merit).
(3) Detective quantum efficiency.
(4) Dynamic range.
(5) Temporal resolution.

*Spatial resolution (SR)*

SR can be determined as a FWHH of the Line Spread Function (LSF). LSF is obtained by differentiating the Edge Spread Function (ESF), which is a histogram of intensity distribution across the image of the test sample edge.

*Contrast sensitivity (CS)*

Minimal deviation of the sample transparency detected in the image. For two adjacent areas of the same size with different transparency it is determined as

$$CS=(I_1-I_2)/ (I_1+I_2)= 2\Delta/(I_1+I_2)= \Delta/I_{av} \qquad (1`)$$

where $I_1$, $I_2$ – image intensity in these areas,

$\Delta$ - deviation of signals from the average value $I_{av}$

One can see that CS should be compared with relative standard deviation of the image intensity due to statistical noise in the considered area.

As CS<<1, CS is equal to the deviation of $(\Sigma_i d_i)$, where $\Sigma_i$ – macroscopic cross section for beam attenuation, $d_i$ – sample size along the beam direction.

CS depends on neutron fluence on the considered area.

Figure of merit: $FOM=1/CS$ (2)

Detective quantum efficiency (DQE)

By definition

$$DQE= (I_{out}/\Delta I_{out})/ (I_{in}/\Delta I_{in}) \qquad (3)$$

where $I_{in}$, $I_{out}$, $\Delta I_{in}$, $\Delta I_{out}$ – input, output signals and their standard deviations.

**Input signal** – number of neutrons impinging certain area of the detector.

**Output signal** – image intensity integrated over the same area.

*Dynamic range (DR)*

DR of the imaging system is the number of quantification steps used for image intensity representation. It depends on the dynamic range of imaging device (film, CCD-matrix).

Real DR of the image itself depends on image statistics and is determined as:

$$I_{max}/\Delta I_{noise}$$

*1.5.6.2.Design of Imaging System*

**Standard layout**

The digital radiography imaging system can be designed using a LiF+ZnS scintillator, front coated mirror, cooled CCD with appropriate acquisition software. Such systems are quite common in many labs world-wide. The specification of CCD will depend upon the resolution and the dynamic range required. Ideally a large area CCD with 1 K×1 K matrix should be used with cooling typically to around –30 degree Celsius. However, a low cost system can also be designed using 512×512 matrixes with around 10-13 micron pixel. The optical lens used should be high numerical aperture better than F1.2. In order to protect CCD and electronics from direct neutron exposure, the mirror is placed at 45 degrees to the scintillator. The dynamic range and resolution depends on size of CCD pixel, its cooling, and number of pixels.

**Intensifier + CCD detector for real time analysis**

For real time applications such as flow visualization, an intensified CCD can be used. Either a lens coupled intensifier CCD combination or at higher end fiber-optic coupled intensifier CCD combination can be used. In the first case, a higher gain image intensifier is needed due to light losses in lens coupling.

**New detectors: imaging plate or flat panel**

Imaging plates containing Gd oxide as converter material are being marketed by some companies. They do provide large area of imaging but the image is not directly available. The imaging plate has to be read in offline mode which can take several minutes.

Flat panel detector is relatively a new arrival. It is yet to be fully evaluated by neutron imaging community for radiography applications.

### 1.6. Results from a Well Developed Facility

Figures 2-5 show some of the recent results obtained using the neutron radiography facility at PSI.

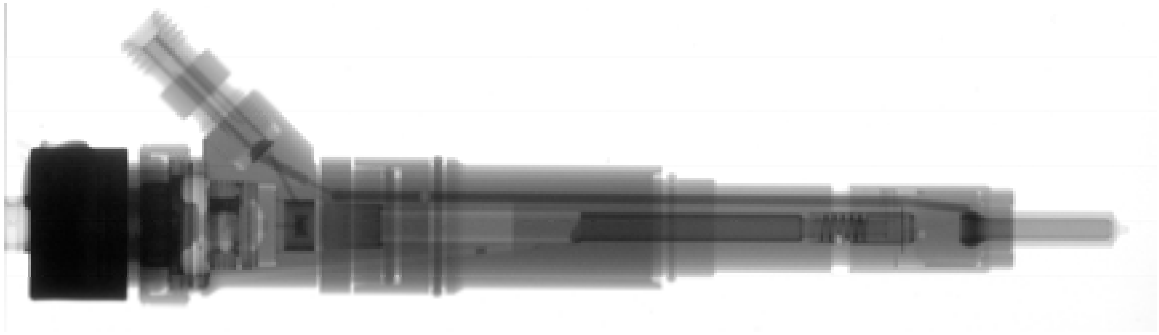

*Fig. 2. This neutron image of the injection nozzle for diesel engines demonstrates the advantage of the method: metallic parts become very transparent, whereas small amounts of hydrogenous liquids (diesel fuel) can be detected, visualized and quantified with high precision. This image was taken at the ICON station.*

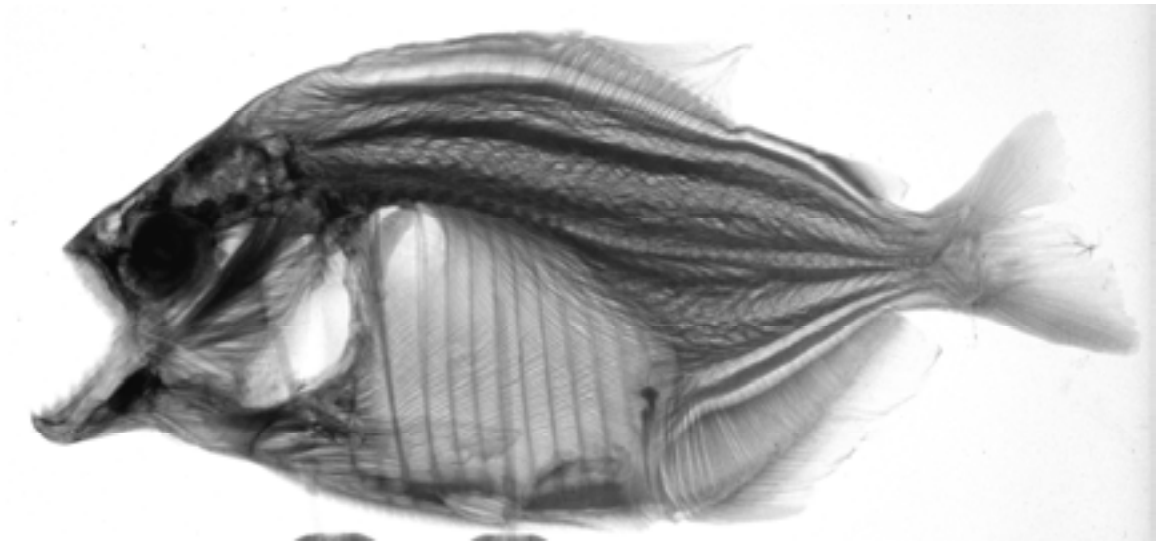

*Fig. 3. Organic materials deliver very high contrasts for neutrons in the transmission mode. This dried fish (Piranha) can be studied in very detail because a high resolution was obtained in the image (50 μm are possible nowadays). There are many interesting aspects in Biology to be investigated with the help of neutrons: root growing, moisture distribution in soil and plants, the detection of pollutions and poisons.*

*Fig. 4. The study of objects from cultural heritage is demonstrated in the example of the "Mercure from Thalwil" – photo left, radiography in the middle and a tomography slice, right. Because such kinds of Roman bronzes contain high amounts of lead, the study by using X-ray methods is very limited. With the help of neutron imaging methods, in particular tomography, a non-destructive analysis is possible and manufacturing processes, corrosion and restoration failures can be shown.*

Fig. 5. The use of neutrons in geosciences has high relevance due to the ability to detect water migration in porous media. This picture shows the water in a rock sample of about 8 cm diameter, where a voxel size of 0.1 mm can be obtained. Both volumetric and temporal information can be obtained from the moisture transport process.

## 1.7. Conclusions

The results of the findings of the work done under the CRP on the Development of Improved Sources and Imaging Techniques for Neutron Radiography done in collaboration by experts of ten countries (Malaysia, India, Bangladesh, Rumania, Russia, Brazil, South Africa, Germany, United States of America and Switzerland) demonstrated impressively how it was possible to transfer knowledge between the type A and type B facilities. The exchange of expertise and sharing of resources allows a much better use of the beam lines in these countries foreseen for practical applications of non-destructive investigations using neutrons.

# COUNTRY REPORTS

# Development of new neutron radiography facility at MINT TRIGA MARK II tangential beam port using CCD camera imaging system

Azali Muhammad[1], Abdul Aziz Mohamed[1], Muhammad Rawi Mohamed Zin[1],
Rafhayudi Jamro[1], Razali Kassim[1], Husain Wagiran[2],
Rosli Jaafar[2], and Wan Muhamad Saridan Wan Hassan[2]

[1.] Malaysian Institute for Nuclear Technology Research (MINT), Malaysia
[2.] Universiti Teknologi (UTM), Malaysia

**Abstract:** The first neutron radiography facility in Malaysia was constructed in 1984 and completed in 1985 at one of the radial beam ports of MINT TRIGA MARK II research reactor. The facility is known as NUR-2 and has been used as a basic R&D and inspection tool for archaeological and biological objects, aircraft and industrial components. However, this facility has low thermal neutron intensity at the sample position, which leads to long irradiation times; it gives many limitations for the industrial applications. The collimator used for this facility is based on step divergent collimator type. The best exposure technique established with this facility was a direct exposure technique, using a combination of Gadolinium (Gd) 25 μm converter and Kodak SR45 (SR5) film. The characteristics of the beam and image quality were studied by using a beam purity indicator (BPI) and sensitivity indicator (SI). The results obtained for image quality were quite good, and comparable with other facilities in the world, where all seven gaps and six holes were visible on the radiograph. A new neutron radiography facility called NUR-3 has been planned and designed, which will be set up at the Tangential Beam Port of RTP. In addition, the new facility will consist of a new collimator design, new imaging system using CCD camera. We present here some information on development of the MINT neutron radiography activities and the current status of the improvement.

## 1. INTRODUCTION

Neutron Radiography is an important technique in non-destructive testing and is the only radiography technique that is able to investigate material with high gamma ray background such as nuclear spent fuel. The development of neutron radiography in Malaysia started with the availability of the country's first research reactor, the 1 MW TRIGA MARK II Reactor, commissioned in June 1982, mainly as a tool for research and development purposes. The development of neutron radiography facility was one of the main objectives. The MINT TRIGA MARK II research reactor (RTP) is a swimming pool-type light water research reactor with enriched uranium-zirconium-hydride fuel and graphite reflector. There are three radial beam ports, one tangential beam port and one thermal column. The maximum steady state operating power of the reactor is 1MW and at this operating power the thermal neutron flux at the edge of the reactor core is around $2.797\times10^{12}$ n/cm$^2$/sec.

In late 1983, a simple neutron radiography test facility known as NUR-1 was constructed and tested. The data collected from this test facility enabled the design and construction of the permanent facility, NUR-2. The construction of NUR-2 started in November 1984 and was completed in February 1985. In January 1987, a new collimator was installed at the beam port of NUR-2. The neutron flux at the outlet of the NUR-2 collimator is about $1.04\times10^{7}$ n/cm$^2$/sec at operating power of 750 kW. The lay out of NUR-2 at RTP is shown in Fig. 6. The direct exposure technique using Gadolinium foil converter and Kodak SR45 (SR5) film was successfully established using this facility. However, due to problems like very long exposure time, and higher dose rate around the facility, more tests and experiments have to be carried out at this facility to improve its performance. These experiments include: study the characteristic of neutron beam, and establish the best/appropriate imaging system. At the same time new NR facility was also planned and designed for tangential beam port. This new

facility, called NUR-3 will consist of a new collimator design and an imaging system using CCD camera.

The outcome of experiments carried out at NUR-2, design of a new collimator and imaging system using CCD camera is presented in this paper.

### 1.1. Present NUR-2 Facility

From the year 2003 till 2005 the facility has been fully utilized for many activities including study of beam characteristic at sample position, evaluation of image quality radiograph using direct and transfer methods, research in various fields, and for testing new imaging system using Charged Coupled Device (CCD) camera. The outcome/achievements or results of the studies are discussed below.

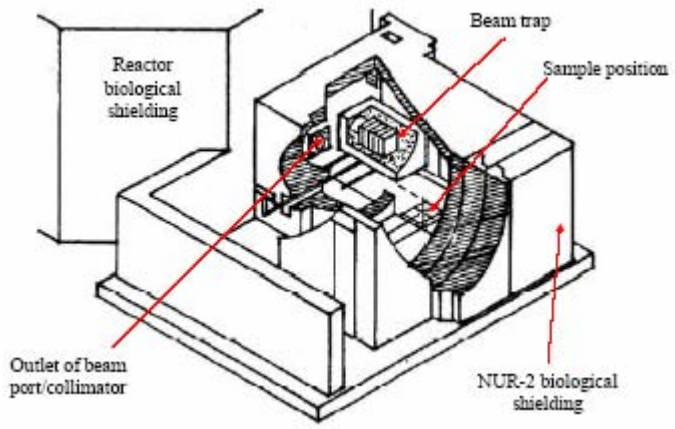


*Fig. 6. Layout of NUR-2 facility.*

#### *1.1.1. NUR-2 beam characteristic and Radiographic Image Quality*

The characterization of the beam and radiographic image quality for NUR-2 facility was done using beam purity indicator (BPI) and sensitivity indicator (SI), respectively. In all cases, the reactor operation power was fixed at 750 kW. Both direct and transfer techniques were studied and compared. For direct exposure technique gadolinium (Gd) converter and Kodak SR45 film were used. The best exposure times for this technique were in the range of 10-25 minutes. The results are shown in Fig. 7 and Tables 1. The comparison of NUR-2 with N-ray facility in Canada [1] is shown in Table 2.

The results show that thermal neutron content is at an acceptable range i.e. in the range from 61.74% to 71.08%. Scattered neutron and gamma contents are also quiet low, with average values of about 2% for both. These values will provide a good beam for better image quality. The SI indicator results show that the facility is able to produce a high quality image.

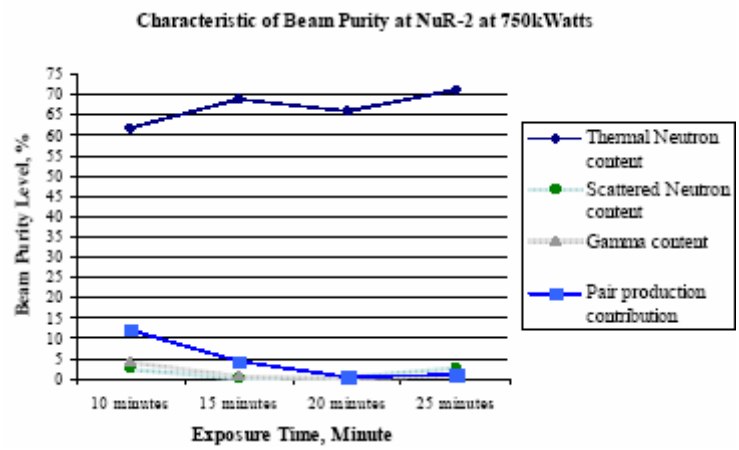


*Fig. 7. Characteristics of NUR-2 measured by ASTM beam purity indicator*

TABLE 1. RADIOGRAPHIC IMAGE QUALITY (DIRECT TECHNIQUE).

| Exposure Time (min.) | Number of Visible Hole<br><br>H | Visible Gap |
|---|---|---|
| 10 | 6 | 7 |
| 15 | 6 | 7 |
| 20 | 6 | 7 |
| 25 | 6 | 7 |

TABLE 2. COMPARISON BETWEEN NUR-2 AND N-RAY FACILITY IN CANADA [1].

| Facility | Sensitivity Indicator (SI) | | Beam Purity Indicator (BPI) | | | |
|---|---|---|---|---|---|---|
| | Holes | Gaps | % Thermal neutron content | % Scattered neutron content | % Gamma content | % Pair production contribution |
| N-Ray[1] | 6 | 7 | 65 | 1.5 | 1.5 | 0.6 |
| NUR-2 | 6 | 7 | 68 | 1.8 | 1.8 | 0.6 |

The results for beam purity and radiographic image quality for transfer technique using indium (In) converter and Agfa D7 film are shown in Tables 3 and 4, respectively.

TABLE 3. BEAM CHARACTERISTIC USING TRANSFER EXPOSURE TECHNIQUE.

| NUR-2 Facility | Beam Purity Indicator (BPI) | | | |
|---|---|---|---|---|
| | % Thermal neutron content | % Scattered neutron content | % Gamma content | % Pair production contribution |
| 50 min | 63.06 | 4.50 | 5.86 | 7.66 |

TABLE 4. RADIOGRAPHIC IMAGE QUALITY (TRANSFER TECHNIQUE).

| Exposure Time (min.) | Number of Visible Hole<br><br>H | Visible Gap |
|---|---|---|
| 50 | 6 | 7 |

From the above results it can be concluded that the best exposure technique NUR-2 facility is direct method. However, the transfer technique still can be used.

### *1.1.2. New imaging system using CCD at NUR-2*

The digital radiography system, NUR-3, is planned to be installed at the tangential beam port in RTP, once the new collimator and exposure facility are finalized and commissioned. In order to familiarize with the operation the system is established and tested at NUR-2. The testing arrangement in NUR-2, include CCD camera, lead shutter, collimator, beam shutter, beam trap, motorized sample holder and trolley. Since the testing of the CCD camera will be carried out at the NUR-2, which consists of a wide range of energies of neutron and gamma rays from the radial beam port, additional shielding is required to ensure that the electronic components in the CCD camera are well protected.

#### *1.1.2.1.Testing Setup*

The CCD camera system is set up temporarily in the NUR-2 exposure room for the testing purpose (Fig. 8 and 9). The operation of the camera is controlled entirely via software. The only manual function is to activate the on/off switch on the rear of the power supply.

#### *1.1.2.2.Shielding Box*

Neutron spectrum at NUR-2 consists of neutron beam of all energy ranges. Not only the fast and thermal neutron, but the beam also contains gamma rays. Electronic components, a part of the neutron camera system, can be severely damaged or rendered unreliable by being exposed to a strong radiation field. For example, the fast neutron will change the chemical and physical properties of the electric component during the bombardment on the material and produce activation gamma rays like $^{27}Si(n,\gamma)^{28}Si$ reaction. Since the emission of the energetic neutron and gamma rays are simultaneous and unavoidable, the device needs to be shielded with particular combination of material such as boronated polyethelyn, boral, and lead of appropriate thicknesses.

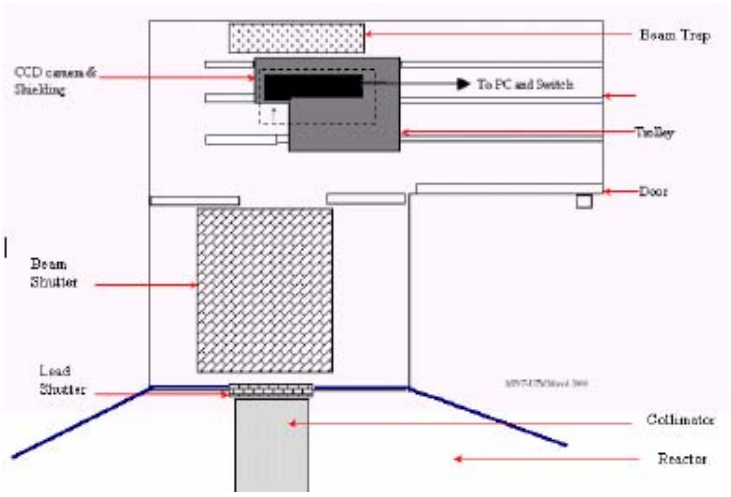


*Fig. 8. Digital Neutron Radiography Testing Set-up in NUR-2 Exposure Room.*

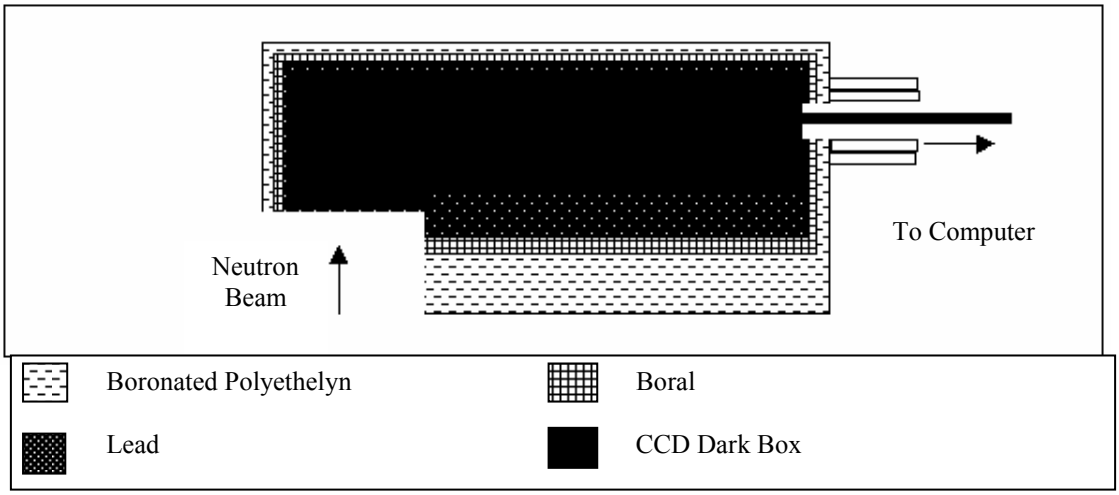


*Fig. 9. Shielded box for CCD camera.*

## 1.2. Applications

During the period of 3 years from the year 2003, NUR-2 has been fully utilized in various research fields, for object inspection like turbine blade, material studies and archaeological artefacts [3, 4, 5]. Examples of these radiographs are shown in Figs. 10 – 14.

*Photograph of Kris (Malay sword)* *NR image*

*Fig. 10. Artifact 1 and their NR image.*

*Photograph of the brass Vishnu deity 6th or 9th century, Lembah Bujang, Kota Kuala Muda, Kedah* *NR image*

*Fig. 11. Artifact 2 and their NR image.*

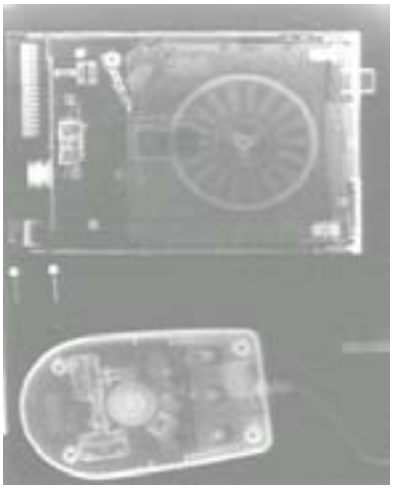

*Standard Blocks (BPI and SI)* *Computer components – hard disk and mouse*

*Fig. 12. NR images of standard blocks and computer components.*

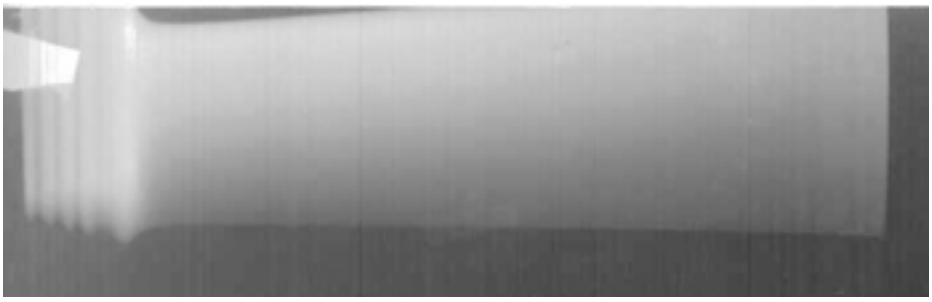

*Fig. 13. NR image of turbine blade.*

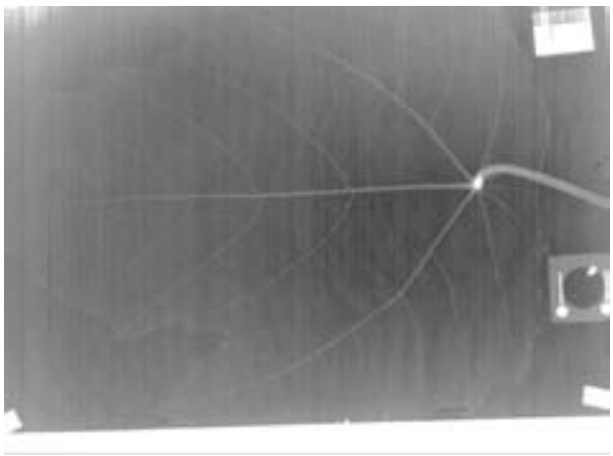

*Fig. 14. NR image of biological sample.*

## 1.3. New NR Facility at Tangential Beam Port

The existing NUR-2 facility is not efficient enough due to the long exposure time that is not practically suitable for the industrial applications. Due to this reason, a new neutron radiography facility has been proposed, which will be installed at tangential beam port of RTP. The development of this new facility, called NUR-3 will be divided into two main parts, namely design and fabrication of a neutron collimator, and the utilization of the CCD camera imaging system. The outcome and achievements of this activity are discussed in the following section.

### *1.3.1. Neutron collimator and its design*

Neutron collimator is the most important component in a neutron radiography facility set-up, which defines the neutron beam characteristic at the object plane. The aim of this research is to design and choose the best geometry and materials for thermal neutron collimator so that a uniform beam, high L/D ratio and maximum thermal neutron flux at the object plane can be determined and achieved. In order to establish the new neutron radiography facility, a collimator shielding has to be designed. Malaysian Institute of Nuclear Technology Research carries out this project in collaboration with Physics Department of Universiti Teknologi Malaysia. The project is now in the final designing stage. From the approved design it will be fabricated and then installed in the tangential beam port.

#### ***1.3.1.1.****Monte Carlo N-Particle Transport Code (MCNP) Software*

The Monte Carlo N-Particle Transport Code (MCNP) software was used for the design of the neutron collimator. The code is able to optimize a few parameters in the designing stage, such as L/D ratio, beam divergence and neutron to gamma ratio. There were six major collimator components to be optimized namely the beam port medium, neutron moderator, collimator aperture, collimator geometry and gamma filter. The optimization of the components has been done by applying variance reduction technique in all the simulations. Besides, each simulation result provided an estimation of Monte Carlo errors and was able to produce output results in various graph styles.

#### *1.3.1.2.Neutron Collimator Components*

After the optimization of each collimator components input variables in the simulation, the estimated thermal neutron flux at the end of the beam port was around $1\times10^{6}$ neutron $cm^{-2}s^{-1}$, whereas, the calculated L/D ratio was around 100. The neutron to gamma ratio for the design will meet the recommended value ($\geq10^{6}$ n $cm^{-2}$ $mR^{-1}$). The table below shows the comparison of the collimator characteristics between the new and the existing collimator design at NUR-2.

TABLE 5. NEUTRON COLLIMATOR CHARACTERISTICS COMPARISON BETWEEN PRESENT NEUTRON COLLIMATOR AT NUR-2 AND NEW NEUTRON COLLIMATOR DESIGN FOR NEW NEUTRON RADIOGRAPHY FACILITY (NUR-3).

| **Characteristics** | **Present Neutron Collimator Design (NUR-2)[1]** | **New Neutron Collimator Design** |
|---|---|---|
| Collimator Type | Step Divergent | Divergent |
| Length | 200 cm | ≈ 200 cm |
| Inlet Aperture Diameter | 5.4 cm | ≈ 2 cm |
| L/D Ratio | 37 | ≈ 100 |
| Thermal Neutron Flux (Sample position) | $1.04\times10^{5}$ n $cm^{-2}$ $s^{-1}$ (at 2 meters from the out let of collimator) | ≈ $1\times10^{6}$ n $cm^{-2}$ $s^{-1}$ (the out let of collimator) |
| n/γ Ratio | $1.02\times10^{4}$ n $cm^{-2}$ $mR^{-1}$ | ≈ $1\times10^{6}$ n $cm^{-2}$ $mR^{-1}$ |

As shown in the table 5, the drastic improvement of the new collimator design was the thermal neutron flux and the L/D ratio. The thermal neutron flux with the new neutron collimator shows an improvement of up to 90% as compare to the present one. The new thermal neutron flux would be able to reduce the irradiation time to 2-3 minutes per radiograph image of certain objects. As shown in Table 5, the diameter of the inlet aperture was reduced to 2 cm rather than 5.4 cm in the existing one to increase the L/D ratio. The changes of the inlet aperture diameter directly improved the L/D ratio to 100, which shows an improvement for about 65% more than the present neutron collimator. This will produce good quality radiographic image with good resolution. The n/γ ratio increased from ~$1\times10^{4}$ to ~$1\times10^{6}$ n $cm^{-2}$ $mR^{-1}$ which will reduce the biological shield required for the NUR-3 facility.

The outcome of thermal neutron collimator design and set-up for the new neutron radiography facility is shown in Fig. 15.

(1) Neutron moderator

The final design and materials for neutron moderator is given below:

Materials: Iron and polyethylene

Shape: Aluminium casing with truncated cone (negative sense) hollow at the centre.

Size: 10 cm long iron, 30 cm long polyethylene, 15 cm in diameter of the casing and 2 cm in diameter for the centre hole.

Location: Place in the inlet of the beam port, located at 5.04 cm till 45.04 cm from graphite reflector outer surface

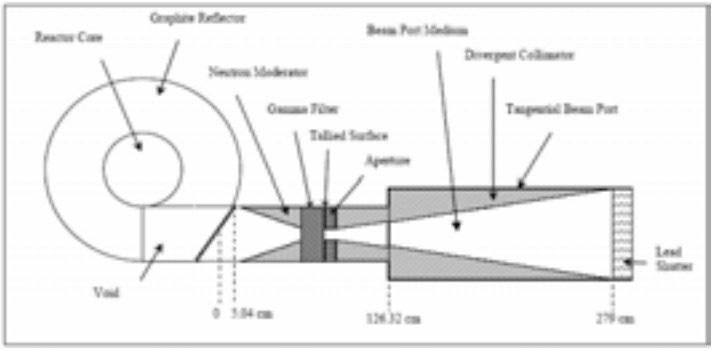


*Fig. 15. Neutron Collimator Design for New Neutron Radiography Facility.*

(2) Gamma filter

The final design and materials for gamma filter is given below:

Material: Single crystal Bismuth

Shape: Cylindrical with aluminium casing

Size: 5 cm long and 15 cm in diameter of the casing

Location: Placed in the inlet of the beam port, located at 45.04 cm till 50.04 cm from outer surface of graphite reflector

(3) Collimator aperture

The final design and materials for collimator aperture is given below:

Material: Boral

Shape: Cylindrical with aluminium casing and hole at the centre

Size: 2 cm long and 15 cm in diameter of the casing and 2 cm in diameter of the aperture centre hole

Location: Placed in the inlet of the beam port, located at 50.04 cm till 52.04 cm from outer surface of graphite reflector

(4) Collimator geometry and material

The final design and set-up of the collimator geometry and materials is given below:

Material: Sandwich of Lead and Boral

Shape: Cylindrical aluminium casing with truncated cone (positive sense) hollow at the centre

Size: 226.96 cm long and 15 cm in diameter of the inner beam port casing, 19 cm in diameter of the outer beam port casing and 2 cm in diameter of the centre hole

Location: Placed after the aperture, from position 52.04 cm till the end of the beam port, 279 cm from the graphite reflector outer surface.

### 1.4. CCD Camera Imaging System

According to prepared specifications, CCD cameras from various manufacturers were evaluated and the cool/view FDI coupled with photonic science zoom lens was selected for imaging system in neutron radiography facility. The technical specifications of the CCD camera and the imaging system are given in Table 6.

TABLE 6. THE TECHNICAL SPECIFICATIONS OF THE NEUTRON RADIOGRAPHY SYSTEM.

| ITEMS | SPECIFICATIONS |
|---|---|
| Camera type | FDI CoolView |
| Image intesifier | Gemsta |
| Lens | f0.95 close focus lens |
| Mirror | 45 degree highly reflectivity polished silicon |
| Camera and electronic shielding | Premadex Shielding materials |
| Pixel resolution | 1392×1040 (max) |
| Input pixel size | Approximately 48 microns square |
| Input active area | Approximately 67×50 mm |
| Scintillator | Li6F/ZnS:Ag 0.4 mm thick & peak emission at 550 nm |
| Energy response | High absorption for thermal neutrons 2-10 Å |
| Light exclusion membrane | 500 micron aluminum |
| Cooling | Dual stage peltier, with secondary air cooling |
| Grey scale resolution | 4096 gray level (12 bits) |
| Readout speed | 20/10 MHz pixel rate software selectable |
| Saturation | Approximately 13,000 electrons at minimum gain |
| Intensifier gain | Software controllable in 100 steps, approx 1000:1 gain range |
| On chip binding | Selectable 1×1 to 8×8 |
| Exposure time | Selectable 1 ms to 30 minutes |
| Control | Via Firewire bus.DCAM compliant |

#### *1.4.1. Current work on CCD*

Since the new NR facility is still not ready the NR group has decided to try this new CCD camera on the NUR-2 facility. However this new CCD camera should be protected from gamma radiation and fast neutron (see section 2.2.2). The calculation and design of this shielding block to protect CCD camera from this radiation is in progress now. The design is

done by Engineering Department in MINT. The image of neutron radiography using CCD camera tested at SANs beam line is shown in Figure 16.

### 1.5. Motorized Sample Holder

The CCD camera has a limitation of the scintillator size of dimension 6.7 cm × 5.0 cm. This will be a problem to the large sample size. To overcome the problem motorized sample holder that will be interfaced to a computer for its control has been developed. The set-up will be tested in the NUR-2 facilities before transferring to NUR-3.

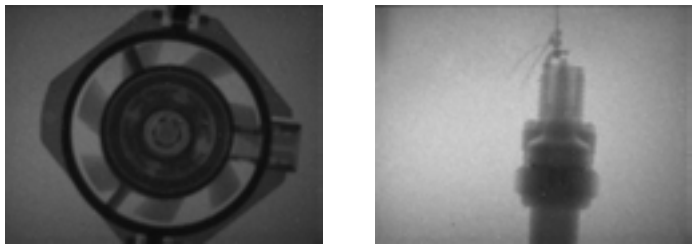

*Microprocessor fan* *Spark plug*

*Fig. 16. Digital thermal neutron radiograph.*

The motorized sample holder was developed based on the commercial x-y plotter 2 axis linear drive unit model: LS-27003. The holder was designed using software AutoCAD Inventor Professional 9.0 by MINT Engineering Department (Fig. 17). The software to control the motorized sample holder was developed using Visual Basic® 6.0.

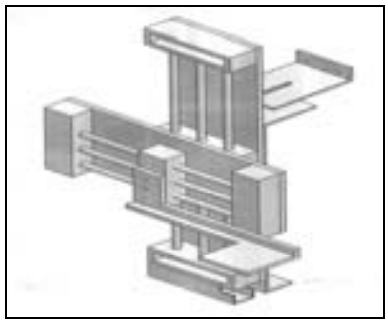

*Fig. 17. Schematic design of Motorized sample holder.*

### 1.6. Devices and Materials Available for the Projects

The existing devices and materials used in this project are listed in Table 7.

TABLE 7. THE DEVICES AVAILABLE FOR NEUTRON RADIOGRAPHY EXPERIMENT.

| **Device** | **Number** |
|---|---|
| Radiographic film KODAK SR-45 | 20 boxes, 2000 films |
| Beam purity indicator | 3 |
| Sensitivity indicator | 3 |
| Aluminum frame | 5 |
| Gadolinium foil | 0.25 mm thickness 1 piece<br>0.75 mm thickness 1 piece<br>0.5 mm thickness 1 piece<br>1.0 mm thickness 1 piece |
| Indium foil | 0.25 mm thickness 2 pieces |
| Densitometry | 1 unit |
| Neutron survey meter (safety) | 1 unit |
| Gamma survey meter (safety) | 1 unit |
| L/D ratio device | 1 unit |
| Steel step wedge | 1 unit |
| Aluminum tape | 100 rolls |
| Aluminum radiographic frame holder | 1 unit |
| CCD camera and imaging software | 1 unit |
| Shielding materials | Boronated plastic, Boron powder<br>Flexi boron, Lead block |
| Neutron scale rate meter | 1 unit |
| NaI scintillation detector | 1 unit |

## 1.7. Conclusions

Some Malaysian sectors have benefited from neutron radiography methods developed at MINT. There are some limitations for industrial applications. Effort to improve and use the tangential beam port has been envisaged. MCNP has been utilized to help the design of the collimator. Real time neutron radiography has been set-up by using CCD and converter to

produce image of the sample exposed to neutron beam. More work will be explored on conventional method (film). Such applications include ceramic electronic, rubber-based products and adhesive problems.

## ACKNOWLEDGEMENTS

Authors are thankful to the Government of Malaysia for the support with providing funds through reactor utilization project under PQRD research grant. Special thanks to the IAEA for supporting this project through financial and technical assistant.

## REFERENCES

[1] Mac GILLIVRAY G. M, Neutron radiography facility at the Chalk River Nuclear Laboratories, Proceedings of the third world conference, Osaka, Japan, May 14–18, 1989, Kluwer Academic Publishers, p.73–79.

[2] ROSLY J, The development of neutron radiography and its potential application in Malaysian industries, Proceedings of the third world conference, Osaka, Japan, May 14–18, 1989, Kluwer Academic Publishers, pp.171–178.

[3] AZALI M., et.al., Radiographic Imaging Techniques For Archaeological Artefacts, Prosiding Persidangan Kebangsaan Sains dan Teknologi dalam Pemuliharaan Warisan Negara, 16–19 Ogos 2004, Melaka, ms 112 – 118, ISBN 967-9970-18-3.

[4] AZALI MUHAMMAD, et.al., Application of Neutron radiography in investigation of Moisture Distribution in Malaysia Wood, Proceeding MINT R&D 2004 Seminar, MINT Bangi, (2004) pp 12–127.

[5] MUHAMMAD RAWI MOHAMED ZIN, et. al., The Comparison of Neutron, Gamma and X-Ray Radiography Images for Materials Evaluation, The 5th National Seminar on Non-Destructive Testing, 1–2 October 2003, Shah Alam, Malaysia (pp. 58–63, ISBN: 983-3006-00-0).

# Overview of facility and development of source and imaging system: Status report of the work done during CRP

Amar Sinha, Yogesh Kashyap, P.S. Sarkar, B.K. Godwal

Laser and Neutron Physics Division, Trombay, Mumbai, India

**Abstract:** The paper summarizes the work done under the research contract for the Coordinated Research Project on Development of Improved Sources and Imaging System for Neutron Radiography. Under this CRP, several processes and systems were developed which include design of improved collimator at CIRUS reactor, design of cooled CCD based detector for neutron, real time neutron imaging detector using intensified CCD for two phase flow, design of a radiography assembly using a microtron, development of simulation tools for phase imaging. The neutron radiography assembly design work at CIRUS reactor has been completed and the components are under procurement for installation. The overall impact of CRP on our work has been quite encouraging and the interaction with other participant has resulted in several new developments.

## 1. INTRODUCTION

The overall objective of the project was to develop:

(1) A state of the art neutron imaging system with improved collimator design.
(2) A neutron radiography and tomography set-up with advanced software tools for visualization.
(3) An image-analysis hardware and software for two phase flow studies and analysis of dynamic events.
(4) A phase sensitive imaging techniques for neutrons and
(5) Tools and techniques for utilization of accelerator based neutron sources such as microtron.

The work carried out during the CRP is reported in this paper.

### 1.1. Development of a State of the Art Neutron Imaging System with Improved Collimator Design

#### *1.1.1. Improved collimator design*

This work involved several steps and are described in the following sections.

##### *1.1.1.1.Flux estimation on CIRUS reactor beam ports*

CIRUS is a heavy water moderated reactor with graphite reflector and cast iron as an annular shielding zone. The core is surrounded by 9" graphite with 24" of additional graphite. This in turn is surrounded by two 6 inch thick layers of cast iron separated by air gap. It is designed to operate at 40 MW with peak thermal flux of $1.4\times10^{13}$ n/cm$^2$/s. There are two types of beam ports available on this reactor for experimentation- one with 4 inches of diameter (Fig.18) and another with 12 inches (Fig.19) of diameter at elevations of approximately 1.25 meter and 2 meters from ground respectively. As these are radial beam holes facing reactor core, any design of collimator has to take into account measures to attenuate gamma flux. Figures 18 and 19 give the schematic layouts of 4-inch and 12-inch beam lines respectively. Some of the measured and estimated values of neutron fluxes at the inner face of the 4-inch beam line are

E <0.625 eV $\phi_0 = 1.4\times10^{13}$ n/cm$^2$/sec

0.625 eV< E <1.0 eV $\phi_0 = 6.2\times10^{12}$ n/ cm$^2$/sec

E >1 eV $\phi_0 = 2\times10^{11}$ n/ cm$^2$/sec

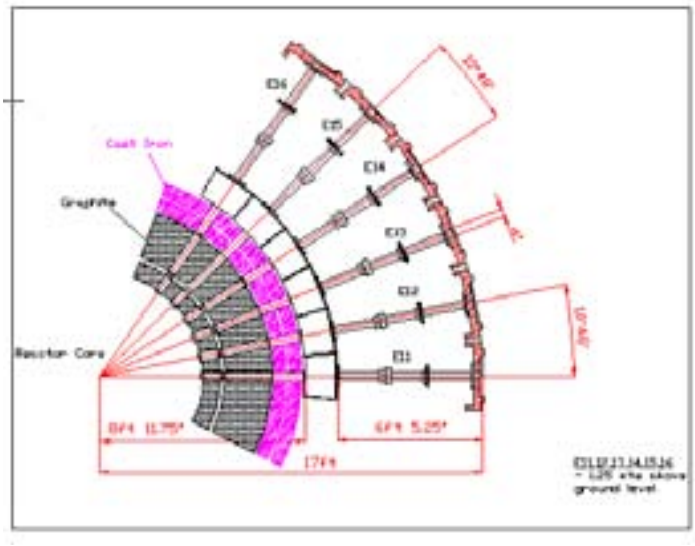


*Fig. 18. Layout of the 4" Beam-holes available at CIRUS Reactor.*

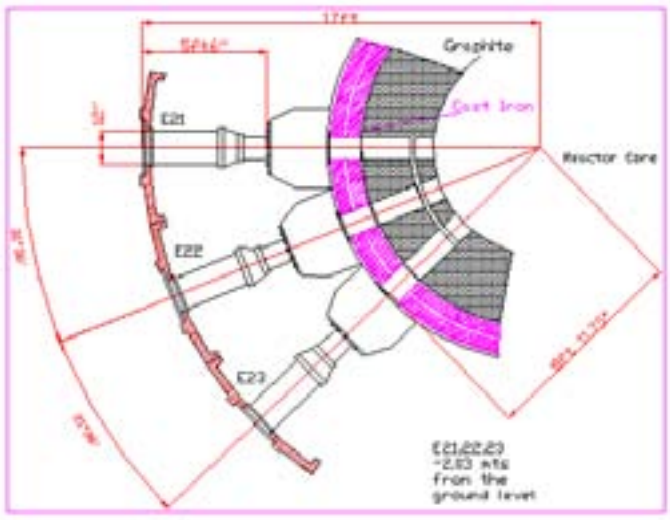


*Fig. 19. Layout of the 12" Beam-holes available at CIRUS Reactor.*

Design calculations have been done for the collimator assembly with both 12-inch and 4-inch diameter beam holes. Monte Carlo code MCNP has been used for these designs. The cut out and full 3D view of the schematic of collimator assembly is shown in Fig. 20 and Fig. 21. The collimator is a conical type consisting of 5 mm thick aluminum tube whose inner surface is lined by layer of boral, cadmium and indium each having thickness of 1mm. The defining

aperture is made up of 20 mm thick boral plate lined with indium. The aperture has a radius of 1 cm. In order to prevent the streaming of gamma rays lead has been inserted at each corner.

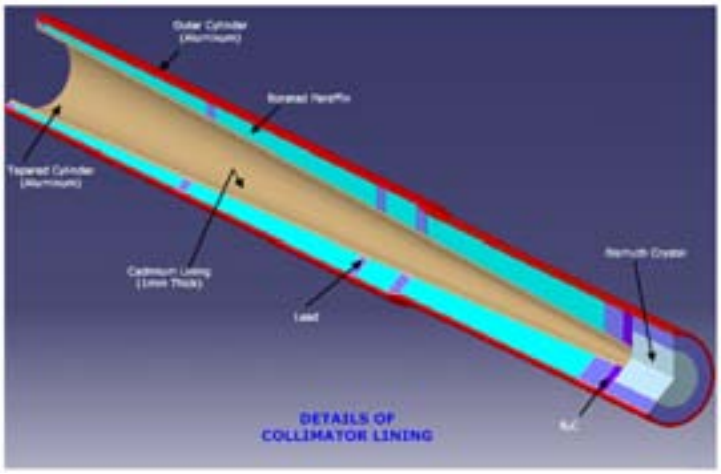


*Fig. 20. Schematic diagram of collimator assembly.*

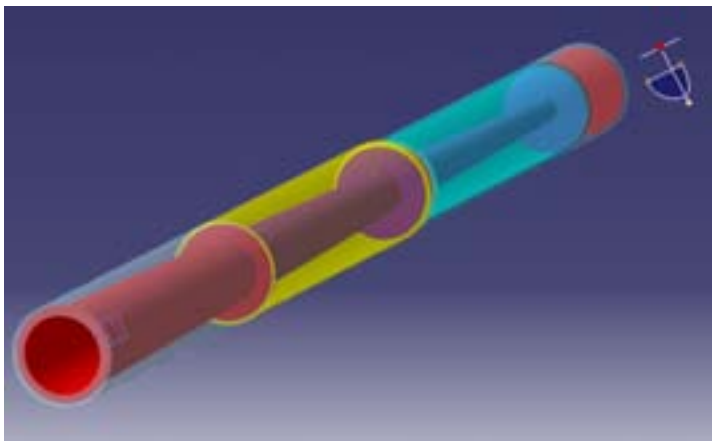

*Fig. 21. Schematic 3D sketch of collimator assembly.*

While the entire opening in the 4-inch beam port will be used in the experiments, only 20 cm of central part of the 12-inch beam hole is being considered for our application. The measured flux at the inlet of the beam-holes inside the core is $10^{13}$ n/cm$^2$/s. From this value, the flux has been estimated at the input face of the collimator. This has been taken as the initial source for the full MCNP calculation of the collimator assembly. Table 8 gives estimated values of neutron flux at the output face of both 12-inch and 4-inch collimator.

TABLE 8. ESTIMATED VALUES OF FLUX AT THE OUTPUT OF 12 AND 4 INCHS DIAMETER COLLIMATOR TUBES.

| Diameter of tube (inches) | Energy of neutrons (eV) | Neutron flux at collimator end with Bi Plug (n/cm$^2$/sec) | L/D |
|---|---|---|---|
| 12 | Upto 0.625 | $1.0\times10^7$ | 90 |
| | Above 0.625 | $3.1\times10^6$ | 90 |
| 4 | Upto 0.625 | $7.5\times10^6$ | 90 |
| | Above 0.625 | $2.3\times10^6$ | 90 |

As can be seen from the Table 8, a neutron flux > $10^6$ n/cm$^2$ /s can be expected from both 4-inch and 12-inch tube diameter at L/D of 90. For phase contrast radiography, it is proposed that a Cd slit with hole of 200-300 micron will be put on the output face of the 12-inch collimator. The object to source distance will be about 2 meters for providing reasonable spatial coherence and detector to object distance will be variable in order to maximize phase effect.

We have also carried out detailed mechanical design of collimator. A design analysis of above collimator assembly has been done using ANSYS code in order to estimate the bend of collimator and stress at various points. Figure 22 shows maximum bending at the end of collimator due to lead weight. Figure 23 gives stress values which show that stress is under tolerance limit.

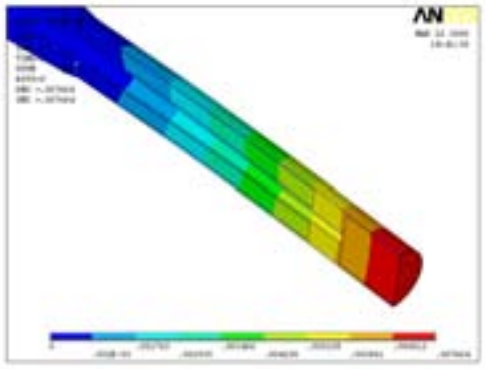

*Fig. 22. Bending in Collimator.*

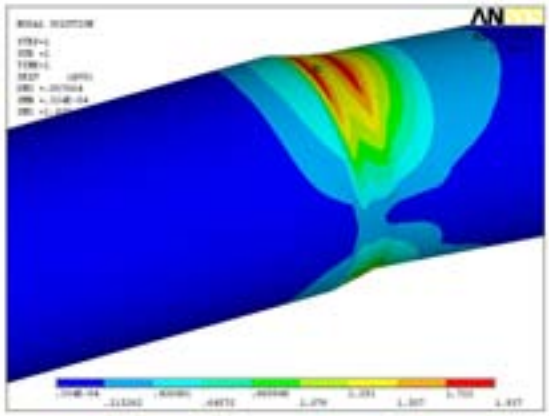

*Fig. 23. Stress analysis at various parts of collimator.*

*2.1.2 Design of shielding of experimental hutch at CIRUS reactor*

In parallel with the design of collimator, design of the shielding of the experimental hutch has been carried out. The shielding wall consists of 9 inches thick lead bricks followed by about 15 inches of borated paraffin. We have also estimated neutron and gamma flux and dose in front of the collimator as given in Table 9. These values are required for ongoing design of the shutter and beam dump for neutrons and gamma-rays.

TABLE 9. ESTIMATES OF NEUTRON AND GAMMA DOSE WITH ABOVE SHIELDING IN FRONT OF BEAMHOLE FOR SHIELDING PURPOSE.

| | Neutron dose | Gamma dose |
|---|---|---|
| 20 cm borated paraffin+ 15 cm lead | 40 mr/hr | 0.5 mr/hr |
| 40 cm borated paraffin+ 15 cm lead | 2 mr/hr | 0.5 mr/hr |

A schematic diagram of experimental hutch and its 3D view is shown below in Figs.24 and 25 respectively. The experimental hutch will have shielding as per the recommendations of safety committee.

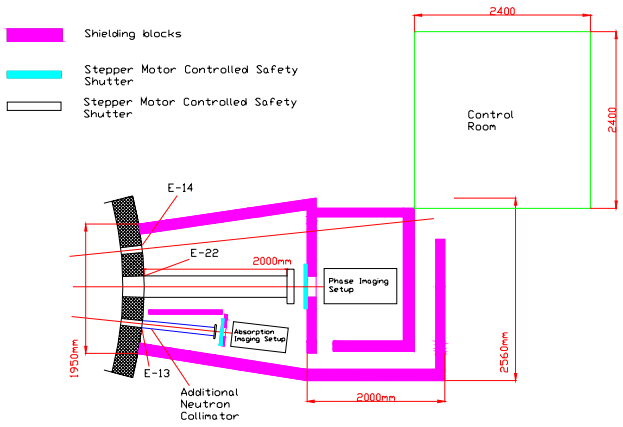


*Fig. 24. Schematic of neutron radiography beam line and experimental hutch.*

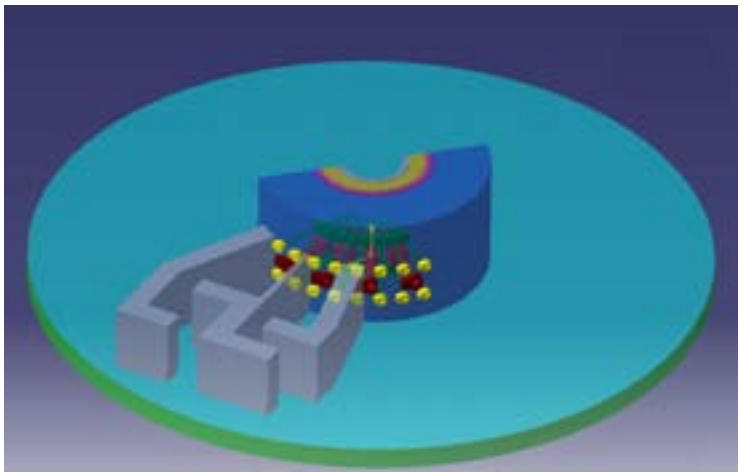

*Fig. 25. 3-D view of the beam ports and proposed experimental hutch of CIRUS reactor.*

*1.1.1.2.Monte Carlo calculation for neutron/gamma optimization*

MCNP simulation has been further carried out with various thicknesses of bismuth plug to optimize neutron to gamma flux. Calculations indicate that a bismuth crystal of 15 cm thickness will have n/γ $>10^6$ n/cm$^2$/mR with a neutron flux $> 10^6$ n/cm$^2$/s

### *1.1.2. Design of imaging systems: cooled CCD based neutron imaging setup*

We have assembled one cooled CCD based detector using $^6$LiF+ZnS scintillator and a front-coated mirror. The CCD used in our design is 1 K × 1 K back illuminated ANDOR CCD with 22-micron pixel. Figure 26 shows the CCD based neutron radiography imaging setup without its shielding assembly.

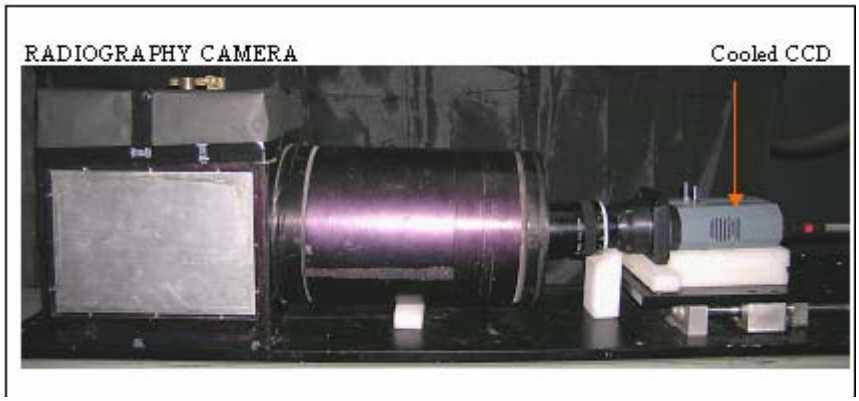


*Fig. 26. Cooled CCD based radiography camera for Neutrons.*

### 1.2. Development of Neutron Radiography and Tomography Setup with Advanced Software Tools for Visualization

The technique of radiography and tomography using electronic imaging technique has already been developed and demonstrated [1,5] by us. Figure 27 shows picture of an object (an aluminum cylinder having 19 rods of SS and copper inside), its radiography image, 2D tomography and 3D tomography carried out earlier using APSAR reactor.

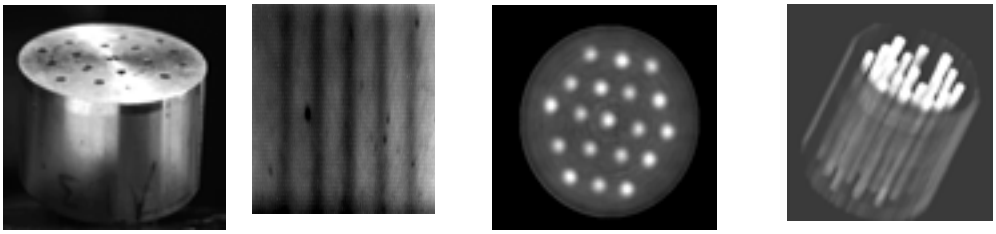

*Fig. 27. Photograph of an object (an aluminum cylinder having 19 rods of SS and copper inside), its radiography image, 2D tomography and 3D tomography.*

The present work is intended to install this technique, already demonstrated by us, at CIRUS reactor beam line using the cooled CCD based imaging system. The major work has been on the development of an in house visualization software using VTK as 3D tomography requires specialized software which can depict 3D volume data to highlight various aspects of the object. Such a software is required to use both volume and surface rendering technique to assign opacity values, do shading correction to depict three dimensional image. Though a stand alone software like VGL is available we need a software which can interface and become part of our tomography software so as to make it interactive. To do this we have developed a software in open source VTK. Figure 28 shows the front end of the software. Some parts of this software are being optimized for interactive display while some more functionalities are being added.

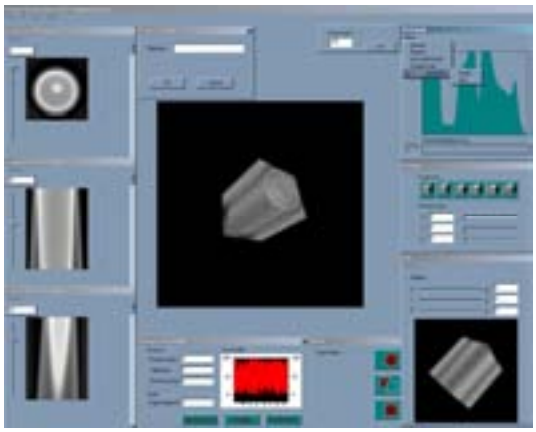

*Fig. 28. GUI of Volume visualization software based on VTK.*

### 1.3. Development of Image-Analysis Hardware and Software for Two Phase Flow Studies and Analysis of Dynamic Events

Two phase flow studies have become important in many field of applied and industrial research. The work on real time radiography and two-phase flow studies have been done [2] and it is being applied for thermal hydraulics studies for Advanced Heavy Water Reactor (AHWR). We have made an attempt to improve the software and hardware for these studies. This system was earlier based on a frame grabber card DT-2867 which works only on P-1 processor using ISA slot and the software was DOS based which has been completely replaced a by new PCI frame grabber card and improved software. We have used MATROX pulsar PCI based Card. The software has been made user friendly and works on any window based platform. The software has been rewritten in Visual C++ and it incorporates many features for online analysis of the data. It can display both the real time images as well as void fraction data simultaneously on the same window on a Window based operating system. The void fraction displayed is instantaneous as well as time averaged (both moving time average and fixed). There is a provision for the online motion correction of the pipes in which the two phase flow is occurring. There is also a provision to account for the fluctuations in neutron flux with respect to time. The software can also account for any changes in the initial conditions of flow parameter such as nonzero initial values of full water condition. The software is fully interactive and region of interest for data analysis can be interactively chosen. Figure 29 shows the front window of two phase flow analysis software.

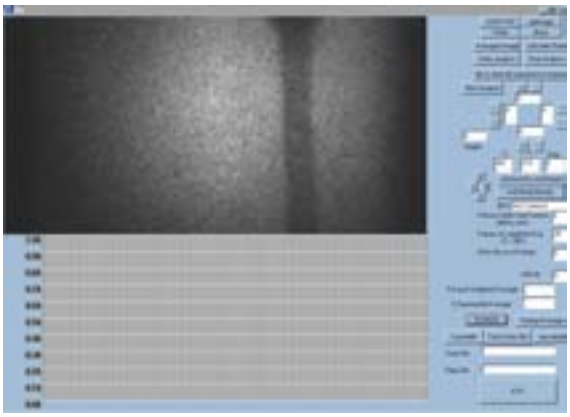

*Fig. 29. Front window of two phase flow analysis software.*

## 1.4. Development of Phase Sensitive Imaging Techniques for Neutrons

A program has been initiated to study the phase contrast neutron-radiography using theoretical simulations [6]. We have tried to use both transport of intensity equation directly as well as Kirchoff integral approach to simulate one and two dimensional phase contrast image on simple objects and these have given quite encouraging results. Figure 30 shows plot of intensity distribution on image plane for a cylindrical object of 10 micron radius for a parallel beam of thermal neutron (25 meV) and object to detector distance of 6 cm. In this case we have assumed pure phase object and absorption has been assumed to be negligible. Many other types of simulation studies for optimum object to detector, source to object have been carried out.

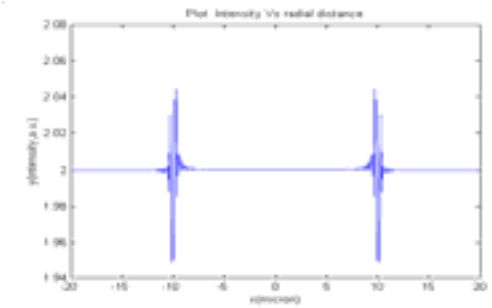

*Fig. 30. Plot of intensity distribution for a cylindrical object of 10 micron radius.*

## 1.5. Develop Tools and Techniques for Utilization of Accelerator Based Neutron Sources such as Microtron

### *1.5.1. Simulation studies with microtron based neutron sources*

We have designed a microtron based neutron source [3, 4] for Microtron Centre, at Mangalore University, India. The design has been carried out using EGS and MCNP. Figure 31 gives

schematic of neutron source interfaced to a microtron (which is basically an electron accelerator).

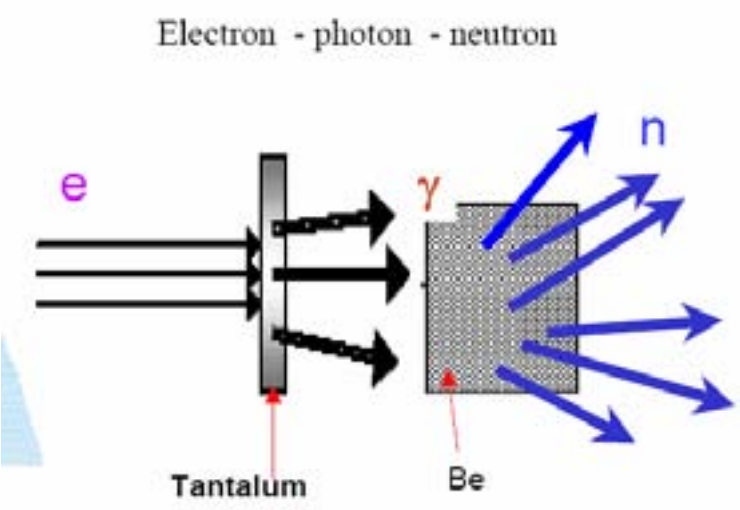


*Fig. 31. Schematic of neutron source interfaced to a microtron.*

Calculations were carried out to estimate the source strength of microtron based neutron source. The results of these calculations have been summarized in the table 10.

TABLE 10. THEORETICAL ESTIMATE OF PHOTONEUTRON YIELD (N/S) FOR VARIOUS THICKNESSES (T) OF BERYLLIUM AS A FUNCTION OF PHOTON ENERGY.

| Photon Energy (MeV) | t =2 cm | t=4.0 cm | t=6.0 cm | t=8.0 cm | t=10 cm |
|---|---|---|---|---|---|
| 8 | 3.84E 09 | 6.67 E 09 | 8.57 E 09 | 9.96 E 09 | 1.10E 10 |
| 9 | 5.23 E 09 | 8.95 E 09 | 1.16 E 10 | 1.35 E 10 | 1.50 E 10 |
| 10 | 6.57 E 09 | 1.13 E 10 | 1.46 E 10 | 1.70 E 10 | 1.89 E 10 |
| 12 | 9.17 E 09 | 1.58 E 10 | 2.05 E 10 | 2.40 E 10 | 2.66 E 10 |

We have made detailed experimental verification of these results using two separate methods.

### *1.5.2. Experimental measurement of neutron source strength using CR-39*

A comparative study between the simulated and experimentally measured neutron yield using CR-39 film has been carried out and shown in table 11. It shows that the results obtained using MCNP simulations are really in good agreement with experimental result.

TABLE 11. EXPERIMENTAL MEASUREMENT OF NEUTRON SOURCE STRENGTH FOR VARIOUS THICKNESSES OF BE.

| Beryllium Thickness (cm) | Neutron Yield (n/s) Expt. | Neutron Yield (n/s) MCNP Simulation |
|---|---|---|
| 2.0 | 0.87 E09 ± 5.2% | 0.91 E09 |
| 4.0 | 1.45 E09 ± 5.2% | 1.51 E09 |
| 6.0 | 2.00 E09 ± 5.2% | 2.04 E09 |
| 8.0 | 2.31 E09 ± 5.2% | 2.38 E09 |

### *1.5.3. Neutron detector based on silver activation technique using GM-tubes*

A customized neutron detector based on Silver activation method has been developed for quick estimation of neutron yield. This detector has been calibrated using the Pu-Be neutron source with source strength of $1\times10^4$ n/sec and then tested at the site.

This detector has been used for estimation of neutron source strength in addition to those measured using CR-39.The results are still under evaluation.

### *1.5.4. Microtron based radiography system simulation study*

Simulations have been carried out to make a radiography set up using the microtron based neutron source. Figure 32 shows schematic of a radiography assembly designed by us.

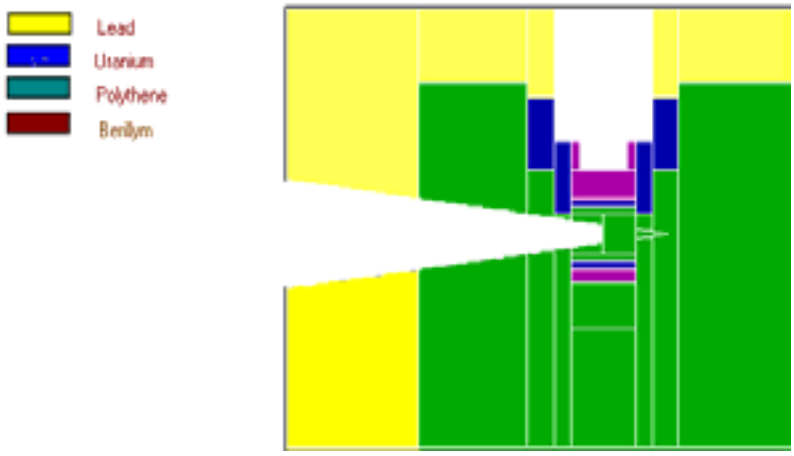


*Fig. 32. Schematic of a neutron Radiography assembly using microtron.*

MCNP calculation shows that for a L/D ratio of 18 we get thermal flux of $1.0\times10^4$ n/sec/cm$^2$ at the exit surface when the Microtron energy is 12 MeV and mean electron current impinging Be target to be about 27 micro amperes. A detailed study of spectral characteristics of this neutron source is being carried out. Meanwhile radiography assembly has been fabricated as per the design mentioned above. The detector for this radiography assembly is being procured. This work has been done in collaboration with Mangalore University.

## 1.6. Conclusions

The CRP has resulted in a very large amount of work covering all the aspects of CRP. Most of the objectives have been fulfilled. The design has been submitted for safety clearance and fabrication and installation at CIRUS reactor will be carried out after detailed review of the design.

## REFERENCES


[1] SINHA, A., SARKAR, P.S., KASHYAP, Y., Applications of digital neutron imaging at BARC (India) using reactor and non reactor sources, IEEE trans., **52**, no 1, (2005) 305.

[2] SARKAR, P.S., et al, Applications of real time neutron radiography for convection driven flow pattern transition studies, IEEE-trans., **52**, no.1 (2005) 290.

[3] ESHWARAPPA, K.M., et al, Estimation of photoneutron yield from beryllium target irradiated by variable energy microtron based bremsstrahlung radiation, Nucl. Instr. Meth. **A540** (2005) 412.

[4] SINHA, A.,.et al, Design of a microtron based photo-neutron source and its applications for radiography and elemental characterization of bulk samples , Poceedings of theInternational scientific and technical conference on Portable Neutron Generators and technolgies on their basis Oct 18–22, 2004 All Russia Research Institute of Automatics, Moscow, Russia (ed. T.G. Novikova).

[5] SARKAR**,** P.S.**,** et al, Development and Characterization of a 3D Cone Beam Tomography System, Nucl. Instr. Meth. **A 524** (2004) 377.

[6] YADAV, P.S.,et al, Study of phase contrast imaging for carbon fiber, polystyrene and lung tissue using monochromatic and polychromatic X ray sources., Nuclear Inst. & Methods, **A 564** (2006) 496–505.

# Development of electronic imaging system for real time neutron radiography at TRIGA MK-II research reactor of AERE, Savar, Dhaka and utilization for research & industrial applications

Md. Nurul Islam

Institute of Nuclear Science and Technology,
Bangladesh Atomic Energy Commission, Dhaka-1000, Bangladesh.

**Abstract:** The neutron radiography facility was installed at the tangential beam port of the 3 MW TRIGA MARK-II research reactor. In the facility only direct film neutron radiography method is being used. The project involves development of electronic imaging system for real time neutron radiography in the existing facility with the aim of utilizing it for research and industrial applications. In establishing the electronic imaging system for real time neutron radiography the improvements of existing facility were almost done during this period. In parallel, the former facility was used for the research: (a) A study of wood and wood plastic composites with and without additive by using film neutron radiography and (b) A study of jute reinforced polymer composites by using film neutron radiography technique.

## 1. INTRODUCTION

The neutron radiography (NR) facility has been installed at the tangential beam port of the 3 MW TRIGA MARK-II research reactor at the Institute of Nuclear Science and Technology, Atomic Energy Research Establishment, Savar, Dhaka, Bangladesh. The facility consists of a Bi- filter, a cylindrical divergent collimator, a beam stopper, a sample and camera holder table, a beam catcher and a semi-building biological shielding house. The schematic diagram of the old NR facility is shown in Fig.33.

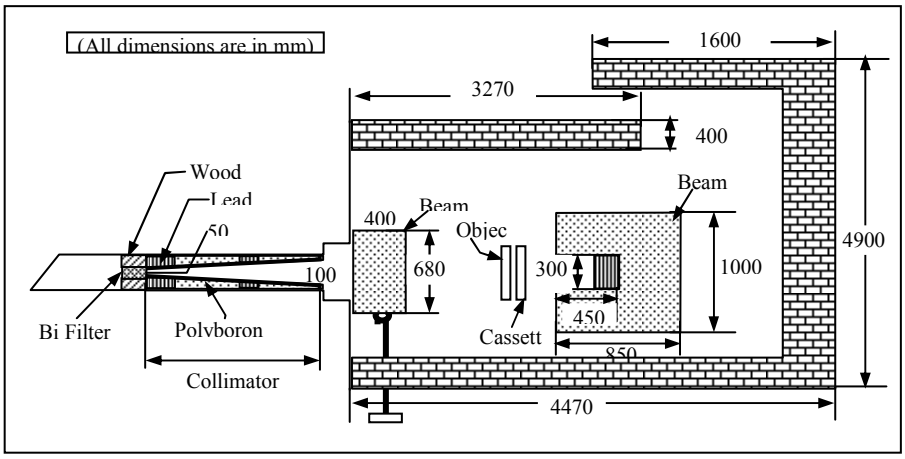


*Fig. 33. Schematic diagram of the previous NR facility.*

### 1.1. Work Done Under the CRP

The following work has been done under the project in order to develop electronic imaging system for real time neutron radiography.

— The new beam stopper has been designed. The previous beam stopper, which was containing only neutron shielding material, has been replaced by the new one by adding

lead blocks for gamma shielding. Figure 34 shows the diagram of the beam stopper with gamma and neutron shielding materials.

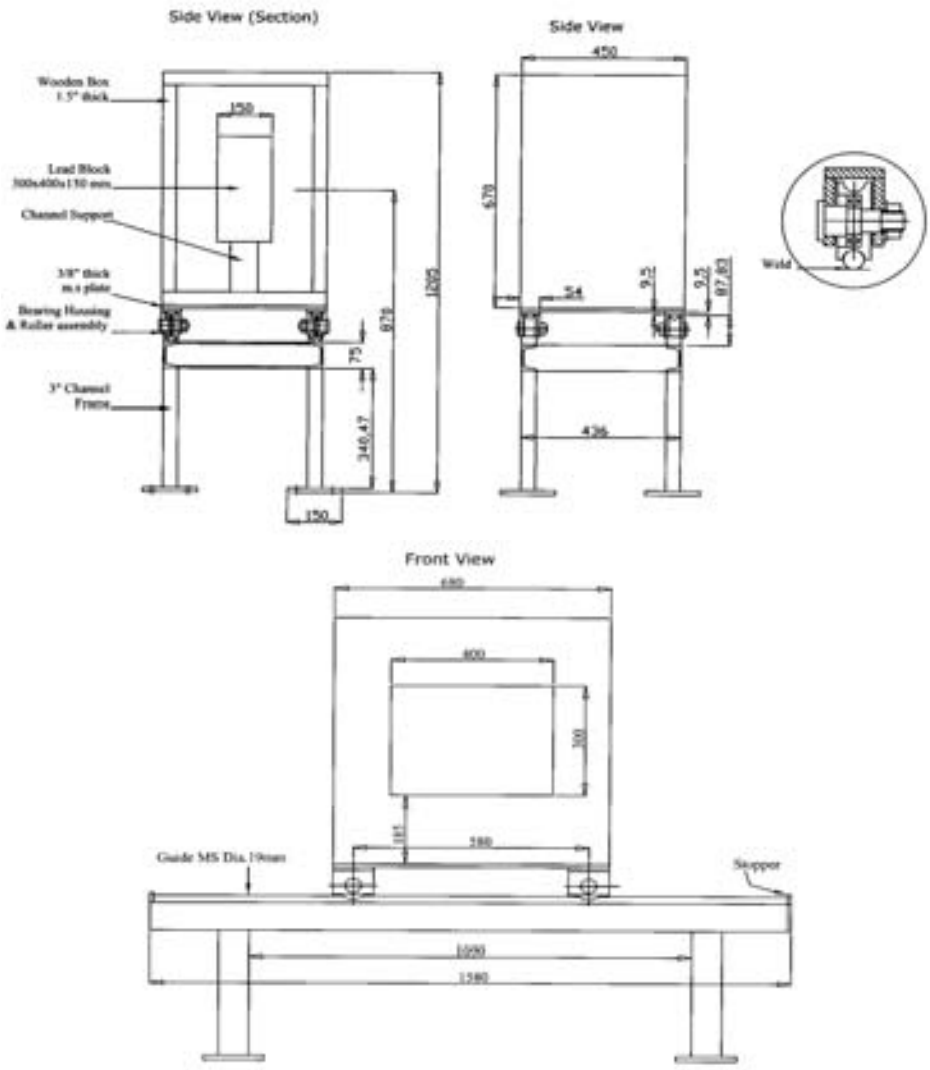


*Fig. 34. Diagram of the beam stopper with lead block.*

The schematic diagram of the facility with modified beam stopper is shown in Fig. 35.

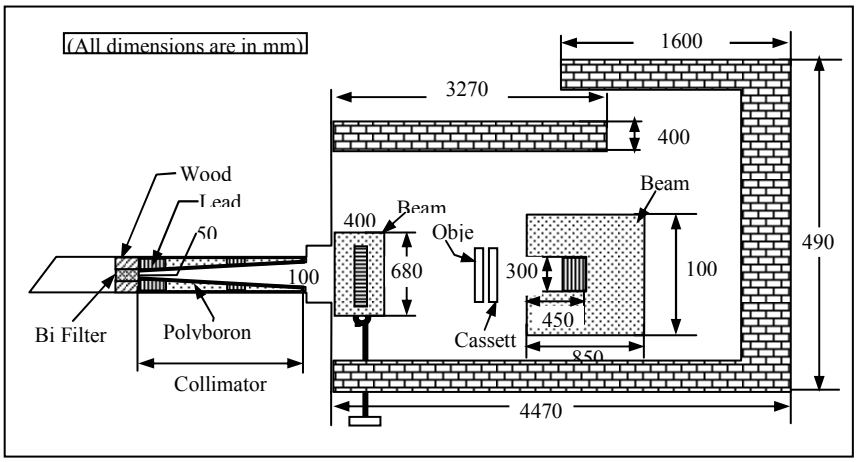


*Fig. 35. Schematic diagram of the modified NR facility.*

— For electronic imaging system it is necessary to use removal beam catcher. Our fixed beam catcher has been changed to moving system. Fig. 36 shows the diagram of the beam catcher with moving system.

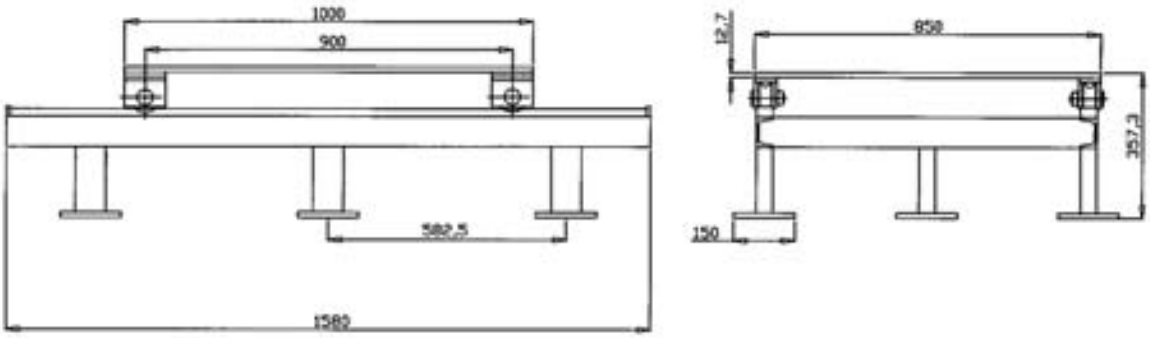


*Fig. 36. Diagram of the Beam catcher with moving system.*

— A rotational sample holder table has been designed and fabricated. Fig. 37 shows the diagram of the rotational sample holder table.
— A light tight box for the CCD camera has been designed and fabricated.
— Gamma and neutron doses have been measured at the sample position of the facility.
— The MCNP code has been trying to implement for simulating the collimator but not yet been succeeded. We have to solve this problem soon.
— In the mean time, the information of equipment for electronic imaging system for real time neutron radiography experiments was gathered in collaboration with other CRP participants. Recently, our Ministry of Science has approved a project for further strengthening the radiography facility. The procurement of equipment is under processing under this project.
— In addition to the development of a real time neutron radiography facility, the existing facility was used for performing the research works:

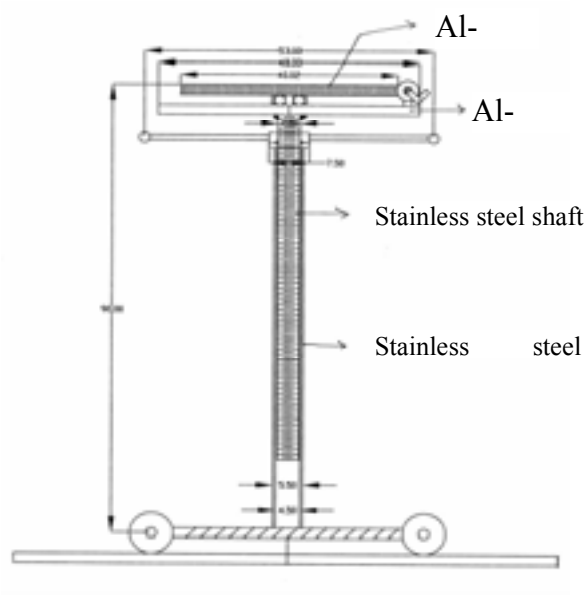


*Fig. 37. Diagram of the rotational sample holder table*

### 1.2. Study of Wood and Wood Plastic Composites of Simul Using Film Neutron Radiography

Film neutron radiography method has been adopted for comparative study of water absorption behavior in wood and wood plastic composites (WPC) of Simul using the thermal neutron radiography facility. Variations of optical density values due to water absorption of these samples are measured from neutron radiographic images. WPC samples were prepared with impregnating monomer methylmethacrylate (MMA) under gamma radiation in order to study their water absorption behavior. The water absorption nature of Simul wood (*Salmalia mamabrarica)* and its composites with and without urea as additive was monitored by optical density measurements. The neutron radiographic image of wood and wood plastic composites with and without additive is shown in Fig. 38.

S2 S1 S3

*Fig. 38. Neutron radiographic images of the samples at dry condition.*

The optical density of the neutron radiographic images of the samples is changed with the increase of water absorption in the samples. So, optical density is related with the thickness of the absorbed water by the samples. The wood (S1) and WPC samples (S2 and S3) of Simul were radiographed at dry condition and after immersion in water for 5 min, 15 min, 35 min and 65 min. A plot of optical density versus water absorption time is shown in Fig. 39.

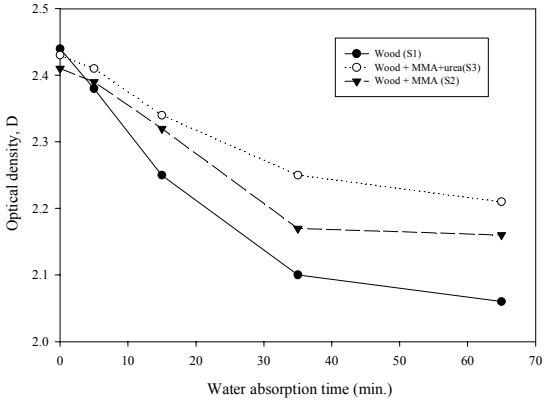


*Fig. 39. Densitometric measurement of wood and wood plastic composites.*

From the measurements we observed that the water absorption with time in wood increases continuously; where as, water absorption with time in WPC is less compared to that in the wood sample. The reason for such reduced water absorption is due to the fact that the polymer fills the void space of wood sample. MMA reacts with OH groups of cellulose backbone of wood through graft co-polymerization and reduce the hydrophilic nature of wood resulting in decrease of the water absorption.

Water absorption in WPC with additive (S3) is also less compared to that in WPC without additive (S2). WPC samples that did not contain urea showed higher water absorption than the samples that contained urea, indicating that urea plays an important role to repel water molecules. The composites with urea as additive also showed the best performance [1, 2]. The carboamide groups of the additive urea gets chemically linked with segment of the MMA monomer and cellulosic chain of wood thereby forming a denser integrated network structure and hence restricting the penetration of water molecules more effectively [3].

### 1.3. Study of Jute Reinforced Polymer Composite

Neutron radiography method has been adopted to study the water absorption behavior in jute reinforced polymer composite using the thermal neutron radiography facility. The composite was prepared with jute fabrics and formulated solution composed of urethane triacrylate oligomer, reactive monomer diluents and an additive urea under Co-60 gamma radiation. Optical density of the neutron radiographs was used for measurements. The neutron radiographic images of jute reinforced polymer composites for dry and different water absorption conditions are shown in Fig.40.

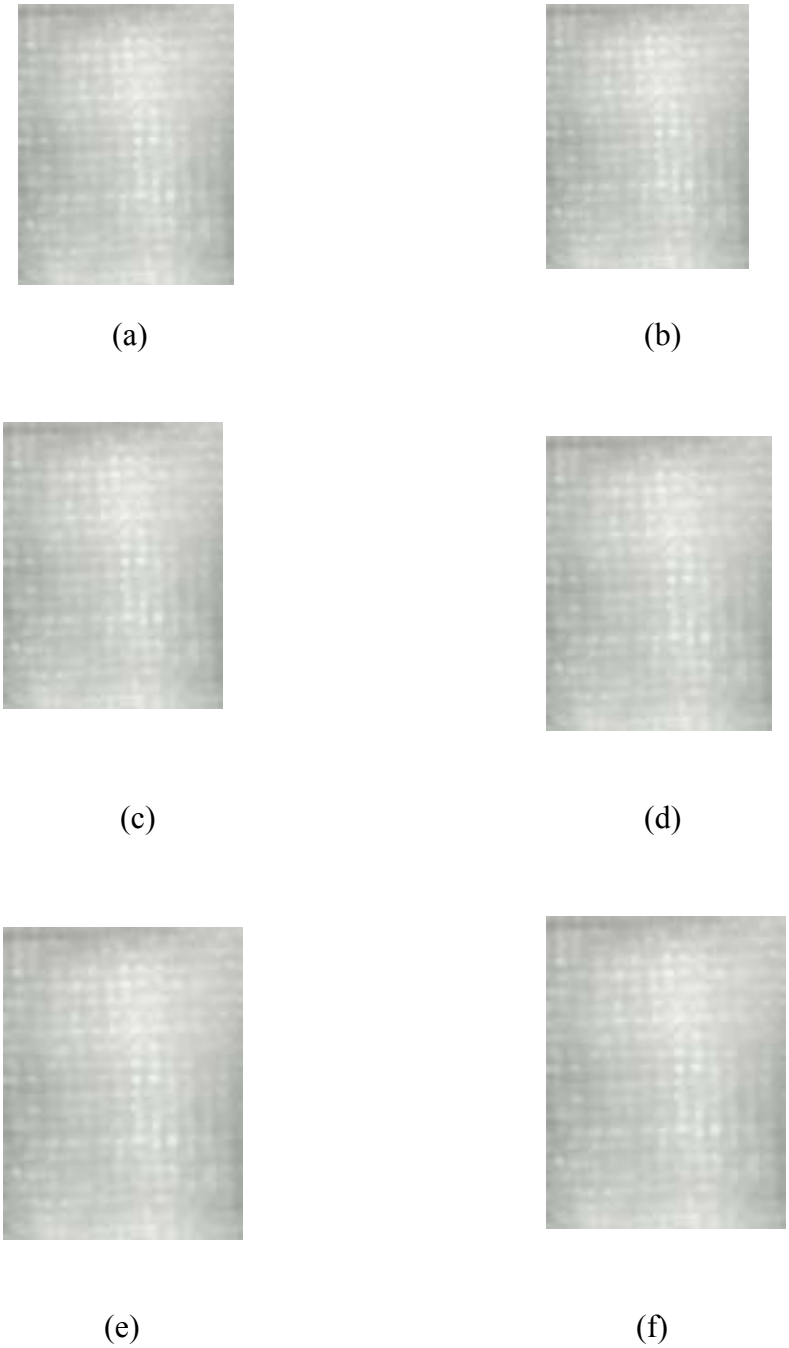


*Fig. 40. Neutron radiographic images of the sample at (a) dry condition, (b) 1 hour immersion time, (c) 2 hours immersion time, (d) 5 hours immersion time, (e) 10 hours immersion time and (f) 15 hours immersion time.*

The neutron radiographic image represents the attenuating behaviour of thermal neutron beam due to constituents within the jute reinforced polymer composites. The attenuation of thermal neutron beam is mainly due to scattering and absorption of neutrons.

The optical density of the neutron radiographic images of the samples changed with the increase of water absorbed by the samples. Optical density is related with the transmitted neutron through the samples. So, density is also related with the thickness of the absorbed water by the samples. A plot of optical density versus immersion time is shown in Fig. 41.

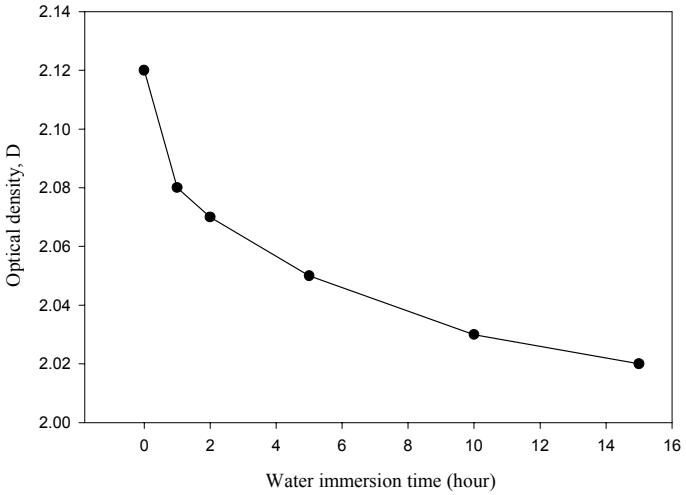


*Fig. 41. Densitometric measurement of jute reinforced polymer composite.*

From the measurements we observed that the water absorption of the composite is very negligible. The water penetration and diffusion are mainly through the fiber matrix interfacial region and cross-sectional portions of the fiber by capillary mechanism. The mechanism involves flow of water molecules along the fiber-matrix interface, followed by diffusion from the interface into the fiber and matrix [4]. Extent of fiber matrix adhesion is a significant factor in determining the absorption behavior of the composite. The reason for such negligible water absorption is due to the fact that the urea plays some important role to repel water molecules. The carboamide groups of the additive urea become chemically linked with segment of the matrix resin and cellulosic chains of jute, thereby forming a denser integrated network structure and, hence, more effectively restricting the penetration of water molecules [5].

### 1.4. Output of the Project

The output of the project may be assessed from the benefits from the completion of research and service works mentioned in the main objectives of the project. Other outputs could be included the extensive use of the facility by researches all over the country (Universities, Government and Non-Governmental research organizations etc.), the earning of revenues, the number of academic degrees achieved, the publications of new data and of noble results in both national and international scientific journals and above all the contributions towards the promotion of science and technology in the country.

### 1.5. Conclusions

When the electronic imaging system for real time neutron radiography will be established, the following research and development works have been taken up:

- Study of water intake in soil of certain areas of the country for root growth in plants (plant research).
- Investigations of defects, voids, cracks, internal continuity, etc. in some metallurgical samples.
- Control the quality of the local industrial products.

— To extend the electronic imaging system for real time neutron radiography using mobile neutron source for online detection of forensic materials such as, explosives, drugs etc. in accompanied and unaccompanied luggages in the airport to check crimes involving drug addiction problems which are posing great threat to the nation.
— Educational training.

## REFERENCES


[1] HUSAIN, M. M.; KHAN, M. A.; ALI, K. M. I.; HASAN, A. J. M., Wood Plastic Composite at Different Urea Concentrations, Radiation Physics and. Chemistry, **45(4)** (1995) 623.

[2] ALI, K. M. I.; KHAN, M. A.; HUSAIN, M. M., Study of Wood Plastic Composite in the Presence of Nitrogen Containing Additives, Radiation Physics and. Chemistry, **44(4)** (1994) 427.

[3] Ali, K. M. I.; Khan, M. A.; Balo, S. K.; Ahad, M. U. J. Applied Polymer Science), **67** (1998) 79.

[4] KARMAKER, A. C., HOFFMAN, A., Hinrichsen, G., Influence of water uptake on the mechanical properties of jute fiber-reinforced polypropylene, Journal of Applied Polymer. Science., **54** (1994) 1803.

[5] KHAN, M. A., BALO S. K., ALI, K. M. I., Polymer-Plastics Technology and Engineering, **34(4**) (1999) 767.

# The implementation of a charge coupled device (CCD) camera in a neutron imaging system for real time and tomography investigations

M. Dinca

Institute for Nuclear Research (INR), Str. Campului Nr.1, 115400 Mioveni, Romania

**Abstract:** The report describes the research contract proposal concerning the development of a neutron imaging system for real time and tomography investigations that is based on LiF-ZnS scintillator and Charge Coupled Devices (CCD) camera like light-electrical signal converter. The necessary components of such a type of detector: scintillating screen, aluminized mirror and CCD camera with proper lenses are presented. It is intended to use the imaging system with large scale objects under static and dynamic investigations under various neutron fluencies obtained from Annular Core Pulsing Reactor (ACPR) in steady state and pulsing mode.

## 1. INTRODUCTION

The new dry neutron radiography facility from Institute for Nuclear Research is placed at the tangential channel of the ACPR and will enlarge the applications of neutron radiography, will diversify the applied methods and will make the neutron radiography easier, in comparison with older underwater facility [1].

The L/D ratio is 86 – 99 depending on the position of the object on the rotary table with 60 cm diameter. The divergent angle of the collimator is $3.3^{o}$.

The neutron beam at the sample position has a diameter from 270 mm to 290 mm depending on the position of the sample on rotary table of the holder. The sample holder is designed to support objects up to 200 kg and assure $360^{o}$ rotation (in at least 200 steps), 60 cm transversal movement and 19 cm vertical movement. All movements are remote controlled and will be observed by a surveillance system based on a remote controlled CCD camera.

A major step in the improvement of the neutron radiography activity is the implementation of the neutron imaging system for tomography and real-time investigations. The utilization of an imaging system based on a scintillator, a front coated mirror, lenses and CCD camera is a guarantee of more reliable and accessible images and a progress for neutron radiography imaging [2,3].

The work in the field of neutron radiography at INR Pitesti has the goal to spread the neutron radiography nondestructive control technique for various scientific studies and industrial applications. This technique is helpful for improvement of the quality assurance in the top level activities of research and development in the nuclear field and industry.

### 1.1. Imaging System Based on CCD Camera

The components of the imaging system are placed in an aluminum light tight box (1274 mm×634 mm×564 mm) sustained vertically by a holder fixed on the metallic frame of the neutron radiography facility.The box has the possibility to be rotated, moved forward-back (300 mm) and rotated horizontally for storage. The schematic design of the neutron imaging detector is shown in Fig. 42. In Fig. 43 there is an outer view of the detector.

For this project, in fact, two scintillators are used (Fig. 44), one $^{6}$LiF-ZnS scintillator for neutrons, one of the preliminary series from PSI, Switzerland with 0.3 mm thickness of

converter-fluorescent layer and one Kodak Lanex regular ($Gd_2O_2S$) for gammas, each with 300 mm×300 mm dimensions and green light emitters. The position of the scintillators in the main window of the detector is changed by a remote controlled step by step motor. The presence of the gamma radiation in the neutron beam offers the opportunity to perform, complementary, nondestructive investigations with gamma radiations.

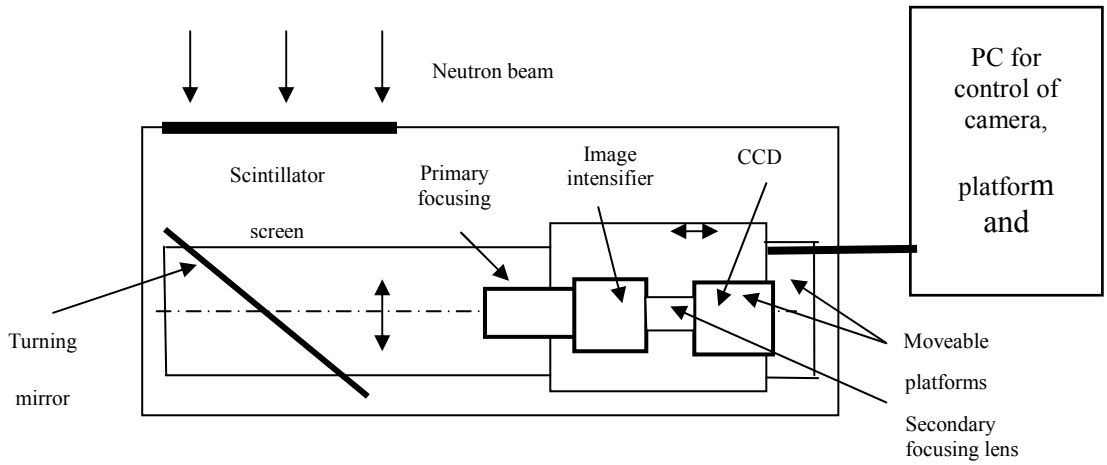


*Fig. 42. Schematic diagram of neutron imaging components.*

*Fig. 43. A view of the detector with scintillators and CCD camera.*

*Fig. 44. The scintillator for neutrons (left) and the scintillator for gammas (right).*

A front aluminum coated mirror on a float glass substrate of 2.3 mm and a surface of 400 mm×300 mm is used. The thickness of the aluminum coating is about 100 nm covered with a thin coating of SiO with the thickness of about 3 nm. The optical efficiency of the mirror (reflection) is about 0.915.

A dual primary lenses, image intensifier, secondary lens and the CCD camera coupled to a PC complete the chain for image acquisition. The optical system was made in collaboration with PROOPTICA Bucharest, a Romanian Research Institute in Optics.

The light of the scintillator screen is reflected at $45^0$ by the mirror and is focused on the photocathode of the image intensifier by the primary lenses. The image of the phosphor of the image intensifier is focused on the sensor of the CCD by the secondary lens. The primary focusing lenses assure two fixed positions to visualize the image of the screen. To protect the photocathode of the image intensifier was considered a common part of the primary lenses and two interchangeable parts to assure the two focusing distances. The change of the optical parts is made manually now but in the future will be used a stepped motor. The principal parameters of the optics are summarized in table 12.

Figures 45 and 46 show the two positions of the primary lenses, first arrangement for the 300 mm field of view and the second for the 100 mm field of view. The image intensifier is a XD-4 type, model XX2051D from DEP. Both the photocathode (Super S-25 with the sensitivity of 600 μA/lm) and the phosphor (P20-AF) have a diameter of 18 mm. The image intensifier has a microchannel electron multiplier plate. The image intensifier assembly includes the high voltage multiplier and oscillator. Two batteries each of 1.5 V or a DC 3 V (minimal 2 V and maximal 3.8 V) are used for operating supply voltage. The gain of the image intensifier at $2\times10^{-5}$lx is between 8000-12000 cd/m$^2$lx.

TABLE 12. PARAMETERS OF THE OPTICAL SYSTEM.

| | Field of view (mm) | Distance scintillator-photocathode (mm) | Distance phosphor-CCD sensor (mm) | Effective focal length (mm) | Working F/# |
|---|---|---|---|---|---|
| Primary lens 1 | 300 | 860 | - | 42.85 | 1.40 |
| Primary lens 2 | 100 | 526.5 | - | 96 | 2.98 |
| Secondary lens | 18 | - | 80.64 | 15 | 6.98 |

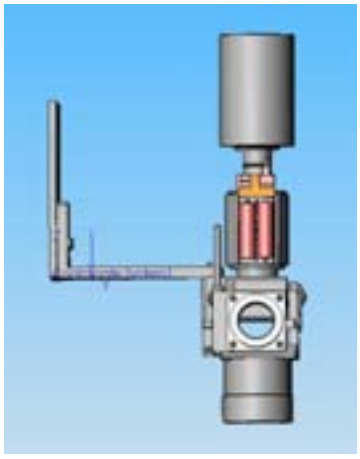

*Fig. 45. Visualization of the entire 300 mm x 300 mm scintillator.*

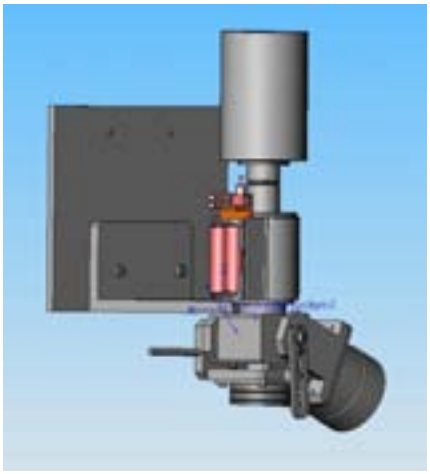

*Fig. 46. Visualization of a 100 mm x 100 mm surface of the scintillator*

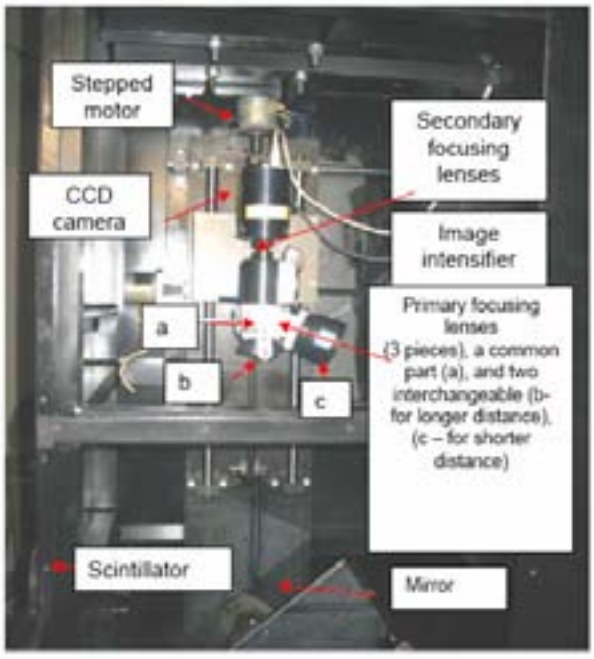


*Fig. 47. A view of the components of the detector.*

Two interchangeable CCD cameras, one cooled for static acquisition and one for real time image acquisition are intended for use. The image of the detector assembled with the cooled static acquisition camera is presented in Fig. 47.

SXV-H9 camera from STARLIGHT XPRESS, intended primarily for astronomical image acquisitions, is used for static acquisition. The characteristics of the camera are:

- Sony ICX285AL Exview HAD CCD sensor with ultra.
- low dark current.
- Pixel size: 6.45 μm × 6.45 μm with 1392×1040 pixels format.
- CCD image area: 8.98 mm (horizontal) × 6.7 mm (vertical).
- Spectral response: QE max at 540 nm (~65%).
- Readout noise: less than 12 electrons (typical 7 electrons).
- Full well capacity: greater than 27,000 electrons (unbinned).
- Dark current: less than 0.02 electrons/second
- Data format: 16 bits.
- Computer interface: built-in USB 2.0 compatible interface (also works with USB 1.1).
- Images download time: typically 3.5-4 seconds at full resolution using USB 2.0 and 7 seconds with USB 1.1.
- Cooling system: single stage thermoelectric cooler to give a CCD temperature of approximately -30C below ambient.
- The thread for lens coupling is M42×0.75 as it is used for photo cameras.

For real time acquisition it is proposed to use in the near future a Basler camera model A201b with characteristics:

- Sensor size (H×V pixels): 1008×1018.
- Pixel size: 9.0 μm × 9.0 μm.
- Maximum frame rate at full resolution: 30 frames/second.
- Monocolor camera.
- Data format: 8 bits single pixel or 10 bits dual pixels.
- Synchronization: via external trigger or free-run.
- Channel link output.

The peak wavelength of the emission spectrum of the LiF-ZnS scintillator is at ~ 520 nm and of the Lanex scintillator is at 544 nm. Figures 48–51 show the spectral characteristics of the photocathode and phosphor of the image intensifier and of the sensors of the CCD cameras.

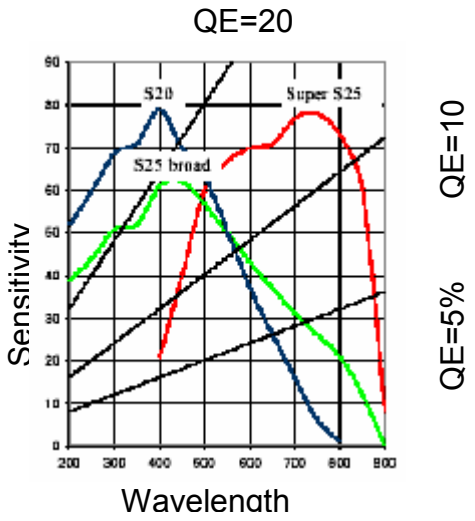


*Fig. 48. The spectral response of the photocathode (Super S25) of the image intensifier.*

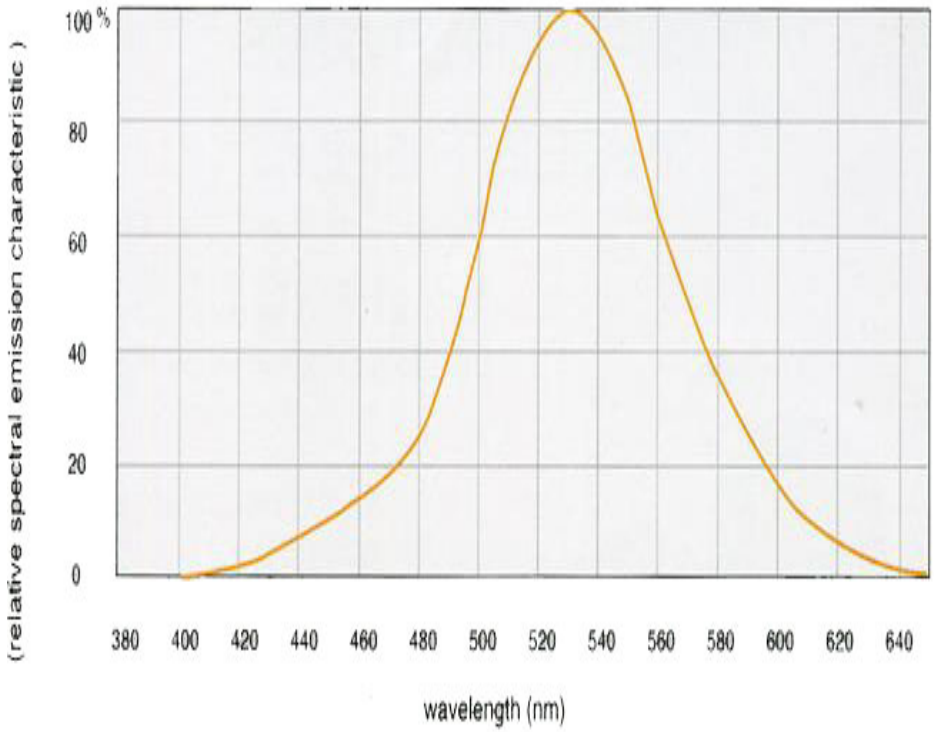


*Fig. 49. Spectral emission characteristic of the fluorescent screen type P20-AF of the phosphor of the image intensifier.*

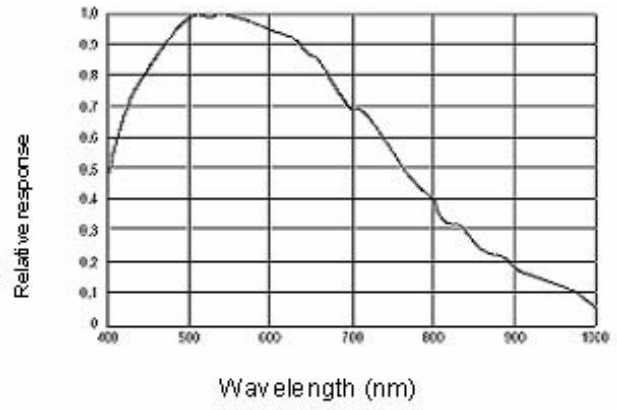


*Fig. 50. Spectral Sensitivity Characteristics for sensor ICX285AL of the Starlight Xpress CCD camera.*

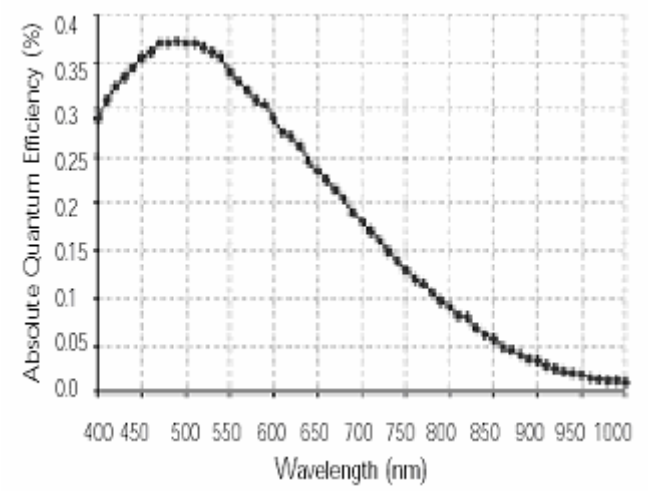


*Fig. 51. Spectral Response Sensitivity for A201b Basler Monochrome Camera.*

The lenses have the chromatic correction between 0.45 nm and 0.65 nm with the maximum at 0.53 nm. The projection of the round image (the neutron beam has a round section with about 290 mm in diameter) on the CCD sensor is like in Fig. 52. For Starlight camera the top and bottom parts of the image are missing and for Basler camera the image match the sensor.

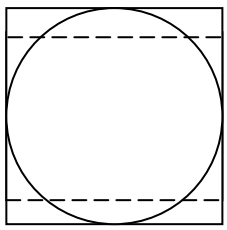

*Fig. 52. The projection of the image on the sensor of the CCD cameras (dashed line on Starlight and continuous line on Basler CCD).*

A calculation for geometrical resolution of the combination Starlight CCD camera (1392×1040 pixels) and standard lens (PENTACON, TESSAR etc.), without an image intensifier, indicated that should be ~ 0.22 mm when it is visualized the entire scintillator (300 mm) and ~ 0.07 mm when it is visualized only a surface of 100 mm × 75 mm of the scintillator [3]. The geometrical resolution is the ratio of the measure of a visualized length and the number of pixels of the CCD sensor on which that length is projected. The detector assures a geometrical resolution for a field of view of 300 mm in concurrence with the geometrical resolution offered by the collimator-object-detector arrangement for a thickness of an object of about 2 cm. Some comparisons of the theoretical geometrical resolutions and experimental geometrical resolutions obtained with the piece of equipment that contains the image intensifier and with one with a standard lens will be done here.

The previous calculation done for a Basler camera (1008×1018 pixels), intended for real time imaging, determines for a field of view of 300 mm and 100 mm the values of ~ 0.3 mm and ~0.1 mm for the geometrical resolution.

The final resolution of an image obtained with a detector with scintillator and CCD camera depends on:

- geometrical resolution of the assembly collimator-object-detector;
- the scattering of neutrons on their path in collimator, object and detection system (previous detection);
- intrinsic resolution of the scintillator;
- the piece of equipment lenses-image intensifier-CCD camera;
- other aleatory processes.


*Fig. 53. The user interface of the software for remote controlled step by step motors.*

There are three remote controlled stepper motors (GAMMA, ML 330/220K type) inside the tight light box. One motor changes the scintillators and two of them change the distance between scintillator and imaging equipment. The hardware that controls the motors is named SAM 01 and the software was programmed in Visual Basic 6.0. An output of the SAM 01 is

now shared on turn between two motors. The window which is used to command the motors is shown in Fig. 53. It is possible to command the movement with an established number of steps or step by step for very fine adjustments.

The SXV-H9 camera from STARLIGHT XPRESS came with its own software for operation, acquisition and analyses of the image, named SXV_H9_USB-HX Camera Image. The acquisition mode (time of acquisition from thousandths to minutes, binning, subframes, single or continous aquisition, auto save, etc.) is selected from the interface window and then the Take Photo button is pushed. The image is saved in diferent formats (tiff, fits, bmp, etc.). The saved images are used subsequently for some adjustments (contrast, luminosity or contour improvements) and some analyses (length measurements, histograms, etc.) and even for tomography reconstruction. An image of the main window and of the interface control is shown in Fig. 54.

Recently, the well known Octopus tomography reconstruction software developed at Gent University in Belgium for the images obtained by neutron radiography also, now in version 8.1 was bought. Octopus works with a modular approach. This means that the user can access a number of modules from the main window (Fig. 55), which are opened in separate floating windows. Next to the menus, a selection of buttons makes it possible to easily access the most common modules. These are, from left to right: *Wizard-Select data set – Crop images – Spot filter – Normalize – Sinograms-Parallel reconstruction – Fan reconstruction – Cone reconstruction-Image viewer – Delete temp files – Manual - Update*

Full dynamic range of the CCD camera will be used the for tomography reconstruction.

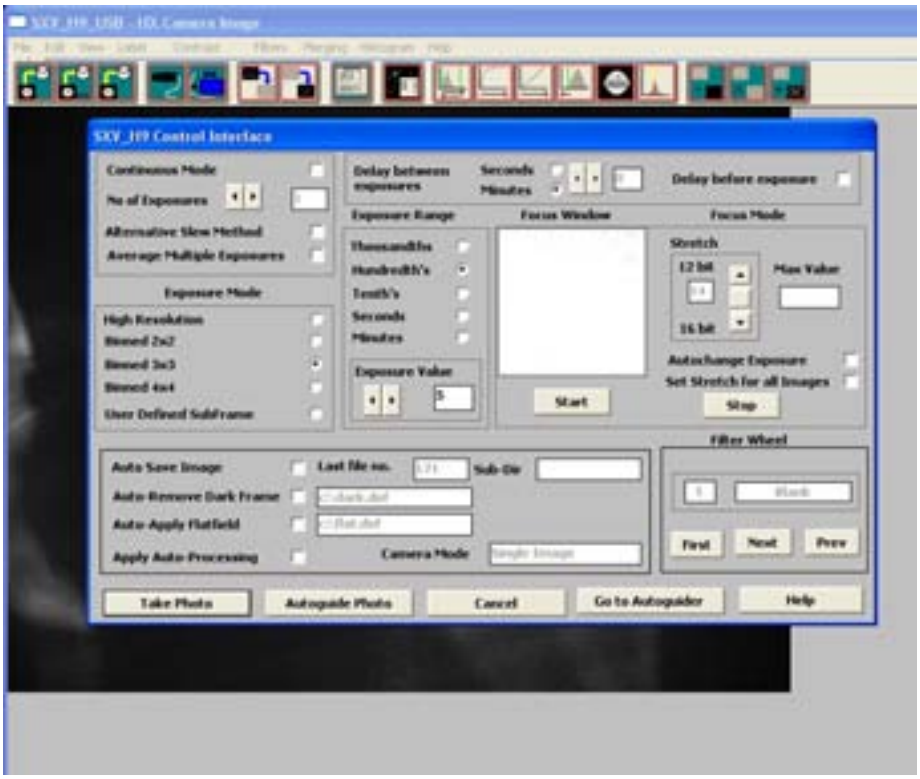


*Fig. 54. The main window and the control interface of the software for SXV-H9 camera.*

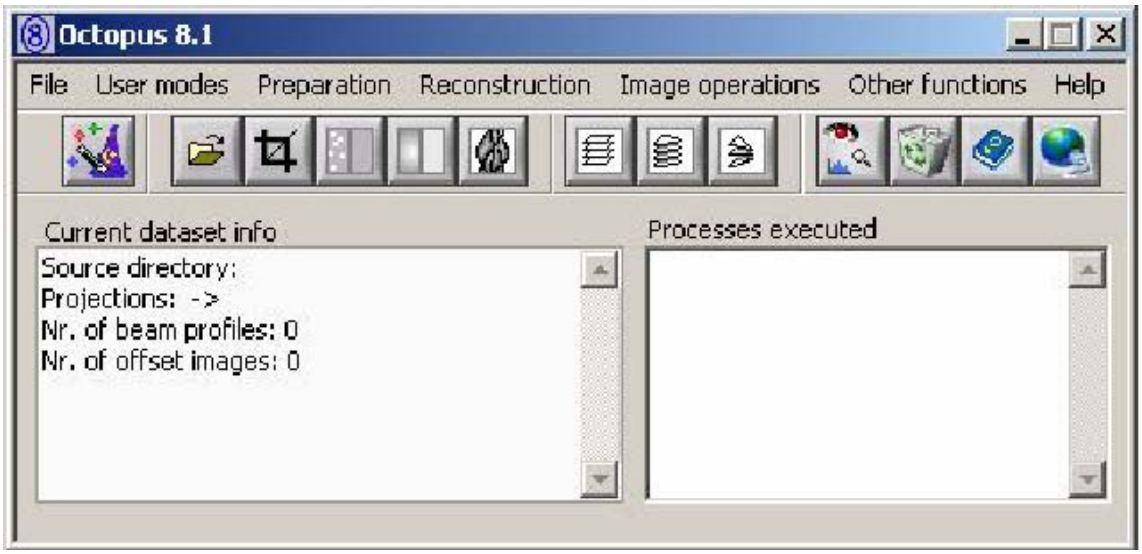


*Fig. 55. The main window of the Octopus 8.1 software for tomography reconstruction.*

### 1.2. Holder for Nuclear Fuel

For the investigation of the fresh nuclear fuel a special holder with 8 positions was built (Fig. 56). It is proper for TRIGA and CANDU nuclear fuel pins. It can be adapted for other types of nuclear fuel pins also. The fuels are rotated simultaneously using a remote controlled stepper motor. The image of the nuclear fuel can be acquired on film with dysprosium or indium (more indicated because the epithermal neutrons penetrate better nuclear fuel and indium has a higher cross section for epithermal neutrons than dysprosium) foils. With the detector based on scintillator and CCD camera a faster investigation can be done with a reasonable geometrical resolution (0.1 mm) using the 100 mm field of view offered by the system. It is intended to do tomography reconstructions for the TRIGA-LEU nuclear fuel pins that will be fabricated at INR Pitesti, for a better characterization of the gaps between pellet-clad, pellet-pellet and soldering rings.

*Fig. 56. Holder for nuclear fuel put on the sample holder.*

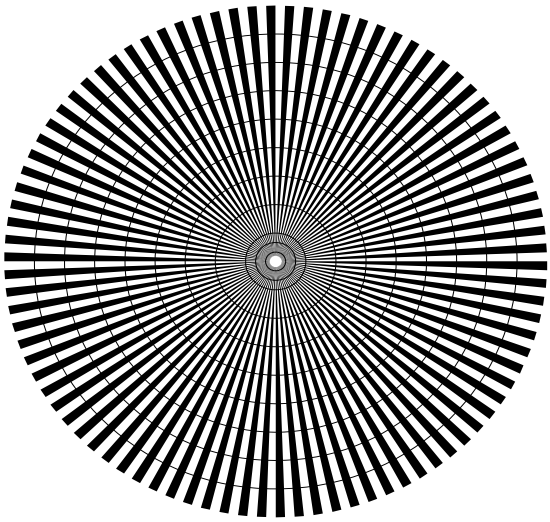

*Fig. 57. The pattern used to establish the resolution of captured images with the imaging system.*

### 1.3. Pattern for Geometrical Resolution Control

For the characterization of the geometrical resolution of the images acquired with the imaging system based on CDD camera was printed on paper a special pattern to be visualized (Fig. 57). The pattern is 270 mm in diameter and has 180 alternative equidistant triangle black-white parts. Between two black parts there is a distance of 0 mm in the centre of the pattern and 4.7 mm at the edge. Other concentric circles mark the position where image has a certain geometrical resolution (table 13) and also characterizes the aspect of the image concerning to possible distortions. The inner part of pattern inside the first circle with 6 mm in diameter was removed. Based on pattern image there are established the alignments and working distances for best images for scintillator-mirror-imaging system.

TABLE 13. LEVELS OF GEOMETRICAL RESOLUTION DICATED BY CONCENTRIC CIRCLES OF THE PATTERN.

| Radius (mm) | 3 | 5 | 10 | 15 | 30 | 45 | 60 | 75 | 90 | 105 | 120 |
|---|---|---|---|---|---|---|---|---|---|---|---|
| Resolution (mm) | 0,1 | 0,175 | 0,350 | 0,52 | 1,04 | 1,57 | 2,09 | 2,62 | 3,14 | 3,66 | 4,18 |

### 1.4. Characterization of the Geometrical Resolution

The control pattern was placed on the Lanex scintillator inside the tight light box. Were established the geometrical resolutions of the images of the pattern obtained for two fields of view, 300 mm and 100 mm as the imaging system will be used. The tests were done with the imaging system that contains the image intensifier and supplementary with the Starlight CCD camera and a TESSAR 2.8/50 CARL ZEISS JENA lens with M 42×0.75 mm thread. The aim was to establish the geometrical resolution offered by imaging system (Figs. 58 and 59) and to compare it with that obtained without image intensifier (Figs. 60). The acquisition time of the image was 1s, exception the image from Fig. 58, with 2s (better result). The light permitted to enter into box to illuminate the pattern was sure different. The theoretical assumptions regarding to geometrical resolution (chapter 2) are verified in the case of image acquisition with TESSAR lens. Using image intensifier with 18 mm diameter there is a loss of resolution, which becomes 1.65 times worse than resolution with standard lens.

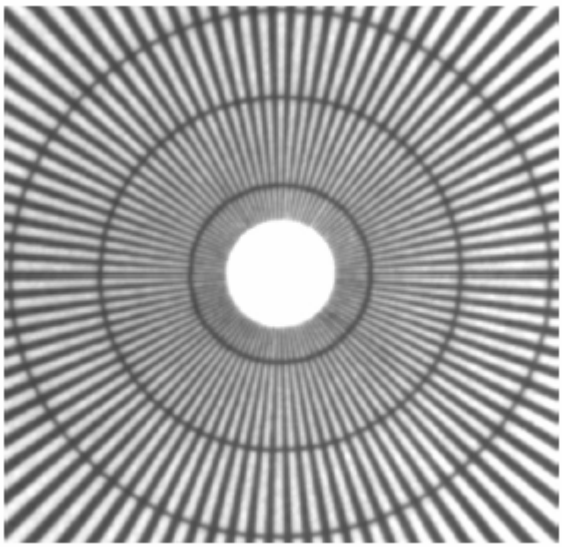

*Fig. 58. Central detail of the image of the pattern (100 mm field of view) obtained with the imaging system with geometrical resolution ~ 0.33 mm.*

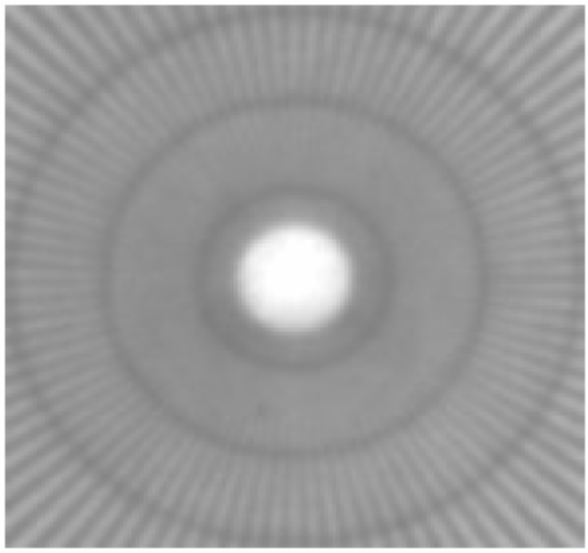

*Fig. 59. Central detail of the image of the pattern (300 mm field of view) obtained with imaging system with geometrical resolution ~ 0.1 mm.*

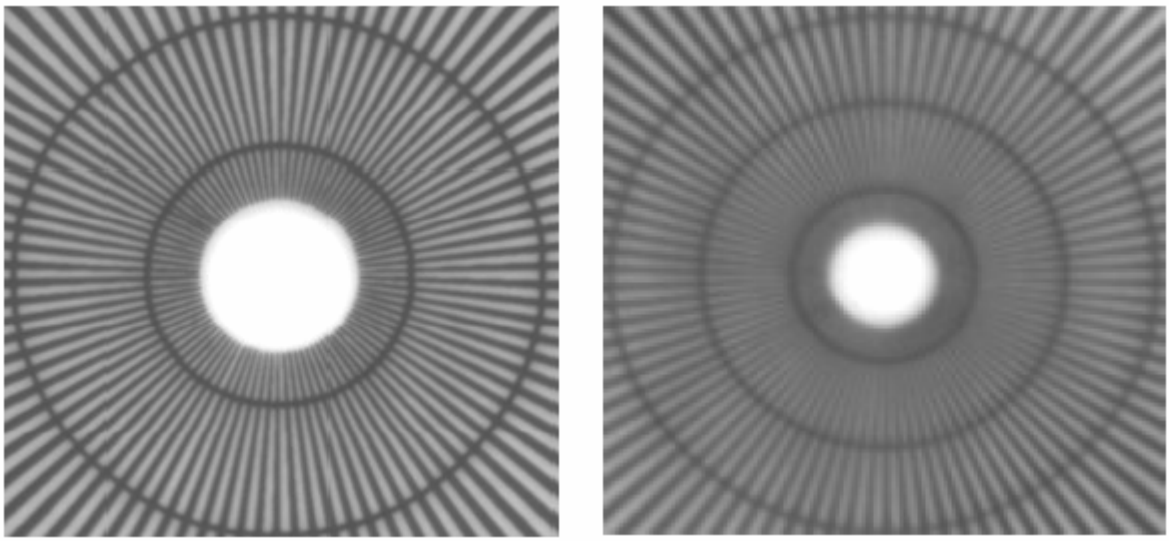

*Fig. 60. (Left) Central detail of the image of the pattern (100 mm field of view) obtained with the TESSAR lens with resolution better than 0.1 mm; (Right) Central detail of the image of the pattern (300 mm field of view) obtained with the TESSAR lens with resolution ~ 0.2 mm.*

The geometrical resolution becomes 0.1 mm using TESSAR lens, for a field of view of about 165 mm.

### 1.5. Neutron Radioscopy Tests

First images with the new detector for neutron imaging were acquired for an object composed of two taps for vacuum, arranged as in Fig. 61. The object contains metals and organic materials [4,5].

*Fig. 61. The test object placed in front of the scintillator screen of the neutron imaging system with CCD camera.*

The images were taken for entire 300 mm field of view with both types of scintillators, LiF-ZnS for neutrons and Lanex for gammas.

The image from Fig. 62 (Left) was taken with bismuth monocrystal filter (3 cm thickness) put in the mixed beam of radiations (neutrons and gammas) and that from Fig. 62 (Right) with bismuth filter raised (remote steel cable). The neutron intensity passing the box of the detector was measured in both situations (the output is a dose rate) and the ratio was 1.6 in concordance with the ratio of integration times on the sensor of the CCD to obtain good images, 60 s, respectively 40 s.

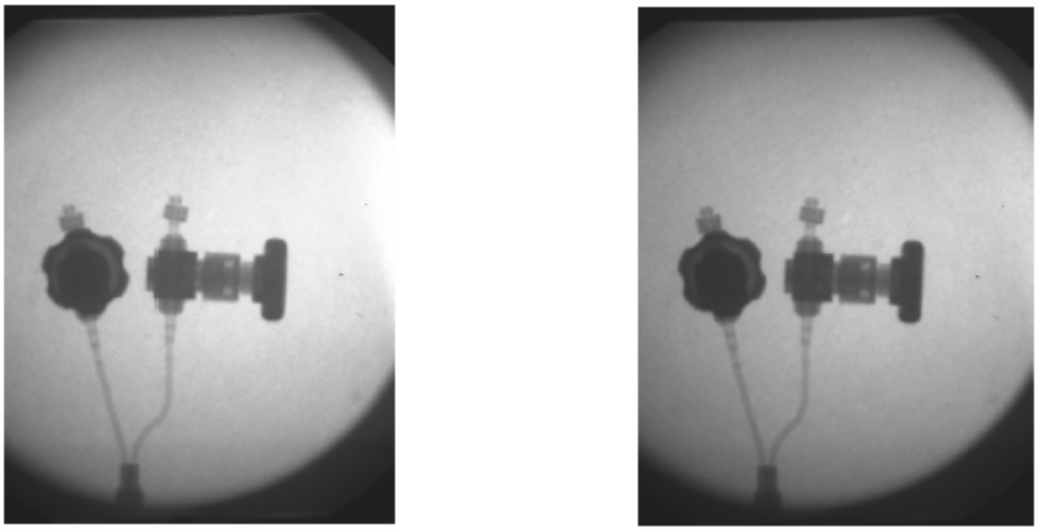

*Fig. 62. (Left) The image of the test object obtained with LiF-ZnS scintillator. Integration time: 60 s; (Right) The image of the test object obtained with LiF-ZnS scintillator. Integration time: 40 s.*

The image taken with the Lanex scintillator is shown in the Fig. 63. The bismuth filter is raised and the integration time on CCD sensor is the same like for LiF-ZnS scintillator. As Lanex scintillator contains gadolinium with the biggest neutron capture section among all elements, it is necessary to remove the neutron content with a foil of cadmium, for example, prior to hit the investigated object. In the image from figure 63 the neutrons were not removed, but can be seen differences between images obtained with the two scintillator types. In the image obtained with Lanex scintillator the gamma content of the beam passed the regions with organic material (knobs of the taps) showing clearly the central screw.

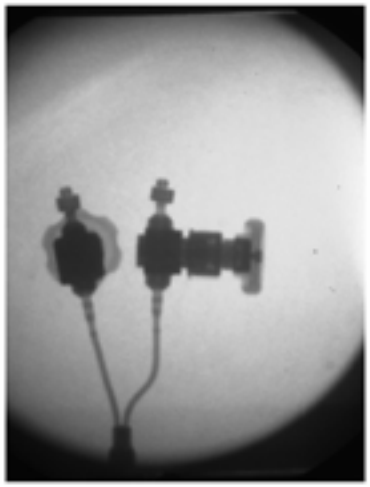

*Fig. 63. The image of the test object obtained with Lanex scintillator. Integration time: 40.*

The neutron beam intensity is estimated to be ~ $10^5$ n/cm$^2$/s. In the near future the neutron beam will be measured by neutron activation analyses with indium foils after some improvements of the neutron transfer from reactor core to tangential beam port.

### 1.6. Conclusions

The main aim of the project under contract No. 12699 is the development of a neutron imaging system based on CCD camera for static (then for tomography reconstructions) and dynamic imaging and to test the imaging system with large scale objects under static and dynamic mode under various neutron fluencies obtained from ACPR reactor (steady state and pulsing mode). The detector assures these applications through its conception. In addition, it is used for investigations with gamma radiations.

As a first step, the neutron imaging system for static image acquisition with a high resolution CCD camera, image intensifier and proper lenses was commissioned. The decision was taken to use two interchangeable cameras, one for static acquisition and one for dynamic acquisition, each of them with best parameters instead to use one very expensive that covers both situations. The images are acquired with 0.1 mm geometrical resolution for 100 mm field of view of a special pattern. To characterize the resolution of the images obtained from scintillator a special gadolinium pattern with 20 mm diameter must be bought or made so that to be present in every image. With the Octopus software for tomography reconstruction we have the possibility to perform this attractive application.

As the subsequent tests and improvement of neutron beam intensity will demonstrate that the real time imaging can be done, the second CCD camera will be put into operation to complete the desirable task to perform real time imaging. The ACPR reactor is operated when some tests are requested for different experiments and it is not possible to perform tests on a continuous scale, a big disadvantage when it is necessary to have an intensive activity.

As the TRIGA-LEU nuclear fuel will be fabricated and will be ready for testing, the imaging system will be used for neutron radioscopy investigations, as the holder for this application is made.

## ACKNOWLEDGEMENTS

The author wishes to express his appreciation of the leadership of INR, IAEA (especially to the coordinator of the CRP). In addition the specialists and colleagues present at the meetings for their support for this project.

## REFERENCES

[1] DINCA, M, Development of a new radiography facility with extended applications at the INR TRIGA reactor, Proceedings of the 7th World Conference on Neutron Radiography, September, 2002, Rome-Italy, 33-39.

[2] DINCA, M. P, AVELESCU, M, A neutron imaging system based on a CCD camera, International Workshop on Neutron imaging using Cold neutron and related topics, 13–14 October 2005, PSI, Villigen, Switzerland.

[3] DINCA, M. PAVELESCU, M, Calculation for a Neutron Imaging System Based on a CCD camera, Romanian Journal of Physics, Volume **51**, Nos. 3-4, (2006), 363.

[4] DINCA, M. PAVELESCU, M, Detector for neutron and gamma radiography based on CCD cameras, 7th World Conference on Neutron Radiography, October , 2006, Gaithersburg MD, USA.

[5] DINCA, M. PAVELESCU, M, Achievements in neutron radiography at INR Pitesti-Romania, Workshop on Imaging And Neutrons 2006 (IAN2006), October, 2006, Oak Ridge TN, USA.

# Development of an efficient imaging system for fast neutron radiography based on portable equipment

V.Mikerov, A.Koshelev, V.Samosyuk, S.Verushkin

All-Russian Research Institute of Automatics,
Sushevskaya 22,127055, Moscow, Russian Federation

**Abstract:** The report describes the work carried out on IAEA CRP project. The aim of the work was to develop a luminescent CCD-detector for fast neutron radiography and tomography with a portable neutron generator. The detector design is intended to provide simultaneously high efficiency and spatial resolution. A 6 cm thick luminescent screen made of polystyrene is used to convert fast neutrons into light. A special optics has been developed to transfer optical image from the screen to the CCD-matrix. The presented results demonstrate the detector performance.

## 1. INTRODUCTION

Fast neutron radiography and tomography techniques are potentially powerful methods for non-invasive inspection and testing due to the extremely high penetration depth of fast neutrons in comparison with other radiations in most materials of industrial interest. Prospects of application of these techniques in many fields depend however on improvements in efficient imaging systems. It is expected that the development and adoption of an innovative detector system conformed to an advanced portable neutron generator in combination with a sophisticated software could provide a rather good productivity and the achievable results in terms of the quality of non-destructive inspection.

One of the promising guidelines in this respect is the development of efficient luminescent CCD-detectors. As a rule these detectors contain projection optics to transfer radiographic image from the luminescent screen to the CCD-matrix. At certain conditions efficiency of such detectors can be increased by application of a transparent luminescent screen long enough (~ 1 cm) in the direction of the neutron beam. This approach results however in a loss of spatial resolution at the screen periphery for a conical fast neutron beam, which is specific for neutron radiography with a portable neutron generator. The screen of special external form and optics containing a diaphragm were suggested in [1] to solve this problem. This paper describes similar but technically simpler solution of the same problem.

### 1.1. Simulations

Detection Quantum Efficiency (DQE) and Spatial Resolution of CCD - detectors for fast neutrons were calculated with the aim to determine the bounds of these parameters, to find out physical reasons they are limited by and to compare operational abilities of existing CCD-detectors. The calculation procedure was based on taking into account stochastic character of processes accompanying neutrons imaging, structure of luminescent screens and optical schemes of CCD-detectors. Validity of the developed approach was checked by comparison of the calculated and available experimental data. The details of this approach were published in [2]. A set of detectors, considered in this paper CCD, included detectors with an image intensifier and without it, having different image reduction factor and two types of luminescent screens: dispersive or transparent one.

The results of DQE calculation have shown that optimal thickness of polystyrene screen for 14 MeV neutrons is about 10 cm and DQE can amount up to several percents depending on image reduction factor.

It was found that the region where the energy of recoil protons is absorbed is quite small and amounts to about 30-40 μm in diameter (FWHH) for 14 MeV neutrons. Due to that the detector resolution depends mostly on used optical scheme and source-to-detector distance.

Following conclusions were made summarizing the results of simulations:

- The efficiency of existing luminescent detectors is limited by low efficiency of scintillating screens.
- While the efficiency of a dispersive screen is limited by low energy deposition of the recoil proton in luminophore and screen opacity, efficiency of a transparent screen is limited by comparatively small amount of emitted photons.
- The prospects to enlarge the efficiency are stipulated by developing more transparent and therefore more thick screens.
- Inherent spatial resolution of a transparent screen is amazingly high, but realisation of this resolution is a problem in the case of a cone shaped beam.
- A special optical condenser can be applied to keep special resolution in this case. An optical scheme containing such a condenser and a diaphragm reduces light emitted or scattered in the screen at directions not coinciding with the primary neutron trajectory.

Besides DQE detector response to gammas was simulated to estimate gammas contribution to the detector signal.

### 1.2. Optical Scheme and Electronics

Optical scheme presented in Fig. 64 was deduced from the analyses of results of simulations [3]. In this scheme photons produced in the screen by a recoil proton are refracted at the external surface of the screen and surfaces of a special condenser in such a way that only photons going in the same direction as the primary neutron can pass through a diaphragm and finally into CCD-matrix.

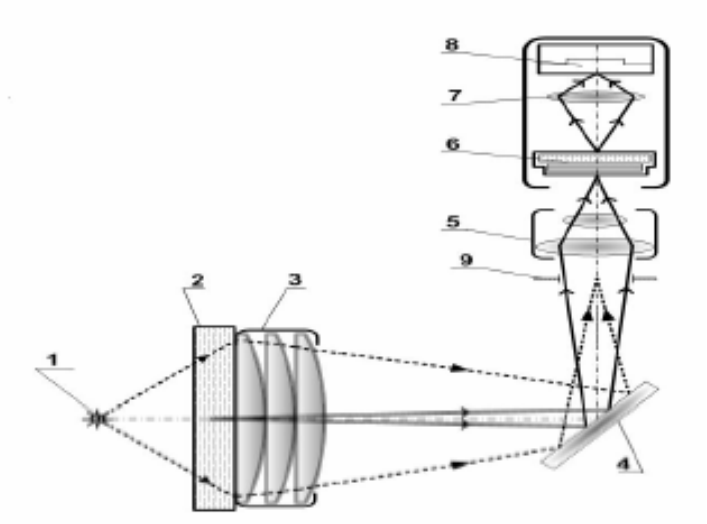


*Fig. 64. Optical scheme of the CCD-detector based on usage of a special optical condenser. 1- fast neutron source, 2 – screen-converter, 3 – condenser 4 – deflecting mirror, 5 – input projection objective, 6 – image intensifier, 7 – scaling objective, 8 – CCD-matrix, 9 – entrance aperture.*

The condenser was calculated taking into account the fact that the luminescent screen was made of polystyrene slab of 225 mm in diameter and 60 mm thick on the assumption of a 500 mm source-to-screen distance. It consists of 3 flat-convex lenses and optically contacts the screen.

A pilot imaging system was developed in accordance with the described optical scheme [4] (Fig. 65). Some of its technical parameters are presented in Table 14.

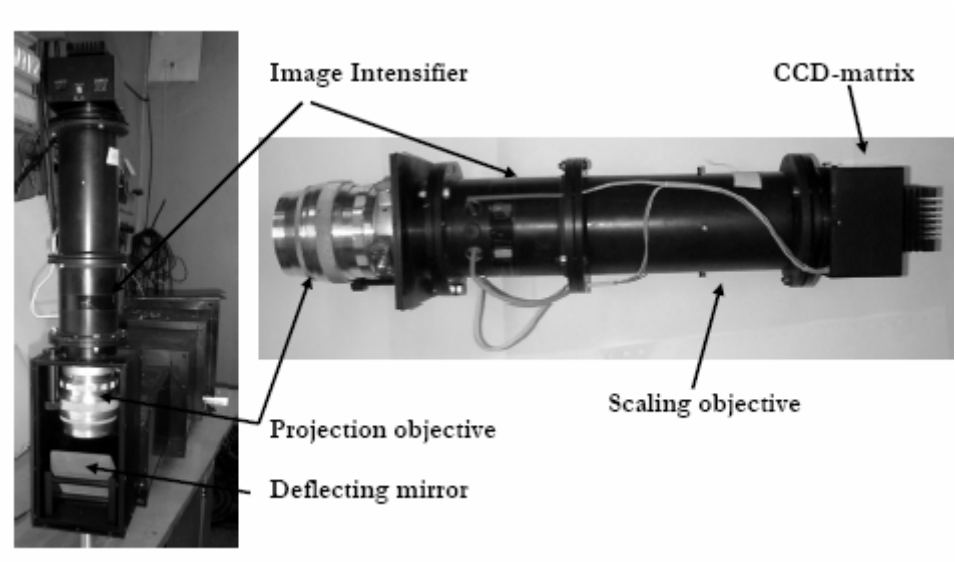


*Fig. 65. Pilot CCD detector for a cone fast neutron beam.*

TABLE 14. PERFORMANCE ATTRIBUTES OF THE PILOT IMAGING SYSTEM.

| Parameter | Value |
|---|---|
| CCD-matrix format | 768×580 |
| Pixel size, μm | 27×27 |
| Dark current, $e^-$/c | 2-5 |
| ADC, bits | 12 |
| Readout noise, $e^-$ (rms) | 20 |
| Image reduction | 12 |

The developed electronic scheme is presented in Fig. 66. It contains intellectual interface to read out data from CCD-matrix, digitize it and transfer it to a PC. Software was developed to adjust detector settings. Adjustable parameters are exposure time and gain factor for the image amplifier.

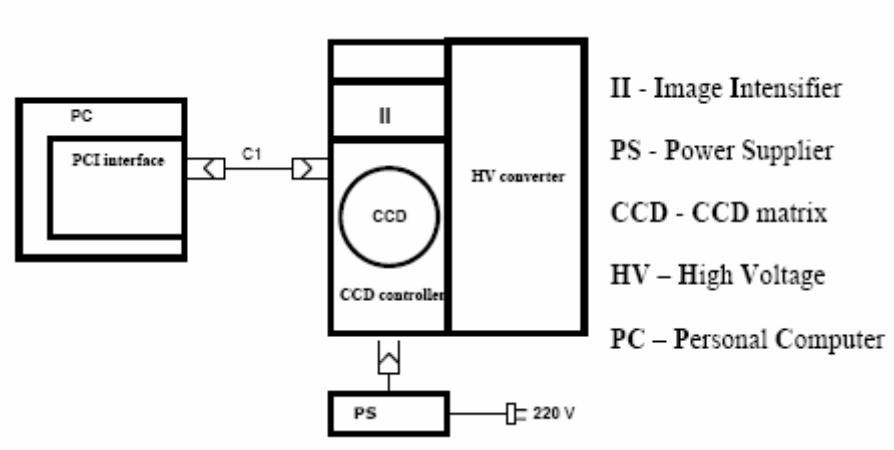


*Fig. 66. Electronic flow block.*

### 1.3. Results

The CCD-detector was tested with an ING-07 portable neutron generator produced by All-Russian Research Institute of Automatics (Moscow). The detector capacity for work has been proved. Image acquisition parameters were the following:

- Fast neutron output of the generator – $2\times10^9$ n/c,
- Source-to-detector distance – 50 cm,
- Exposure time - 5 min.

Two techniques based on the determining Line Spread Function (LSF) have been developed to measure spatial resolution of the detector. A narrow (about 100 μm) and long (about 10 mm) light source was used to simulate linear neutron source in the first technique. The second technique is based on measurement of Edge Spread Function with neutrons (Fig. 67). It was shown that both the techniques give similar results. The obtained resolution (about 2 mm) is confirmed by a radiographic image of the test objects presented in Fig. 68. Holes of

4 mm and 2 mm diameter are observable in the radiographic image of the polyethylene disk (c) despite of their off-axis position in the cone fast neutron beam.

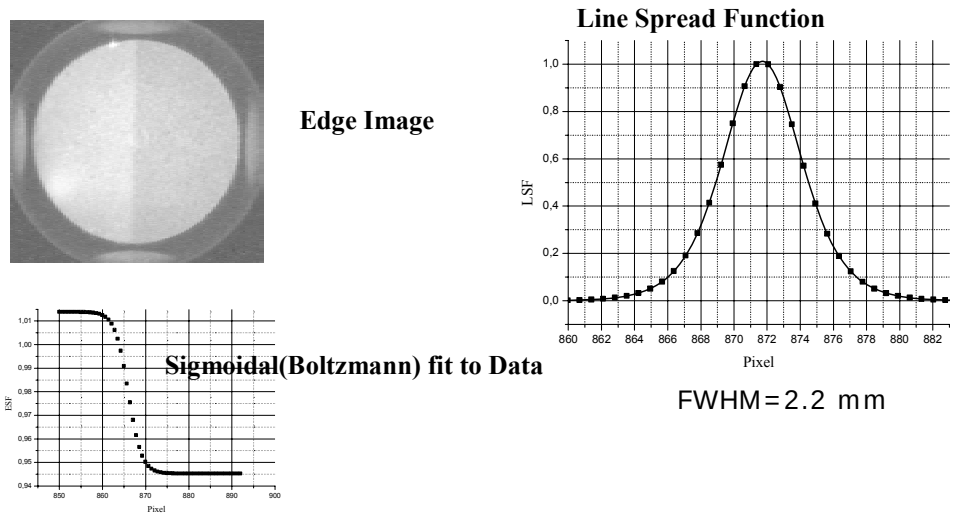


*Fig. 67. Edge and Line Spread Functions used to measure spatial resolution of the detector.*

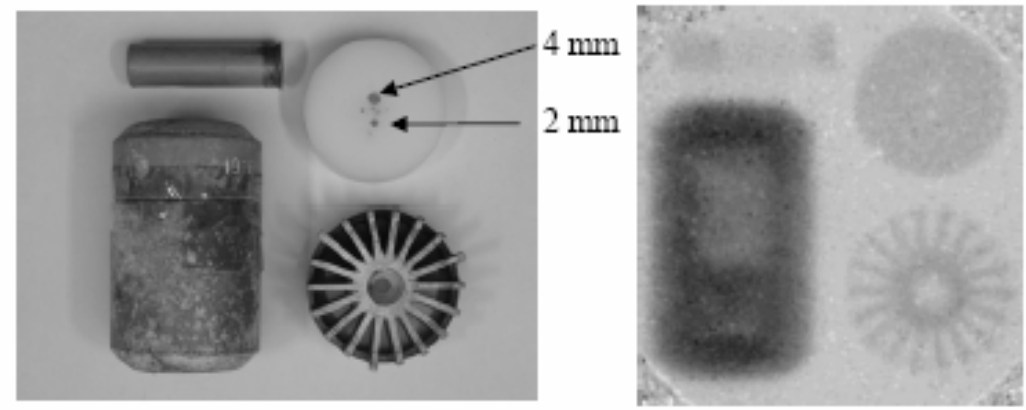


*Fig. 68. Radiographic image of test samples. Holes of 2 mm and 4 mm in diameter are clearly observable on the radiographic image of a polyethylene (PE) disk.*

It was shown that systematic deviations in image intensity over the view field interfere in the measurements of DQE. As a result the detector sensitivity determined as a relative standard deviation of the image intensity over the detector view field was used to describe the detector detective characteristics. At the moment this parameter amounts to about several percents.

A luminescent detector has been made to monitor fast neutron beam intensity. It consists of a polystyrene slab of 2 mm thick, PM and corresponding electronics. The monitor was calibrated with activation Cu detector.

Scattered neutrons and capture gamma rays are emitted from the generator components containing oil, from radiographed sample and from surroundings. Their contribution to the detector signal can vary. Major problem of the background investigation is simultaneous presence of both types of background and interdependence of their intensities.

A HPG spectrometer was used to measure gamma spectra (Fig. 69) at the detector position. At the same time fast neutron signal was measured. One can see that major components of gamma background are the following:

- Complimentary X ray radiation of the generator;
- Radiation capture gamma rays (2.23 MeV);
- Gamma rays from electron-positron annihilation (511 keV).

Figure 67 shows that X rays can be easily avoided by a 5 mm thick lead screen.

Spectrum measured with 5 mm thick lead filter was used to determine intensities of both gamma lines taking into account spectrometer efficiency.

A Cs-137 (661 keV) standard gamma source was used to estimate contribution of 511 keV gammas to the detector signal. Contribution of 2.23 MeV gammas was estimated using simulated in advance sensitivity of the detector to gammas (Fig. 70). It turned out that contribution of gammas with energy 511 keV and 2.23 MeV is about 2%.

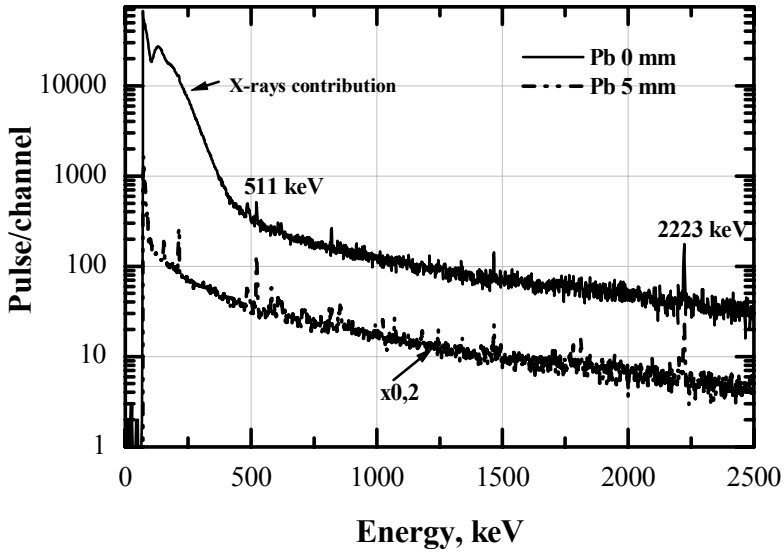


*Fig. 69. Gamma spectra measured at the detector position with ING-07 portable generator.*

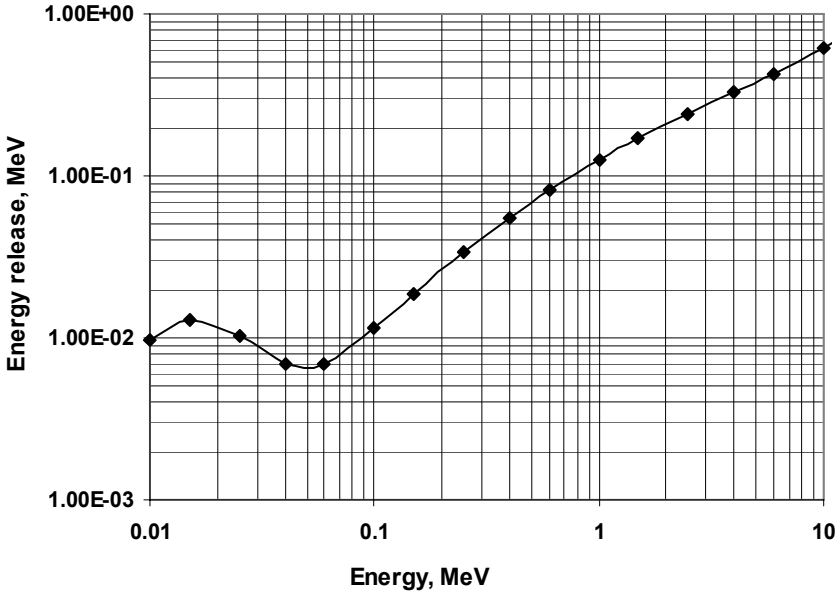


*Fig. 70. Detector sensitivity to gammas.*

## 1.4. Conclusions

The tasks of the CRP are fulfilled. The efficient imaging detector for fast neutron radiography and tomography with a cone beam has been developed. The operational ability of the designed CCD-detector has been experimentally proven.

Major characteristics of the radiographic system have been measured. A spatial resolution of the system amounts to about 2 mm and is appropriate for fast neutron radiography and tomography with a cone fast neutron beam. A relative standard deviation of the image intensity over the detector view field amounts to about 1%. This restricts dynamic range of the detector. It was shown that systematic spatial deviations in image intensity interfere also in the measurements of DQE.

The contribution of gamma background was estimated using measured gamma spectra, detector response to 661 keV gamma and fast neutrons, results of simulations as well. This contribution is acceptable and amounts to about 2%.

## REFERENCES

[1] MIKEROV, V.I.et al., Prospects for efficient detectors for fast neutron imaging, Applied Radiation and Isotopes, **61**, 4, (2004) 529.

[2] BARMAKOV, Yu., BOGOLUBOV, E., KOSHELEV, A., MIKEROV, V., RYZHKOV, V., Detection quantum efficiency and spatial resolution of neutron CCD-detectors, Nucl. Inst. Methods **B 213** (2004) 241.

[3] BOGOLUBOV, E., et al., CCD detectors for fast neutron radiography and tomography with a cone beam, Nucl. Inst. Methods **A 542** (2005) 187.

[4] BOGOLUBOV, E., MIKEROV, V., SAMOSYUK, V., VERUSHKIN, S., Fast Neutron Imaging with CCD Detectors and Image Plates, to be published in proceedings of International Workshop on Fast Neutron Detection and Applications (FNDA2006), Cape Town, South Africa, April 3–7, 2006.

# New radiographic images from old neutron converter screens

R. Pugliesi , M.L.G. Andrade, M.A.S. Pereira, F. Pugliesi, M. Olimpio de Menezes

Instituto de Pesquisas Energéticas e Nucleares IPEN - CNEN/SP
São Paulo SP - Brazil

**Abstract:** This report summarizes the activities under the IAEA Coordinated Research Project (CRP) on "Development of Improved Sources and Imaging Systems for Neutron Radiography". Firstly a brief historical regarding the development of the Neutron Radiography – NR technique in IPEN with emphasis to the ideas to obtain new images from old neutron converter screens is provided. The NR working group of IPEN began to develop these ideas in 2000 using the available infrastructure. Because of the good preliminary results a CRP has been proposed to the IAEA. During this period of development several modifications, improvements and optimizations have been carried out in the NR facility as well as in the digital system to capture and process radiography images. As consequence most of the previous radiography data were improved resulting in the implementation of a new radiography technique the "neutron induced electron and alpha radiography" having as most important feature the possibility to inspect low-thickness samples (~ μm). Other important consequences of this CRP for our working group were the improvement of the track-etch neutron radiography sensitivity, the possibility to inspect radioactive samples in an almost real-time mode and as a future plan, the development of new researches such as the neutron induced proton radiography.

## 1. INTRODUCTION

The neutron radiography (NR) activities in the Research Reactor Department of IPEN-CNEN/SP began in 1987. The first tests have been performed by using the neutron beams of two spectrometers installed at the beam-holes 03 and 10 of the IEA-R1, 2MW pool - type nuclear research reactor. In 1988 the neutron radiography working group was formed having as main objective to design and construct a neutron radiography (NR) facility. Since 1992 this facility is operational and is installed at the radial beam-hole 08 of the same reactor.

The group has developed the neutron radiography technique by employing metallic dysprosium, gadolinium and boron converter screens together with conventional X-ray films and track-etch foils. In 1998 the first real-time system, was installed in the same facility and several other screens (evaporated gadolinium and lithium fluoride) have been also used. Further improvements in the neutron beam quality, facility's shielding and the installation of a first generation real-time system, consisting of a high sensitivity digital video camera, were performed in 2001 under the IAEA project BRA1032. Nowadays the IPEN has a neutron radiography facility with a neutron flux of $10^6$ n/s.cm$^2$ at the sample irradiation position and, a basic digital system to process and film real-time images which provide some service and develop high level research.

In order to obtain "new images from old neutron converter screens" the NR working group of IPEN, began to work in three research lines in 2000, by using the already available infrastructure and equipments:

Line 1- Neutron Induced Radiation Radiography – NIRR to inspect low-thickness samples on the order of μm.

Line 2- Digital system for track etch neutron radiography to improve the radiography sensitivity to discern thickness.

Line 3- Dy - TV neutron radiography system to inspect high radioactive samples in an almost real-time mode.

## 1.1. Before the CRP

### *1.1.1. Line 1: neutron induced radiation radiography (NIRR)*

NIRR is a new non destructive testing technique in which low energy electrons or alphas generated by a natural gadolinium metal foil or by a natural boron screen, under neutron irradiation, are employed as penetrating radiation. The former technique is the "Neutron Induced Electron Radiography" – NIER and the later the "Neutron Induced Alpha Radiography" – NIAR.

The radiographs are obtained by using a film, a sample and one of the cited screens which are kept in a tight contact, inside an aluminum cassette, during irradiation, as shown in Fig.71. The neutron beam passes through the film, through the sample, and will induce (n,γ) or (n,α) reactions in the screens. The gadolinium metal foil generates 70 keV conversion electrons and the boron screen 1.47 MeV alpha particles. The generated beam impinges the sample and the transmitted intensity will be registered either in a conventional X ray emulsion film or in a track-etch foil, which are developed according to the standard procedures.

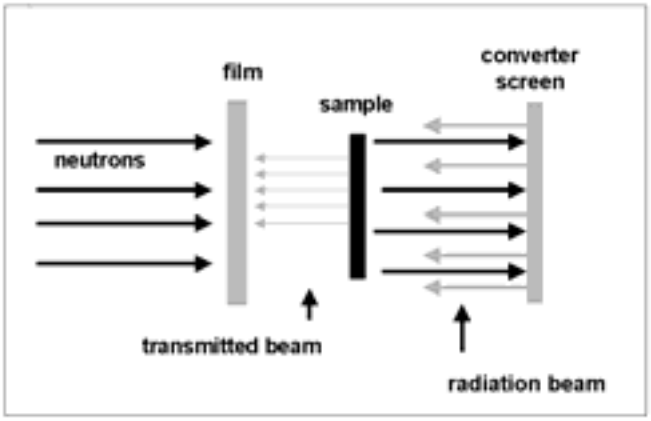


*Fig. 71. Set up for the NIRR.*

**NIER** - In order to characterize the NIER method regarding its sensitivity (capability to discern thickness) and spatial resolution, it was firstly necessary to determine the conditions for which the radiographs must be performed to obtain the best contrast in the image. For such purpose several film strips are irradiated with the gadolinium screen and after the development, the light transmission readings are evaluated as functions of the exposure. Here the transmitted light was evaluated by using an optical densitometer (in optical density units). The optical density is defined as:

$$D_{op} = \log(I/Io) \qquad (1)$$

where $I_o$ and $I$ are the intensities of the incident and transmitted light through the film respectively.

Since the electron beam is generated by a neutron beam, the *optical density vs exposure* curve has been obtained as functions of the neutron exposure-E (n/cm$^2$). The obtained curve for the film Kodak – AA (conventional for X-ray) with a gadolinium screen (25 μm thickness) is shown in the figure 72 and the highest contrast(indicated by arrows) was achieved for $3\times10^7$n/cm$^2$ < E < $1.2\times10^8$n/cm$^2$ and for 1.3 < Dop< 3.5.

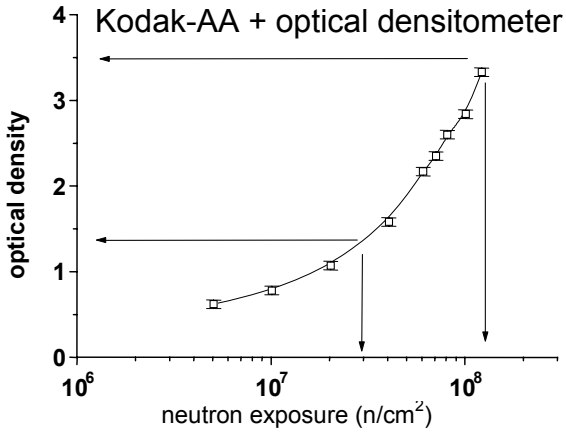


*Fig. 72. Optical density as functions of the neutron exposure for the NIER.*

The sensitivity has been determined for some materials and the samples are step wedges with thicknesses in the following range: adhesive tape – 50 to 300 μm, aluminum foil 10 to 70 μm; polymer "Makrofol-KG" 10 to 100 μm; ordinary white paper 100 to 400 μm. The samples were radiographed and the behavior of the optical density as function of the sample thickness, are shown in Fig. 73.

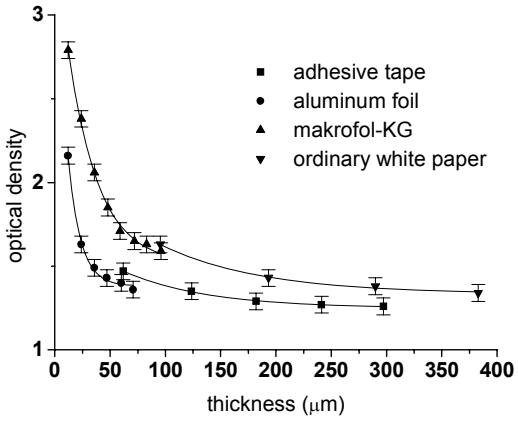


*Fig. 73. Behavior of the optical density as functions of the sample thickness.*

To these data, the best fitted function was a first order exponential given by:

$$D_{op} = A+B.\exp(-C.X) \qquad (2)$$

where *A, B,* and *C* are free parameters in the fitting and, "X" is sample thickness.

The sensitivity was calculated from its derivative as:

$$\Delta X = -\Delta Dop.\exp(C.X)/(B.C) \qquad (3)$$

with $\Delta D_{op}$ = 0.05, being the minimal discernible optical density capability of the optical densitometer.

The plots of the sensitivity as functions of the sample thicknesses are shown in figure 74

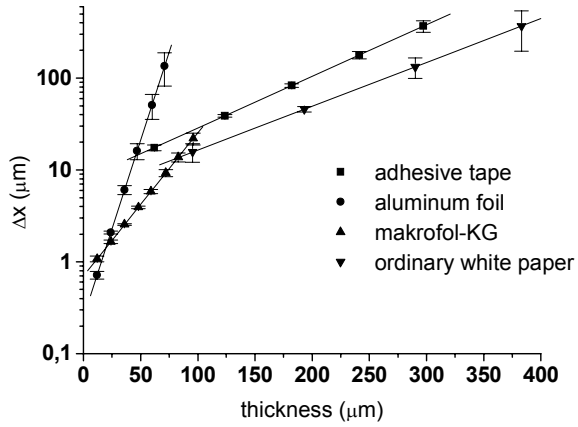


*Fig. 74. Behavior of the sensitivity as a function of the sample thickness.*

As evaluated, the method is able to discern, ~0.8 μm of aluminum in 10 μm, ~1 μm of the Makrofol KG in 10 μm. Table 15 shows the minimal discernible thickness or the minimal amount of these materials, detectable by the method.

TABLE 15. MINIMAL DISCERNIBLE THICKNESS FOR THE NIER METHOD.

| Material | Minimal disc thick.- (μm) |
|---|---|
| Adhesive tape | 8±1 |
| Aluminum foil | 0.25±0.05 |
| Makrofol - KG | 0.69±0.07 |
| White paper | 6±2 |

The resolution was quoted as the total unsharpness ($U_t$) and it was obtained by scanning the optical density distribution at the interface between the images of a knife edge opaque object (aluminum foil 100 μm) and, the one to the direct electron beam. The scanning was performed by using the microphotometer with a light beam width of 3 μm and length of 700 μm. A typical distribution is shown in Fig. 75.

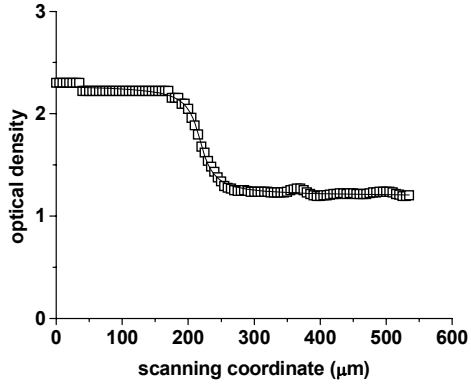


*Fig. 75. Scanning of the optical density distribution for an aluminum foil (100μm).*

The following Edge Spread Function-ESF was fitted to this distribution:

$$ESF = p1+p2.atan[p3(X-p4)] \qquad (4)$$

where "*X*" is the scanning coordinate and p1, p2, p3, and p4, are free parameters in the fitting.

The resolution is given by U = 2/p3 and the obtained result was 30±1 μm.

The Figures 76 and 77 are typical examples of NIER after some digital processing.

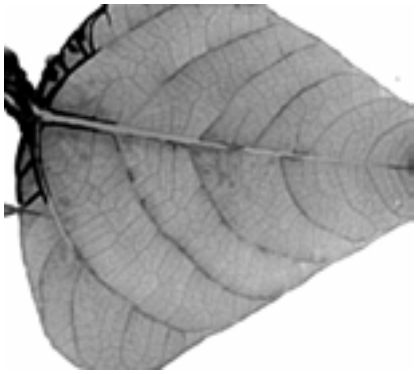

*Fig. 76. NIER of a plant showing some nutrients (dark points) inside the stems.*

*Fig. 77. NIER of a regular Brazilian bill showing one of the security marks.*

**NIAR** - In the case of NIAR, the radiographs are obtained as in the NIER but using a 60 μm thickness boron screen and the track-etch foil CR-39. Since the optical densitometer is not

useful to quantify the light transmitted through the track-etch foils, only photographs of the radiographs using an optical microscope coupled to the digital system could be obtained. Figure 78 is a typical example.

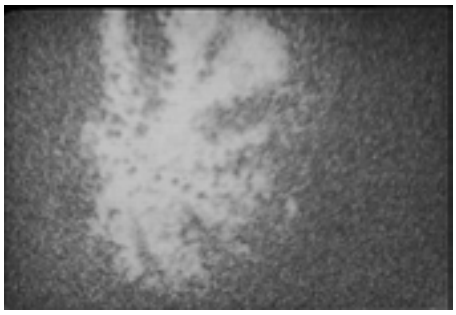

*Fig. 78. Staphilococus bacteria colony as seen by the NIAR.*

The results here presented have demonstrated that both techniques show a high potential to inspect low-thickness samples with a high resolution. In order to try to improve the results for the NIER technique a light transmission scanner to evaluate the light transmitted through the films will be used. For the NIAR technique two systems to evaluate the light transmitted through the track-etch foils will be tested. The first will be a light transmission scanner and the second a photo enlarger coupled to a digital system. In this last system the photo enlarger is coupled to a video camera and to a computer. In this system a parallel light beam impinges the films perpendicularly and the transmitted intensity is projected in a white screen forming the image. This image is captured by the video camera and a capture frame grabber, installed in a standard computer, converts it to the digital form which can be processed. In this case the transmitted intensity is evaluated in an 8 bit gray level scale ranging from 0 to 255.

### *1.1.2. Line 2: track etch neutron radiography*

The employment of track-etch foils to record neutron radiography images is a well known technique. The radiograph is obtained by irradiating a sample in a uniform neutron beam and a converter screen transforms the transmitted neutron intensity into ionizing radiation which is able to cause damages into the foil. Usually boron based converter screens are used and, in this case, alpha particles and lithium ions cause the damages. By means of a chemical etching the damages are enlarged and are called tracks and, they form two-dimensional image which is visible by naked eye. The insensitivity of the track-etch foils to visible light, beta and gamma radiations, the high resolution achieved in the image, the feasibility of stopping the etching at intermediate stages are some of their attractive characteristics for radiography purposes. One of the main disadvantages of the track-etch foils is the low-intrinsic optical contrast in the recorded image.

In order to characterize this method the same methodology applied in the research line 1 was used. However, here the light transmission readings through the images have been performed by using the optical microphotometer.

The curve for the CR-39 foil, is shown in the fig. 79 and the highest contrast (indicated by arrows) was achieved for $2\times10^{9}$n/cm$^2$ < E < $2\times10^{10}$n/cm$^2$ and for 0.2 < $D_{op}$ < 1.6.

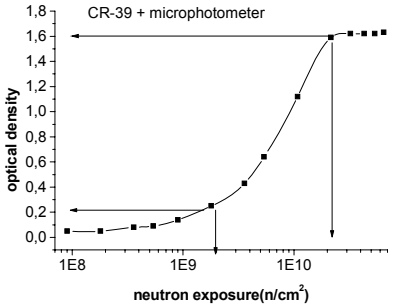


*Fig. 79. Optical density as functions of the neutron exposure for NR.*

The samples used for the sensitivity were step wedges of iron and perspex with thicknesses varying from 2 to 12 mm and 2 to 11 mm respectively. Figure 80 shows the behavior of the light transmitted as functions of step wedge thickness.

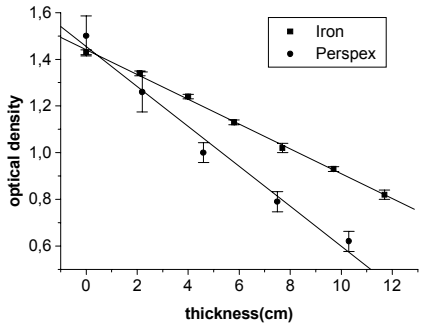


*Fig. 80. Behavior of the optical density as functions of the sample thickness.*

In this case the best fitted function is linear of the type:

$$D_{op}(x) = D_o - C.X \qquad (5)$$

where $D_o$ is the optical density for X = 0 and C is the slope of the straight line.

The sensitivity was calculated as:

$$\Delta X = \Delta Dop/C \qquad (6)$$

with $\Delta D_{op}$ = 0.02, being the minimal discernible optical density capability of the optical microphotometer.

The results thus obtained demonstrate that it is possible to discern 0.37±0.01 mm of iron and 1.0±0.1 mm of perspex.

For the resolution the opaque material was a gadolinium foil (100 μm) and a typical distribution, is shown in fig. 81. The resolution obtained was 20±3 μm.

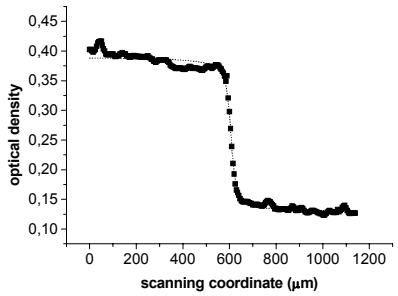


*Fig. 81. Scanning the optical density distribution for a gadolinium foil (100 μm).*

Although the images present a high resolution, the results for sensitivity show a low capability to discern thickness. This is expected because, as already mentioned, the track-etch foils exhibit a low intrinsic contrast in the registered image. In order to improve the sensitivity of this method, the new digital system, mentioned above for NIER and NIAR, consisting of the photo enlarger coupled to a video camera and a computer was used.

### *1.1.3. TV neutron radiography*

The indirect or transfer neutron radiography method is commonly used to inspect high radioactive samples. The radiograph is obtained by irradiating the sample and a dysprosium screen, in a neutron beam. The radioactive dysprosium is put in tight contact with a conventional X-ray film and after a typical period of several hours, the image is transferred. Insensitivity to gamma radiation and the high dynamic range are the main characteristics of this method.

The idea proposed for this research line is to provide an alternative methodology to inspect the radioactive samples, in an almost real-time mode.

In the proposed method the material under inspection is irradiated in a close contact with the dysprosium screen. After irradiation the screen is put in a tight contact with a scintillator screen and a bright image, which is visible by naked eye, is promptly formed. This image is captured by a digital video camera and then processed. The method was characterized following the same procedures employed before in the NIER and NIAR techniques. The preliminary results have demonstrated that for an irradiation of 3 half-lives of dysprosium screen (~ 7 hours) the time to capture the image is 7 sec. For such conditions the minimal discernible thickness for perspex was 68±10 μm (in 0.2 cm) at a resolution of 732±80 μm.

In order to try to improve the results, a light tight box was designed. The sensitivity and the resolution were again determined and the results compared with those obtained by using conventional X-ray film.

## 1.2. The Work Plan for the CRP

The main objectives of the proposed project were centered on the improvement of the radiographic images and make reliable data quantification. In order to reach these objectives following modifications and optimizations were proposed in present set up:

— **Minimize the neutron scattering in air**. The NR facility has a large internal free space of 3×2×2 $m^3$, and provides several irradiation positions. Since the minimal distance from the neutron collimator outlet aperture to the sample position is about 1 meter and

the maximal about 3 meters, the neutron beam is strongly scattered by the air before impinge on the sample. This means a loss of beam quality as well as an increasing of the neutron dose rate outside the facility's shielding. In order to minimize such problems an aluminum tube, ~2 m in length and ~40 cms in diameter, was installed inside the shielding along the neutron beam. Experiments were carried out with the tube evacuated and with He gas filled in the tube. In both the cases, the reduction of the scattered neutron intensity was ~10%.

- **Construct a sample holder for irradiation.** The NR facility provides several irradiation positions. This holder provides precise adjustments and reproducibility in the sample position, at any one of the irradiation positions.
- **Optimize the present beam catcher**. We have programmed two optimizations for the beam catcher. The first regarding the reduction of the back-scattered neutrons and the second regarding its mobility to make easy eventual modifications.

For the first purpose it was necessary to increase its present dimension along the neutron beam direction, allowing the beam be scattered inside it. The reduction of the back-scattered neutrons has optimized the signal to noise ratio in the radiographs as well as reduced the radiation dose outside the facility shielding. For the second purpose we have designed a mobile base and to minimize the radiation background outside the facility we have also constructed a mobile roof.

- **Optimizing the photo enlarger.** Allow a controlled light intensity impinging the film as well as small angle light incidence for the images registered in track-etch foils.
- **Optimizing digital system.**. Basically the improvements were regarding the changing of the frame grabber for image capture, as well as the computer for image capture and processing.
- **Design and construction of a light tight box for the TV - Dy based system.**
- **Use of a light transmission scanner to perform light transmission readings.**

During the development of the present CRP, several other improvements, modifications and optimizations have been suggested by the participants of the meetings which also have been implemented. As a result an excellent infrastructure has become available at IPEN to keep the development of the proposed techniques as well as to develop other ones.

- An upgraded neutron radiography facility;
- Adequate sample holder;
- Adequate equipment for NR with track etch foils;
- Three reliable systems for image analysis-- microscope coupled to a digital system; photo enlarger coupled to a digital system and transmission scanner.

### *1.2.1. NIER using the scanner to evaluate light transmission readings*

The basic procedures to characterize this NIER are the same as the ones used with the optical densitometer. Figure 82 shows the behavior of the light transmitted in units of "gray level" as functions of the exposure, by using the scanner to perform the readings. The film as well as the screen were the same ones used previously. The best contrast was achieved for $1.5\times10^{7}n/cm^{2} < E < 1.5\times10^{8}n/cm^{2}$ and for $0 < GL < 200$.

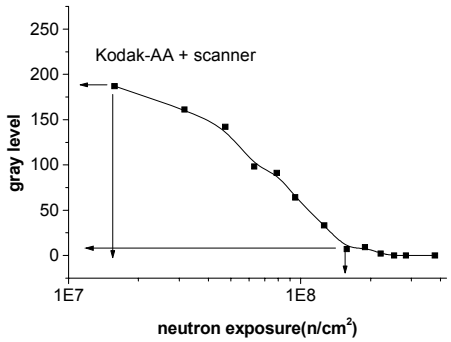


*Fig. 82. Gray level as functions of the neutron exposure for the NIER.*

In order to study the sensitivity the same step wedges, employed before, have been used and the behavior of the light transmission readings, for the aluminum sample, as functions of the sample thickness, are shown in the figure 83. After mathematical analysis, the best fitted function was an exponential given by:

$$GL = P1 + P2.\exp(-P3.x) \qquad (7)$$

Figure 84 shows a typical result regarding the behavior of the sensitivity as functions of the sample thickness for the aluminum sample. In order to show the high potential of the scanner as a light transmission reader, in this figure the results obtained for aluminum by employing the densitometer are also presented. As can be seen, the results provided by the scanner are smaller, that is, better.

Table 16 shows the minimal discernible thickness or the minimal amount of these samples, detectable by the method.

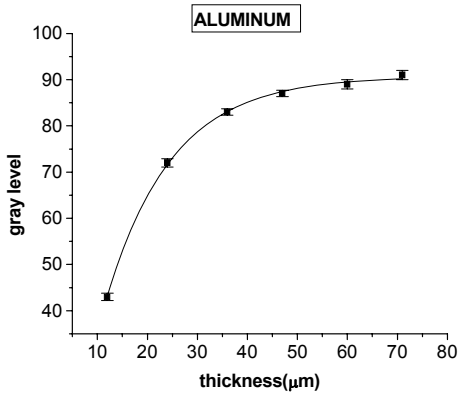


*Fig. 83. Behavior of the gray level intensity as a function of the aluminum thickness.*

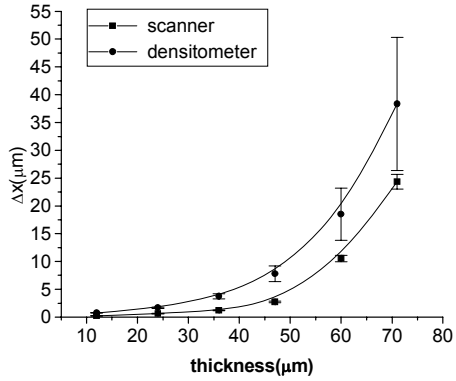


*Fig. 84. Behavior of the Δx values as a function of the aluminum thickness.*

TABLE 16. MINIMAL DISCERNIBLE THICKNESS FOR THE NIER METHOD.

| Material | Min disc thick.- (μm) |
|---|---|
| Adhesive tape | 1.2±0.5 |
| Aluminum foil | 0.11±0.03 |
| Makrofol – KG | 0.22±0.05 |
| White paper | 2.6±0.8 |

In order to determine the resolution the opaque material used was a 100 μm thick aluminium foil. Figure 85 shows a typical gray level distribution observed as functions of the scan coordinate provided by the scanner. A value of 23±2 μm was determined and this is a very good result since it is near the theoretical limit of the range of the 70 keV electrons into the film emulsion which is about 20 micra.

In order to compare the results for the NIER using the optical densitometer and the scanner, to evaluate the light transmitted, the values for minimal discernible thickness and resolution are summarized in Table 17.

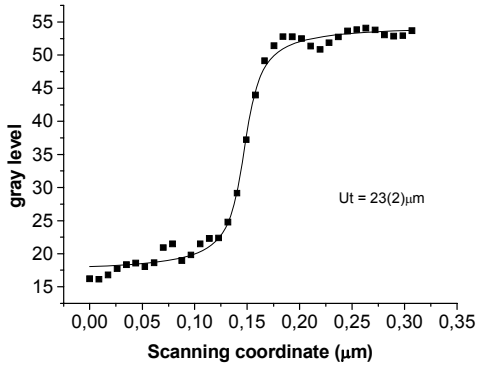


*Fig. 85. Scanning of the gray level distribution for aluminum foil.*

TABLE 17. COMPARISON OF THE NIER DATA AS OBTAINED WITH THE SCANNER AND WITH OPTICAL DENSITOMETER.

| Material | Min disc thick.- (μm) Scanner | Min disc thick.- (μm) Optical densitometer |
|---|---|---|
| Adhesive tape | 1.2±0.5 | 8±1 |
| Aluminum foil | 0.11±0.03 | 0.25±0.05 |
| Makrofol – KG | 0.22±0.05 | 0.69±0.07 |
| White paper | 2.6±0.8 | 6±2 |
| Resolution | 23±2 | 30±1 |

As demonstrated in Table 17, the scanner is able to provide better results either regarding the minimal discernible thickness or regarding the resolution than the ones provided by the optical densitometer. Such improvement can be attributed to the smaller uncertainties and to the higher linearity in the light transmission readings.

### *1.2.2. NIAR using the photo enlarger digital system and scanner.*

In order to characterize the NIAR method the conditions to obtain the best contrast in the image have also been determined. Figure 86 shows the behavior of the light transmitted in "gray level" units as functions of the exposure, for the CR-39 in three different etching times using this method. The best contrast was achieved for 25 minutes, $6\times10^{7}$n/cm$^2$ < E < $3.5\times10^{9}$n/cm$^2$ and for 70 < GL < 240

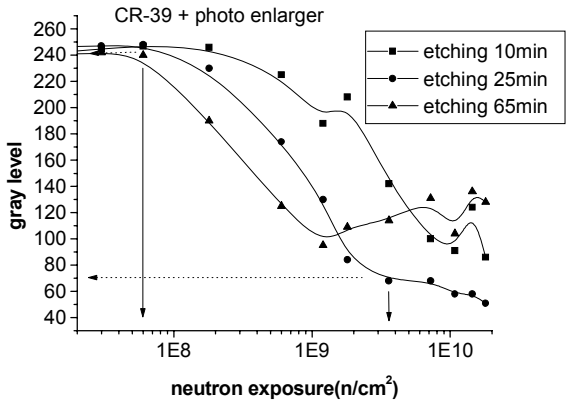


*Fig. 86. Gray level as functions of the neutron exposure for the NIAR.*

For this etching time the track diameter, track production rate are shown in Table 18. These parameters have been determined using the optical microscope coupled to the digital system. The resolution was determined by using the gadolinium (100 μm) opaque material and the light transmission readings performed by using the photo enlarger system. The result is also shown in Table 18.

TABLE 18. PARAMETERS REGARDING THE RADIOGRAPHY IMAGE FOR THE NIAR.

| Etching time min | Track-diameter μm | Track prod. Rate tr/n | Resolution μm |
|---|---|---|---|
| 25 | 2.5±0.2 | $17\pm1\times10^{-3}$ | 110±18 |

In order to compare the characteristics of the NIAR technique, the behavior of the light transmitted in units of "gray level" as functions of the exposure, for the same etching times, by using the scanner to evaluate the light transmitted are shown in the figure 87. The best contrast was achieved for 25 minutes, $8\times10^{8}$n/cm$^2$ < $E$ < $8\times10^{9}$n/cm$^2$ and for 170 < GL < 250.

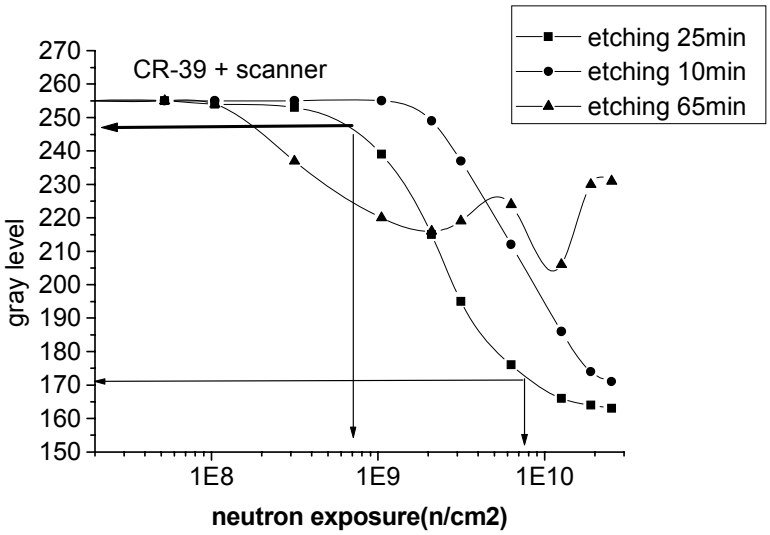


*Fig. 87. Gray level as functions of the neutron exposure for the NIAR.*

The resolution, 19±1 μm, was obtained using gadolinium(100 μm) as opaque material and the light transmission were performed by using the scanner.

From the figures 86 and 87 it is possible to compare several characteristics of the NIAR method using the photo enlarger and the scanner to evaluate light transmission and they are complementary to each other. While the photo enlarger system shows a higher dynamic range and contrast, the scanner shows a resolution ~ 5 times better in the image. The improvement in the resolution can be explained taking into account the scanner characteristics. At a resolution of 3200 dpi, it is able to provide an 8 μm pixel in the image which is approximately the range of the alpha particle in the foil. The choice of the light transmission reader to be employed then depends on the information required from the inspection (see Table 19). For example, if the sample is small (some mm in size) the most adequate equipment, in spite of the lower contrast, is the scanner. The photo enlarger is not adequate because the projected image is still very small and details will be lost because of the low resolution.

TABLE 19. COMPARISON OF THE NIAR DATA AS OBTAINED WITH THE SCANNER AND WITH PHOTO ENLARGER.

| Material | Photo enlarger | Scanner |
|---|---|---|
| Dynamic range | 170 | 80 |
| Contrast | 96 | 72 |
| Resolution | 110±18 μm | 19±1 μm |

Regarding the sensitivity of the method, we had problems to get very thin samples, on the order of units of μm (the range of the 1.47 MeV alphas emitted by the boron screen, in most of the organic materials) with precise thicknesses. Hence the sensitivity could be not quantified. The best we could get were nice brain tissue samples with approximate thicknesses of 3, 6, 9 and 12 μm. These samples have been radiopgraphed and the resulting images scanned. As shown in the figures below, the best result, in terms of contrast (evaluated by visual inspection) was achieved for thickness between 6 μm and 12 μm. This example

together with the other ones regarding the radiographs of a finger print and of a bacteria colony (shown in the previous progress report) demonstrate the high potential of the present method to inspect thin samples.

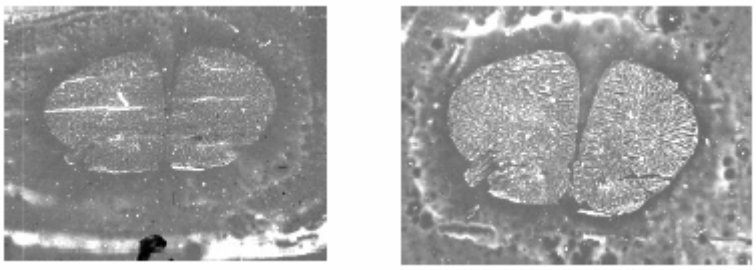

*Fig. 88. Brain tissue 3μm (Left) and Brain tissue 6μm (Right).*

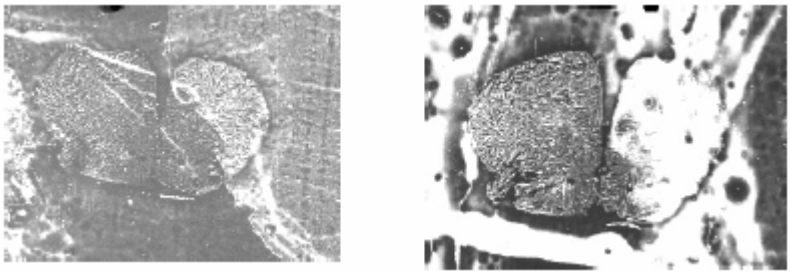

*Fig. 89. Brain tissue 9μm (Left) and Brain tissue 12μm (Right).*

For the NIAR another converter screen was employed. This is the Lithium fluoride which under neutron irradiation provides 2.05 MeV alpha particles and 2.73 MeV protons. Since the ranges of such particles in the CR 39 are about 7 μm and 108 μm respectively, we have two alternatives to perform radiography. The first with alpha particles and in this case the etching time is about the same as used with the alphas from boron screen (25 minutes) because the "dE/dx" and the range in the CR-39 are nearly the same. The second with protons (a new technique - NIPR) in which the etching time is somewhat greater, to reach the depth of 108 μm. For the purpose of the present project our primary interest is in the first one. Hence, in order to characterize the NIAR method by using the LiF screen, we have proceeded to determine the conditions to obtain the best contrast in the image and the resolution. Figure 90 shows the data regarding the behavior of the light transmitted in units of "gray level" as functions of the exposure using the scanner to evaluate the light transmitted.

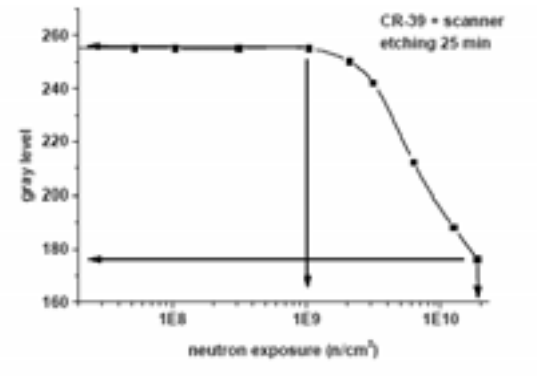


*Fig. 90. Gray level as functions of the neutron exposure for the NIAR – LiF.*

The best contrast was achieved for $1\times10^{9}$n/cm$^2$ < E < $2\times10^{10}$n/cm$^2$ and for 170 < GL < 250, shown by arrows. For such condition the resolution was about 30±1 μm.

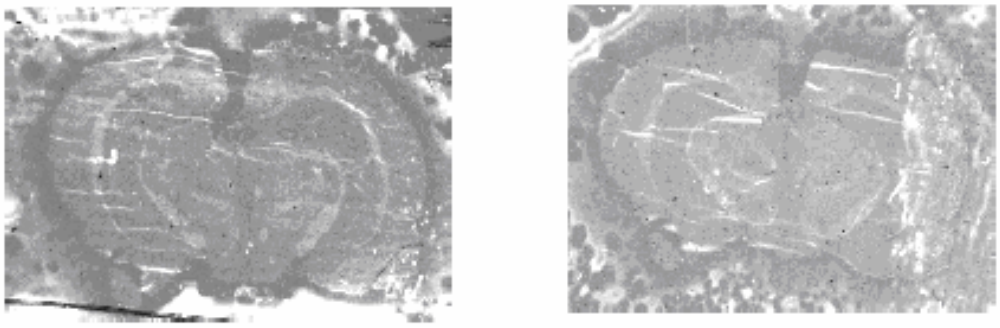

*Fig. 91. Brain tissue 3 μm (Left) and Brain tissue 6 μm (Right).*

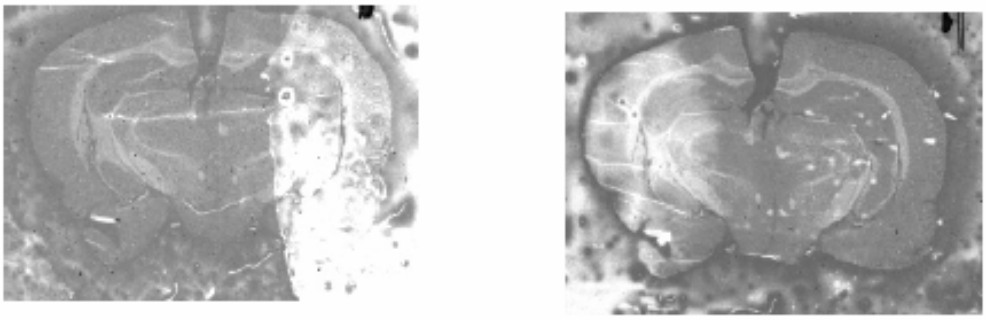

*Fig. 92. Brain tissue 9 μm (Left) and Brain tissue 12 μm (Right).*

The problem of the sensitivity of the method, mentioned above, remains and again the sensitivity could not be quantified. The samples are very similar and have been radiographed. The resulting images were scanned and as shown in figures above the best result, in terms of contrast (also evaluated by visual inspection) was achieved for thickness between 9 μm and 12 μm. At present we are exploring the possibilities of the NIPR method.

### *1.2.3. Digital system for track etch neutron radiography using the photo enlarger digital system*

In order to try to improve the previous results regarding the NR technique by using track-etch foils, the photo enlarger digital system, instead of the microphotometer, was used to quantify the light transmitted through the samples.

Such improvement was evaluated by comparing the values of the sensitivity to discern thickness and resolution obtained in both methods. The procedures to characterize this method were the same as employed before and the track-etch foil was also the CR–39.

Figure 93 shows the behavior of the light transmitted in "gray level" units as functions of the exposure, for the CR-39 for three different etching times, using the photo enlarger. The best contrast was achieved for 25 minutes, $6\times10^{7}$n/cm$^2$ < E < $3.5\times10^{9}$n/cm$^2$ and for 70 < GL < 240.

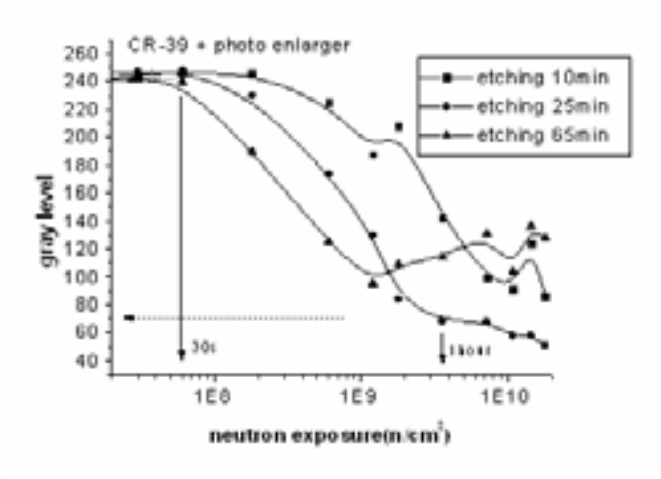


*Fig. 93. Gray level as functions of the neutron exposure for NR..*

The samples used to evaluate the sensitivity were the same step wedges of iron and perspex with thicknesses varying from 2 to 12 mm and 2 to 11 mm.

The behavior of the light transmitted as functions of step wedge thickness are shown in figure 94. In this case the best fitted function is a linear one as:

$$GL(x) = GLo - C.X \qquad (8)$$

where GLo is the gray level for X = 0 and C is the slope of the straight line.

The sensitivity was calculated as:

$$\Delta X = \Delta GL/C \qquad (9)$$

with ΔGL, the minimal discernible gray level capability of the photo enlarger coupled to the digital system.

The results show that it is possible to discern 0.28±0.01 mm of iron and 0.53±0.03 of perspex.

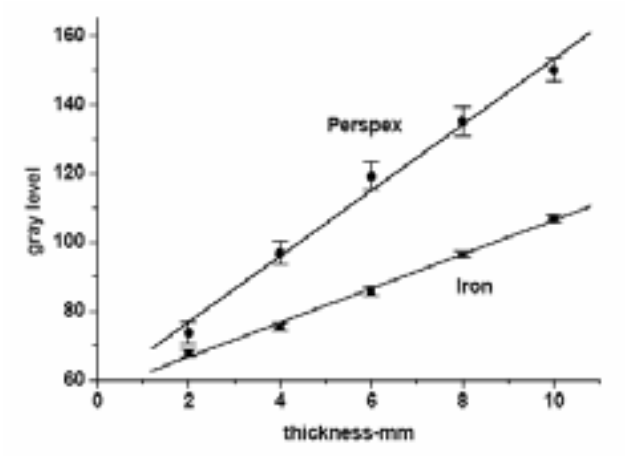


*Fig. 94. Behavior of the optical density as a function of the sample thickness.*

The resolution obtained was about 150 μm using gadolinium foil (100 μm) as the neutron opaque material.

In order to compare the potential of the photo enlarger system the results for the minimal discernible thickness obtained by using the microphotometer are also shown in Table 20. As can be seen the results provided by the former are better. Such improvement can be attributed to the smaller uncertainties and to the higher linearity in the light transmission readings of the photo enlarger system.

Another important characteristic of the photo enlarger system is the quickness in data acquisition. Each gray level intensity reading is evaluated by averaging the intensities of about 1700 individual pixels in an area corresponding to about 0.4 $cm^2$ of the image. This procedure takes few seconds. For the microphotometer the reading procedure takes about 30 minutes in an area approximately 200 times smaller.

The main limitation of the photo enlarger system is the low resolution achieved in the image. For the same radiography conditions, the microphotometer is able to provide a resolution of about 20 μm, while the present system provides about 150 μm. This value is the pixel size in the digital image, which is limited by the capture frame grabber used.

TABLE 20. COMPARISON OF THE RESOLUTION AND MINIMAL DISCERNIBLE THICKNESS FOR PLEXIGLAS AND IRON OBTAINED BY USING THE PHOTO ENLARGER SYSTEM AND THE MICROPHOTOMETER.

| **Material** | **Min disc thick.- (μm) Photo enlarger** | **Min disc thick.- (μm) Microphotometer** |
|---|---|---|
| Iron | 0.28±0.01 | 0.37±0.01 |
| Plexiglas | 0.53±0.03 | 1.0±0.1 |
| Resolution | 150 | 20 |

### *1.2.4. TV neutron radiography system to inspect high radioactive samples*

The experimental arrangement is nearly the one used previously, but now we have used an adequate light tight box. The scintillator was the Kodak Lanex having a thick plastic base covered with the scintillator. The conditions regarding irradiation time as well as capture time were the same as obtained in section 7.2.3., that is, 3 half-lives and 7 seconds respectively. The results for the sensitivity for the perspex and iron samples with thickness ranging from 0.2 to 1.2 cm as functions of the sample thickness and for the resolution by using a knife edge opaque object, a gadolinium foil (100 μm), are shown in figures 95, 96 and 97 respectively.

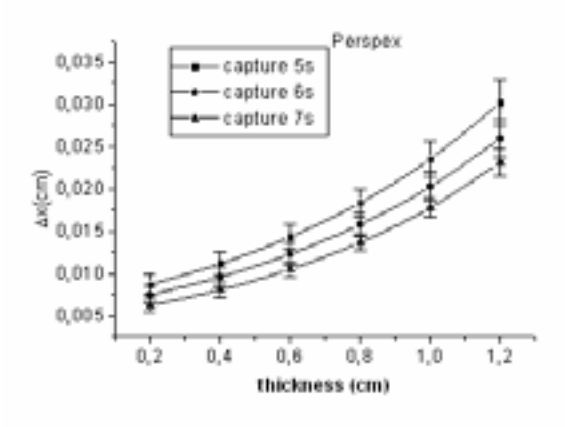


*Fig. 95. Behaviour of the sensitivity as a function of the sample thickness.*

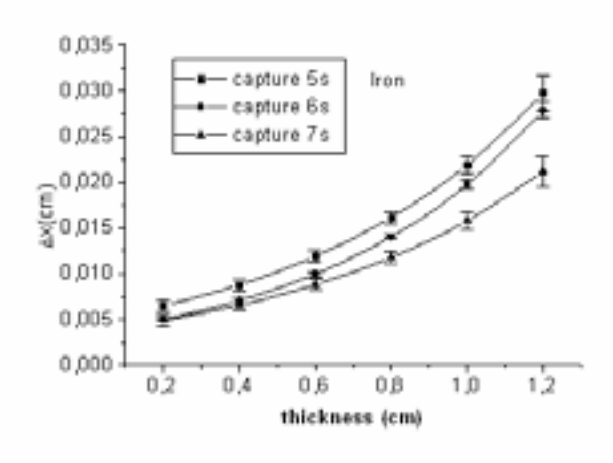


*Fig. 96. Behaviour of the sensitivity as a function of the sample thickness.*

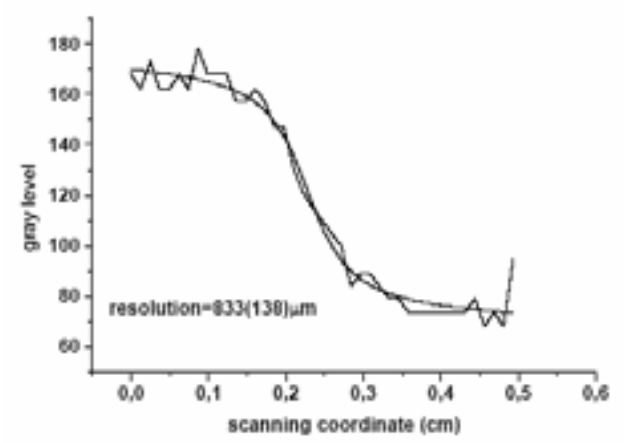


*Fig. 97. Scanning of the grey level distribution for the gadolinium foil.*

The data for the minimal discernible thickness for iron and perspex and the resolution achieved are given in Table 21.

TABLE 21. COMPARISON OF THE RESOLUTION AND THE MINIMAL DISCERNIBLE THICKNESS FOR PLEXIGLAS AND IRON OBTAINED BY USING THE TV DY SYSTEM AND A CONVENTIONAL X-RAY FILM.

| **Material** | **Min disc thick.- (μm) TV system** | **Min disc thick.- (μm) Conventional film** |
|---|---|---|
| Iron | 37±8 | 290±0.01 |
| Perspex | 48±7 | 210±0.1 |
| Resolution | 833±138 | 355±10 |

In order to compare the high potential of the proposed method, the values for the Dy method using a conventonal X-ray film to register the image are also presented in this table. The higher sensitivity can be attributed to the smaller uncertainties and the higher linearity in the light transmission readings of the TV system used.

Another important characteristic of the TV system is the quickness in data acquisition since the image transfer is not necessary.

The main limitation of the TV system is the lower resolution achieved in the image. For the same radiography conditions, the method with the X-ray film is able to provide a resolution ~ 2.4 times better. This value is limited by the Dy - screen scintillator set up since the beta radiation, generated by the Dy, before reach the scintillator, passes firstly across the thick plastic base. In order to improve the resolution, perhaps the next development regarding this technique should be to paint the Dy screen surface, with the scintillator substance.

### 1.3. Cooperation between Institutions

Work in collaboration between IPEN-CNEN/SP and Paul Scherrer Institute (Switzerland) PSI.

Several measurements on NIER using imaging plates and other converter screens were carried out at PSI, Switzerland in collaboration with Eberhard Lehmann. The objectives were:

- To compare and to discuss the improvements in the contrast for the track-etch foil images.
- To perform irradiations in the PSI neutron radiography facility, by using the method of the "Neutron Induced Radiation Radiography (NIRR)". In this case image plates will be employed, instead of the conventional X-ray films and the track-etch foils. Because of the high intrinsic dynamic range of these plates, the images show higher quality as compared to the ones obtained by using films and track-etch foils in IPEN-CNEN/SP. The results were published.

## REFERENCES


[1] BERGER, H. Neutron Radiography – A state of art report. NTIAC–SR–98–01. NASA (Center for Aerospace Information): Aug, 1998.

[2] BRYANT, L.E; MCENTIRE, P. 2nd ed. Radiography and radiation testing. American Society for Nondestructive Testing (Nondestructive Testing Handbook); 1985.

[3] HARDT P. VON DER; ROETTGER H. Neutron radiography handbook: nuclear science and technology, Dordrecht, D. Reidl, 1981.

[4] THOMS, M.; MYLES, D. AND WILKINSON, C. Neutron detection with imaging plates part I. Image storage and readout. In E. Lehmann, H. Pleinert, S. Korner, editors, Proceedins of the Third International Topical Meeting on Neutron Radiography, volume 424 of Nuclear Instruments and Methods in Physics Research A, pages 26–33, 1998.

[5] BARTON J.P.; BADER J.W.; BRENIZER J.S.; HOSTICKA B. Feasibility of neutron radiography for space shuttle inspection. Proceedings of the Fourth World Conference on Neutron Radiography, pp 123–132. San Francisco, California, USA May 10–16, 1992.Edit by John P. Barton. Gordon and Breach Science Publishers.

[6] LEHMANN, E.; PLEINERT, H.; WILLIAMS T. and PRALONG, C. Applications of new radiation detection techniques at the Paul Scherrer Institut, especially at the spallation neutron source. In E. Lehmann, H. Pleinert, S. Korner, editors, Proceedins of the Third International Topical Meeting on Neutron Radiography, volume 424 of Nuclear Instruments and Methods in Physics Research A, pp. 158–164, 1998.

[7] KOBAYASHY H; WAKAO H; IKEDA Y; OHOKUBO K; TSURUNO A. macroscopic cross section measurements and defect detection in materials using neutron radiography technique. Journal of Nuclear Science and Technology, **29**(11), (1992) 1045–1053.

[8] Ilic' R. and Najzer M.. Image Formation in Track-Etch Detector-I. The Large Area Signal Transfer Function. Nucl. Track Radiat. Meas. **17**, (1990a) 453–460

[9] Ilic' R. and Najzer M.. Image Formation in Track-Etch Detector-II. The Space-Dependent Transfer Function in Thin Detectors. Nucl. Track Radiat. Meas. **17**, (1990b) 461–468

[10] Ilic' R. and Najzer M.. Image Formation in Track-Etch Detector-III. The Space-Dependent Transfer Function in Thick Detectors. Nucl. Track Radiat. Meas. 17, (1990c) 469–473

[11] Ilic' R. and Najzer M.. Image Formation in Track-Etch Detector-IV. Image Quality. Nucl. Track Radiat. Meas. 17, (1990d) 475-481

[12] K.R.Castleman. Digital Image Processing. Prentice Hall Upper Saddle River, New Jersey, 07458, 1996.

# Neutron scattering corrections for neutron radiography

F.C. de Beer[1], N. Kardjilov[2], E.H. Lehmann[3], R. Hassenein[3]

[1]Necsa, Pretoria, South Africa, SANRAD Facility.
[2]Hahn-Meitner-Institute (HMI), Berlin, Germany, CONRAD Facility.
[3]Paul Scherrer Institut, Switzerland, NEUTRA Facility

**Abstract**: This article describes the problem of scattering artefact in neutron imaging, hindering a precise quantification of the sample content in many practical applications. This was found especially important when hydrogen is involved as sample material or agent.
The problem was tackled from both sides: the experimental determination of the scattering effect under well-defined conditions at three different imaging beam lines and the theoretical description of the scattering in the sample by means of Mont-Carlo simulations. In the latter case, the concept of Point Scattered Functions (PScF) was used to determine the scattering contribution of the sample interaction. This knowledge can be used to withdraw the scattered component for each pixel in the image, whereas the "real" attenuation data will result.
This effort was finalized recently by the issue of the first version of the correction software QNI 1.0 based on IDL scripts as the main result of the dissertation of R. Hassanein (PSI). It is available for the whole neutron imaging community for testing and application on request.

## 1. INTRODUCTION

The digital processing of the neutron radiography images gives the possibility for data quantification. In this case an exact relation between the measured neutron attenuation and the real macroscopic attenuation coefficient for every point of the sample is required. The assumption that the attenuation of the neutron beam through the sample is exponential:

$$I/I_0=exp(-\Sigma*d) \qquad (1)$$

where $I_0$ and $I$ are the intensities of the beam before and after the transmission and $\Sigma$ and $d$ are the linear attenuation coefficient, and the thickness of the sample in beam direction is valid only in an ideal case where a monochromatic beam, non scattering sample and non background contribution are assumed. In the real case these conditions are not fulfilled and in dependence on the sample material we have more or less deviation from the exponential attenuation law. Because of the high scattering cross-sections of hydrogen ($\sigma_s$=80.26 barn) for thermal neutrons, the problem with the scattered neutrons at quantitative radiography investigations of hydrogenous materials (as PE, PMMA, Oil, $H_2O$, etc) is not trivial. For these strong scattering materials the neutron beam attenuation is no longer exponential and a dependence of the macroscopic attenuation coefficient on the material thickness and on the distance between the sample and the detector appears. When quantitative radiography (2D) or tomography investigations (3D) are performed, some image correction procedures for a description of the scattering effect are required. Examples for this approach are shown in references [5, 7] where preliminary simulated point scattered functions by Monte Carlo code MCNP-4C were used. The aim of the current study is to show that the contribution of the scattering effect in neutron radiography investigations of hydrogenous materials is very strong using a comparison between experimental and Monte Carlo simulated data. A correction procedure based on analytically described point scattered functions was tested and the results are presented.

## 1.1. History of the Problem

As late as 1992 and only until the 4th World Conference on Neutron Radiography (WCNR-4), Murata et al. [1] published the two-dimensional neutron image excluding the effect of scattered neutrons where the effect of scattered neutrons was identified and acknowledged. At the same conference Raine et al. [2], Unesaki et al. [3] and Maghadam et al. [4] reported the scattered effect correction for high resolution neutron radiography and computed tomography as well as the improvement of images by elimination of contribution of the scattered neutrons in computed tomography. One important paper by Pleinert et al. [5] investigated the effect of hydrogenous distributions in quantitative neutron radiography measurement.

Takenaka et al. [6] extended the neutron radiography application of quantitative measurement method to void fraction of two-phase flow in a rod bundles. It was only until reported in 2001 through a study by Kardjilov et al. [7] about the representation of the image formation in applied neutron radiography in terms of a Point Spread Function (PSF) superposition, that this problem is addressed in order to find a solution and to apply it in practical applications such as for petroleum engineering mentioned by Middleton et al. [8].

A first attempt for the corrections for scattered neutrons in quantitative neutron radiography by Kardjilov et al [9] as PhD student in this field, was followed by another paper by the same author and collaborators, participating in the IAEA-sponsored and initiated collaborative research project (CRP) during 2004 [10] where Point Scattered Functions (PScF) were used in the scattering corrections in neutron radiography. In a comprehensive study and continuation of the IAEA-CRP, Hassanein et al. [11] investigated the methods of scattering corrections for quantitative neutron radiography as part of his PhD thesis, continuing the work initiated by Pleinert and Kardjilov. Preliminary results the scattering Correction Algorithm created for neutron radiography and tomography tested at facilities with different beam characteristics were reported [12]. A final paper where the scattering correction software and performance through a series of tests are being described will be published at the Proceedings of WCNR-8 at NIST 2006 [13].

This development concluded in the software tool QNI 1.0 (Quantitative Neutron Imaging), based on IDL scripts, which will be made available for interested applicants in the field.

## 1.2. Experiments

### *1.2.1. Samples under investigation*

*1.2.1.1.Hollow Al cube types*

These sample holders are filled with $H_2O$, oil and $D_2O$ alternatively for simulating the experimental conditions for the typical samples from the Civil Engineering and Geological fraternities.

Extreme care must be taken that these samples holders themselves do not contribute to the scattering effect onto the neutron radiographs. After the first attempt (Fig. 98) where the sample holder was constructed from Al but was assembled by means of Si rubber and stainless steel nuts and bolts, separate sample holders were manufactured from Al with no other material that can contribute to the scattering. (Fig. 99)

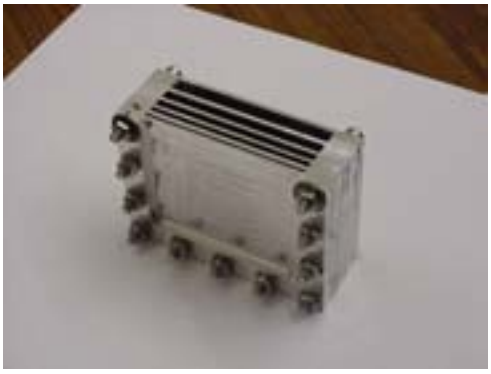

*Fig. 98. Old sample holder.*

*Fig. 99. New sample holders.*

The new design (Fig. 99) improves on the current aluminium container (Fig. 98) in order to remove all hydrogenous materials (glue or plastic) from it. High neutron scattering materials like stainless steel bolds were also removed to minimize the scattering contribution from any source. Fig. 99 shows the number of containers for different thickness of fluid, manufactured from only aluminium. The sizes of the sample holders are as in Table 22 and Fig. 100. Calibrated fluid thicknesses are given in Table 23.

TABLE 22. DIMENSIONS OF SAMPLES.

| **Water thickness (mm)** | **X1 (mm)** | **X (mm)** | **Height Sample Holder (mm)** | **Height Fluid (mm)** |
|---|---|---|---|---|
| 0.97 | 50.0 | 44.3 | 50.0 | 40.0 |
| 1.91 | 49.3 | 43.6 | 50.0 | 40.0 |
| 3.00 | 50.0 | 43.9 | 49.6 | 39.6 |
| 4.99 | 49.9 | 43.6 | 49.3 | 39.3 |
| 6.94 | 49.9 | 43.1 | 49.2 | 39.2 |
| 9.97 | 49.2 | 43.3 | 49.5 | 39.5 |

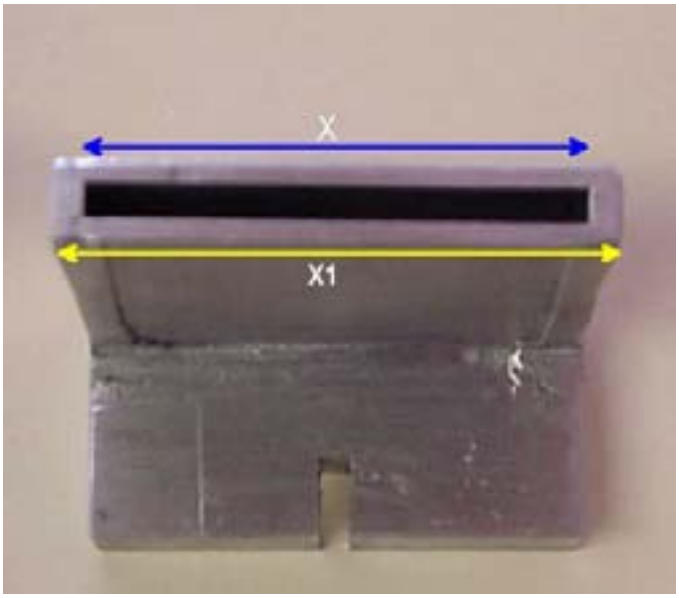


*Fig. 100. Dimensions of sample.*

TABLE 23. CALIBRATED FLUID THICKNESS DIMENSIONS OF EACH CONTAINER.

| *Intended Thickness* | *1 mm* | *2 mm* | *3 mm* | *5 mm* | *6 mm* | *10 mm* |
|---|---|---|---|---|---|---|
| *Calibrated thickness of slit.* | *0.97 mm* | *1.91 mm* | *3.0 mm* | *4.99 mm* | *5.98 mm* | *9.97 mm* |

### *1.2.1.2.Cylindrical (plug) type*

These samples (Al and STST) are used to simulate the conditions and characteristics such as porosity, for the typical samples of the Petrophysics and Geology fraternities. (Fig. 101).

*Fig. 101. Cylindrical samples.*

TABLE 24. SIMULATED POROSITY WHEN HOLES ARE FILLED WITH WATER.

| **Number of holes** | **Porosity** |
|---|---|
| 1 | 1.9% |
| 2 | 3.7% |
| 3 | 5.6% |
| 4 | 7.4% |
| 5 | 9.3% |
| 6 | 11.2% |
| 7 | 13.0% |
| 8 | 14.9% |
| 9 | 16.7% |
| 10 | 18.6% |
| 11 | 20.5% |
| 12 | 22.3% |
| 13 | 24.2% |

The dimensions of the cylindrical samples are:

| | |
|---|---|
| Diameter | 22 mm |
| Height | 55 mm |
| Diameter of holes | 3 mm |
| Height of holes | 50 mm |

*1.2.1.3.Solid metal (Al, STST or Cu)*

These samples are for simulating the conditions for the typical samples of the mechanical engineering fraternity.

*Fig. 102. Al (Left); Cu (Right).*

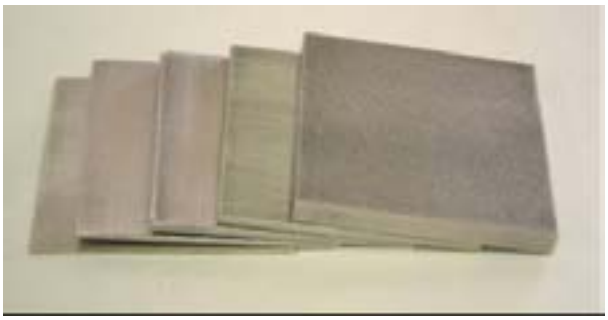

*Fig. 103. STST.*

TABLE 25. CALIBRATED SAMPLE THICKNESSES FOR SOLID SAMPLES.

| | 1 mm | 2 mm | 3 mm | 5 mm | 7 mm | 10 mm |
|---|---|---|---|---|---|---|
| Al | 0.9 | 1.92 | 2.92 | 2.92<br>+1.92 | 5.92<br>+0.9 | 5.92<br>+ 2.92<br>+ 0.9 |
| True value | 0.9 | 1.92 | 2.92 | 4.84 | 6.82 | 9.84 |
| STST | 0.72 | 2.0 | 2.0<br>+0.72 | 5.22 | 5.22<br>+1.98 | 5.22<br>+2.0<br>+1.98 |
| True value | 0.72 | 2.0 | 2.72 | 5.22 | 7.20 | 9.20 |
| Cu | 1.22 | 2.04 | 3.16 | 3.16<br>+2.04 | 3.16<br>+2.04<br>+1.22 | 6.38<br>+2.04<br>+1.22 |
| True value | 1.22 | 2.04 | 3.16 | 5.2 | 6.42 | 9.64 |

### *1.2.2. Imaging instrumentation*

#### ***1.2.2.1.****Sample holder equipment*

A suitable translation table (Fig. 104), designed for the existing neutron tomography system, was utilized to set the distance between the container and the detector surface with a better precision of 0.5 mm. A positioning pin for the cube water holders, shown in Fig. 105, was designed and manufactured to position the sample holders on top of the extension bar.

*Fig. 104. Translation table.*

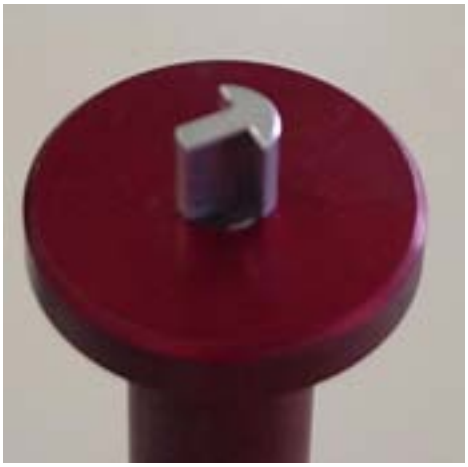

*Fig. 105. Positioning pin.*

An Al sample holder, to minimize the scattering effect under investigation, is manufactured that fits into the hole of the translation table to position the samples parallel to the scintillator screen as the 1 mm thick sample can not stand alone upright and needs some sort of support. A thin Al adhesive tape is used to secure the sample to the holder.

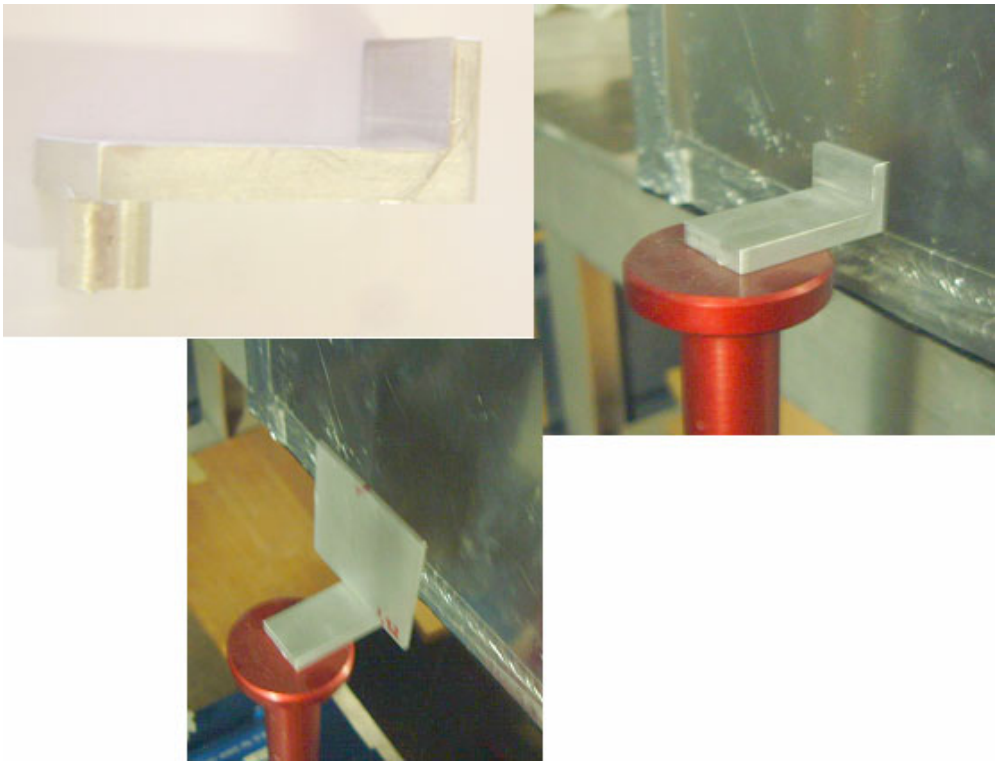

*Fig. 106. Shows the sample holder and its position on the turntable.*

### *1.2.3. Detection system*

It was a real advantage to have the same detection principle and involved CCD-camera system available in all three involved labs. As shown in Fig. 107, the primary detector, consisting of a Li-6 doped ZnS scintillation screen is observed with the high-sensitive and thermal stabilised (Peltier cooled) CCD-camera via a mirror within a light-tight box. Although this principle is common now in many other labs too, the installations in the current study can be considered as very state of the art. This is valid mainly for the camera itself, where the performance parameters are given in Table 26.

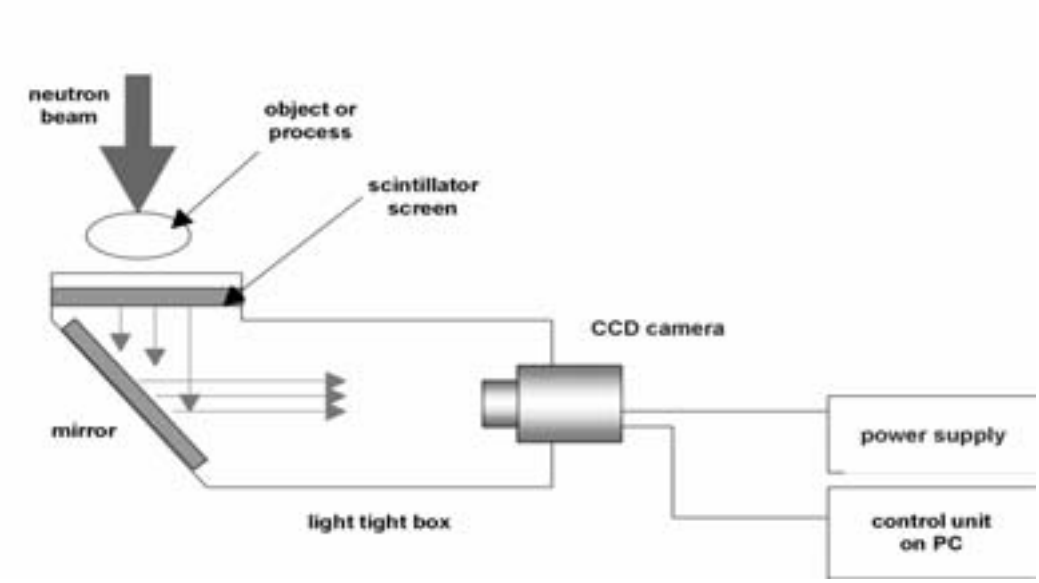


*Fig. 107. Principle setup of the used detection system for all inspections in this report.*

TABLE 26. MAIN CHARACTERISTIC FOR THE USED CAMERA SYSTEM.

| **Specification of the CCD-camera** | |
|---|---|
| Type | ANDOR-DU934BV |
| Active Pixels | 1024×1024 |
| Pixel Size [micro-m] | 13.5×13.5 |
| Image Area [mm] | 13.3×13.3 |
| Peak Quantum Efficiency | 95% |
| Min. operation temp. | 200 K |
| Pixel Read-out Rate | 1 MHz |
| Read-out Noise | 7.5 e@1 MHz |
| Digitisation | 16 Bit |
| Dark Current (@200K) | $10^4$ e/pixel/s |

### *1.2.4. Experimental conditions.*

All the samples, prior to investigation, were cleaned with acetone to ensure no greasy fingerprints might influence the signal, especially the Al samples.

To maintain a relative constant neutron flux during the experiments, the imaging of all the samples respectively was conducted during the same period of time.

The same spatial resolution and dynamic range set-up of the CCD camera were maintained for all experiments.

### *1.2.5. Numbering of neutron radiographs:*

A number of neutron radiographs were generated. They were numbered according to the following numbering system:

Metal (Liquid)-X-Y-Z-A-B

Where:

Liquid = $H_2O$, Oil or $D_2O$

X = Calibrated Thickness (1, …, 10 mm)

Y = Distance from the scintillator (mm) (5, 20, 30, 50)

Z = L (Resolution) (L = Large, M = Medium, S = small)

A = O (open beam)

B = E (open beam with empty holder = no liquid in holder)

### *1.2.6. Experimental procedure:*

The following procedure was followed:

(a) Set-up of the translation table in order to move the sample the appropriate distances from the detector. This requires the precise alignment (vertical, horizontal and perpendicular to the detector plane) of the translation table so that movement is perpendicular to the detector and no distortion exists between images taken at 5 mm and 50 mm from the detector plane (See the setup in Fig. 104 or Fig. 106).

(b) The cooled CCD camera system (Chapter 8.3.3), normally used for tomographic imaging was used to capture the 2D neutron radiographs in the following manner:

(c) Take dark current image (Image without the neutron beam).

(d) Take background image with no sample holder in beam ("open beam").

(e) Take background images with sample holder in beam (no liquid) at 5 mm, 20 mm, 30 mm and 50 mm from the detector plane.

(f) Clean the samples with acetone.

(g) When working with liquid: Fill 1 mm holder with liquid (use a syringe and needle for 1 and 2 mm thick sample holders).

(h) When working with liquid: Put sample in desiccators and evacuate to 30 TORR to get rid of all the air bubbles in the liquid (See Fig. 108).

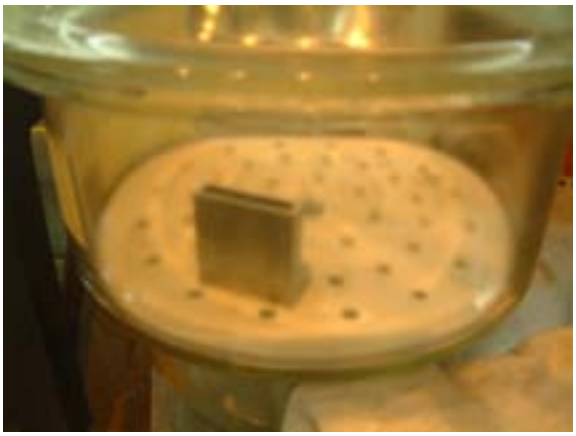

*Fig. 108. Desiccator set-up.*

(i) Put sample holder with liquid at imaging position (Fig. 104 or 106).

(j) Take neutron radiographs at 5 mm, 20 mm, 30 mm and 50 mm from the detector plane.

(k) Repeat (c) to (j) for 2 mm, 3 mm, 5 mm, 7 mm and 10 mm thickness of liquid / metal samples.

(l) Clean the sample holders with acetone and dry it with compressed air after measurements (See Fig. 109).

*Fig. 109. Cleaning of liquid holder.*

### *1.2.7. Cylindrical samples:*

Neutron tomography is being done with the same experimental set-up for each sample with the nearest surface of the sample to the detector to be 10 mm from the detector.

- Tomography with solid sample
- Tomography with empty holes
- Tomography with holes filled with water. 1 hole filled with water

— 6 holes filled with water
— 13 holes filled with water. (Centre hole included)

*1.2.7.1.Experimental setup*

To maintain constant neutron flux during the experiments, the imaging of the samples was conducted during the same period of time.

The same spatial resolution and dynamic range set-up of the CCD camera were maintained for all experiments.

Before the experiments the samples were cleaned with acetone.

## 1.3. Theoretical Description of the Scattering Contribution to the Imaging Signal

The signal obtained in the radiography measurement can be regarded as a result of superposition of two different mechanisms of interaction between the neutrons and the investigated sample. The neutron flux after the interaction can be divided into the following components: the *collided* flux – the component of neutrons that reach the detector after being scattered in the sample and the *un-collided* flux – the component of neutrons that penetrate the sample without interacting with it. A graphic representation of this model for a parallel neutron beam is shown in Fig. 110.

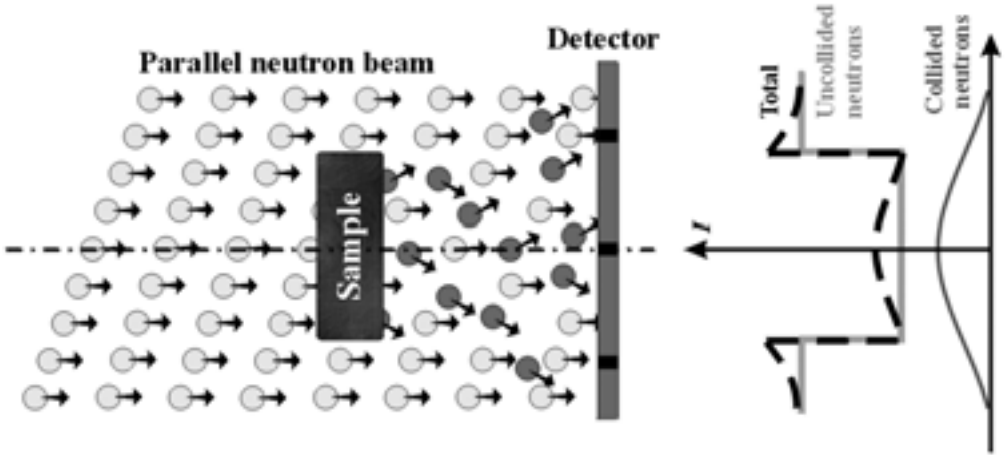


*Fig. 110. A schematic representation of the image formation process.*

It can be demonstrated that the scattering contribution depends on the distance between the sample and the detector. This dependence is clearly illustrated in Fig. 110 where a radiography investigation of PMMA slabs (1×5 cm) with different thicknesses was performed at two distances to the detector. The experiment was performed at the thermal radiography setup NEUTRA at SINQ, PSI. The detector system was a standard CCD camera system described elsewhere [14].

The obtained distance-dependent transmission in Fig.111 can be explained with the fact that the attenuation of the neutron beam in a hydrogenous material (such as PMMA - $C_5H_8O_2$) is determined mainly from the scattering properties of hydrogen. Hydrogen possesses a very high scattering cross-section for thermal neutrons (80.26 barn). As it is known that the scattering cross-section has two components, which concern the coherent and incoherent interaction between the neutrons and the matter. The coherent part is angular dependent while the incoherent part is not angular dependent and its contribution goes into the whole space – $4\pi$. Since hydrogen scatters dominantly incoherently we can expect that behind the illuminated sample the scattered neutrons will be distributed uniform in space and the projection of the scattered neutron component on some plane behind the sample will depend on the distance between the scattering medium (the object) and the plane (the detector). Consequently, the cross-sections of the so defined scattering cloud with the detector plane will form different neutron distributions, which will be more smoothed at larger distances between the sample and the detector. Such examples are shown in Fig.112 where two MCNP simulations are presented.

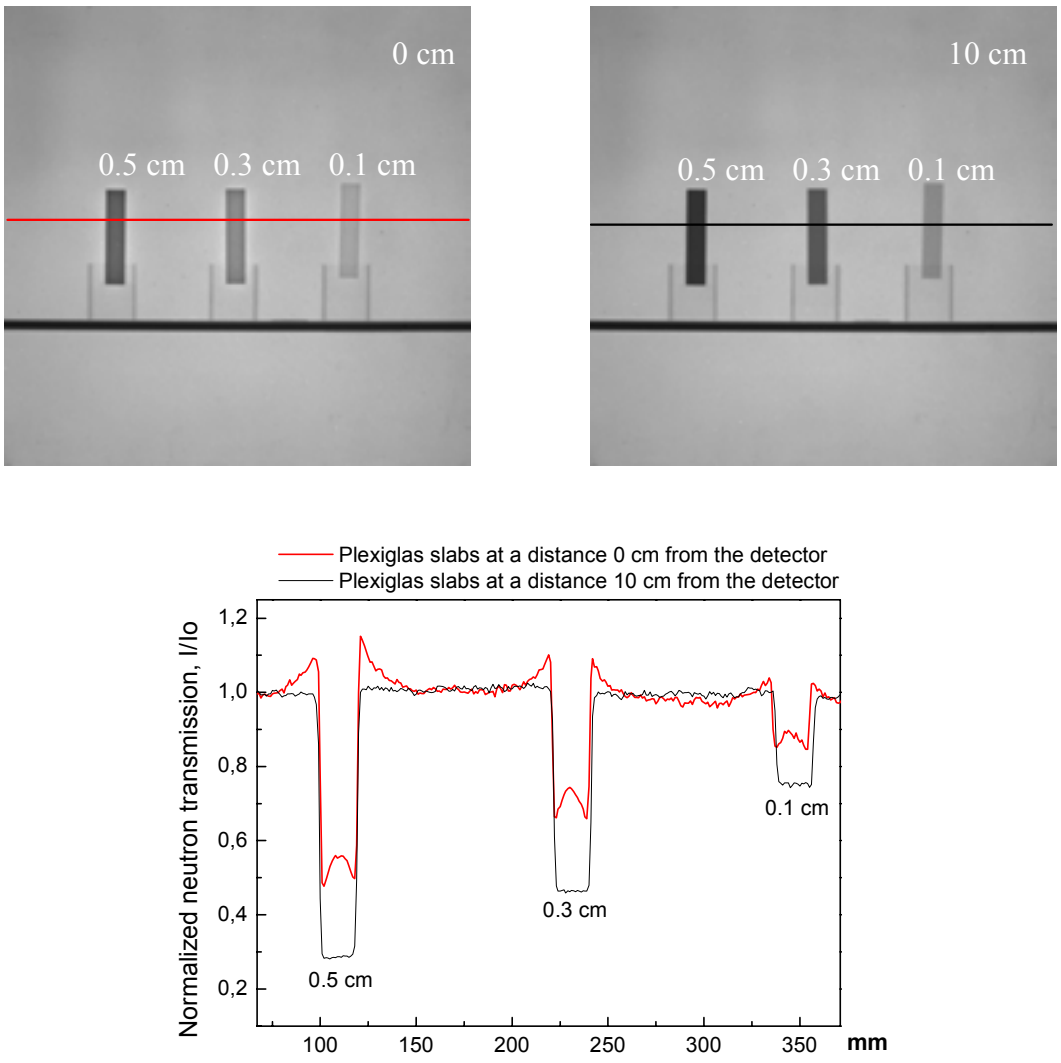


*Fig. 111. Radiographs of PMMA slabs (1x5 cm) with different thickness at (Left) 0 and (Right) 10 cm from the radiography detector. (Bottom) The intensity profile through the slabs is shown below.*

For the shown simulations, parameters close to these at the NEUTRA radiography station (neutron spectrum, beam divergence, etc.) were used. It can be seen that simulated profile in Fig.112 a) follows very well the image formation model presented in Fig.110.

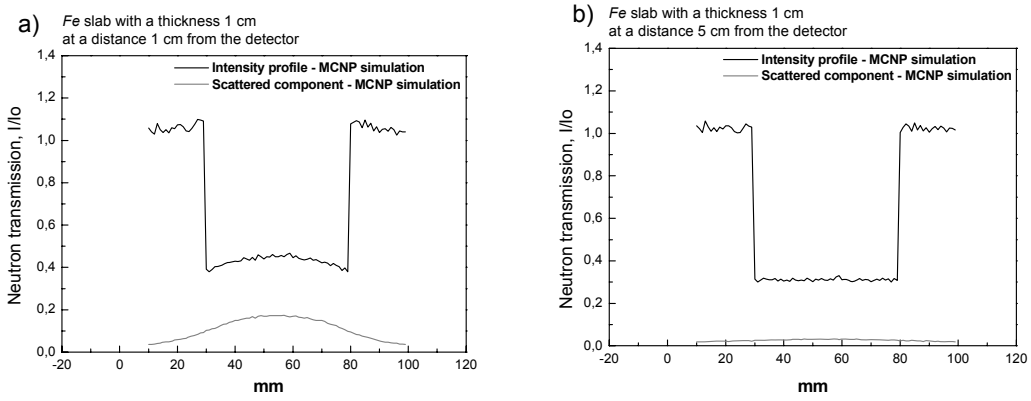


*Fig. 112. Monte Carlo simulations of a neutron radiography of a iron slab (1 x 5 cm) with a constant thickness of 1 cm at two distances to detector of (a) 1 cm and (b) 5 cm. The contribution of scattered neutrons was calculated separately.*

### *1.3.1. The scattering correction procedure*

The process of a neutron radiography image formation can be described in terms of a Point Spread Function (PSF) superposition for a given space discretization. If one uses the same discretization for the detector as well as for the neutron source then the PSF can be represented as a sum of two parts - the collided and un-collided neutrons for one volume element. The neutron distribution corresponding only to the collided part of the PSF can be defined as Point Scattered Function (PScF). In these terms the superposition of PSF with a step equal to the discretization step will give the full picture of the investigated object while the superposition of PScF will describe only the scattered neutron part in the radiography experiment. The scattering effect is position dependent since the scattering events are possible only in the sample area. The neutron scattering contribution depends of course on the sample material and its thickness as well on the distance between the sample and the detector. Taking into account these factors an image correction algorithm can be developed using a subtraction of the corresponding PScF for each pixel belonging to the sample area. In this way the scattering contribution to the radiography image will be eliminated.

Our attempts to measure the PScF for different water layers using a small pinhole in a 1 mm thick Cd plate showed that the signal from scattered neutrons was below the noise level of the detector system. Because of that a Monte Carlo model was used for a calculation of the PScF for homogenous materials. The geometry of the used model is shown in Fig.113. MCNP-4C code [15] was used for the calculations. The source and the detector surfaces were composed of small square areas (pixel discretization). The PScF was calculated as a spatial distribution of scattered neutrons over the detector surface for one emitting source element. For simplification of the model a parallel neutron beam was used.

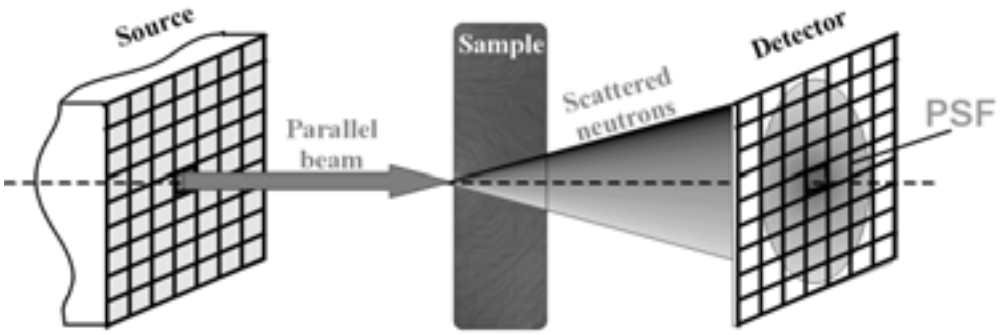


*Fig. 113. The used Monte Carlo model for a calculation of the PSF for defined material, material thickness and distance between the sample and detector.*

### *1.3.2. Approximation and analytical description*

The scattering correction procedure was based on the simulation of the scattering component for different layer thicknesses of liquids and various distances between the layer and the detector using a Monte Carlo computation method. For this purpose the MCNP-4C code [15] was used. The reliability of the calculation of the scattering component, so-called Point Scattered Function (PScF) was tested by using different tallies (detector types). The comparison presented in Fig. 114 shows that the obtained behaviour of the scattering properties for a thin $H_2O$ layer of 3 mm is similar for all the used tallies. The observed drop in the central area of the PScF could be explained by uncertainties in the MCNP calculations for very narrow collision angles. This problem comes from the uncertainty of the MCNP code in case of using the $S(\alpha,\beta)$ treatment for processes of inelastic scattering from bounding materials like water [16].

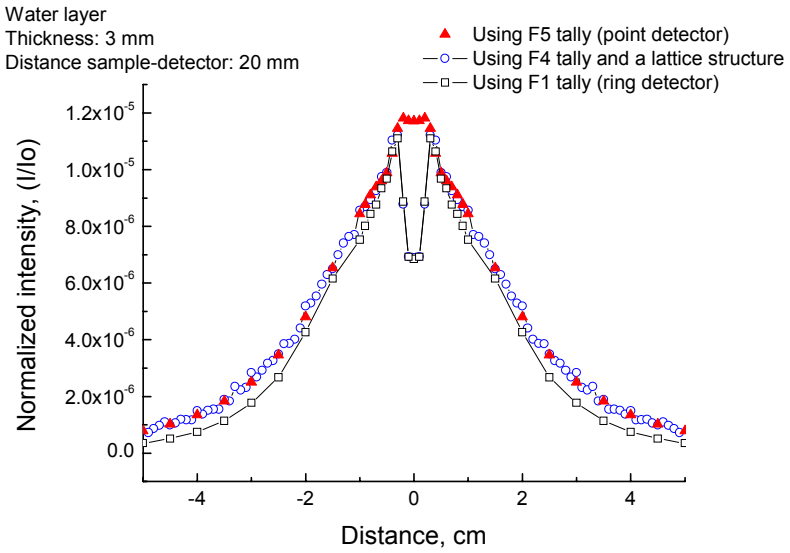


*Fig. 114. Point scattering functions calculated by using different MCNP tally structures.*

To overcome this problem we used an analytical description of the Point Scattered Function by Gaussian functions. The shape of the Gauss function was chosen due to the good agreement at large collision angles (the wings of the scattering function). The central area is also adequately described by the Gauss (see Fig. 115).

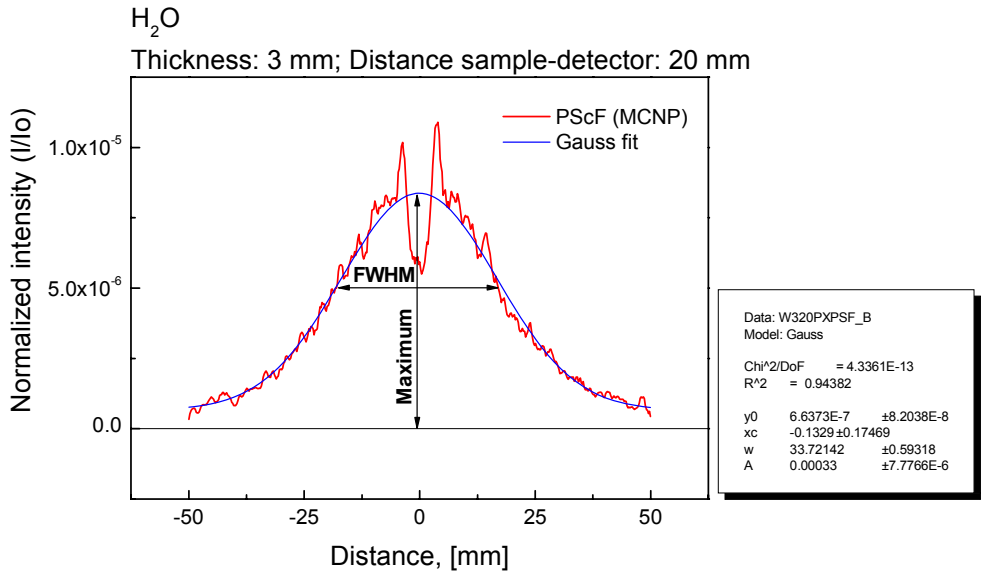


*Fig. 115. Fitting of the calculated PScF by a Gauss function.*

For the analytical description the behavior of the Gaussian maximum and FWHM were investigated for different $H_2O$ thicknesses at a fixed distances between the sample and the detector of 20 mm as shown in Fig. 115. Analogically the Gaussian parameters were

investigated for different sample-to-detector distances at a defined liquid thickness of 3 mm water, Fig. 116.

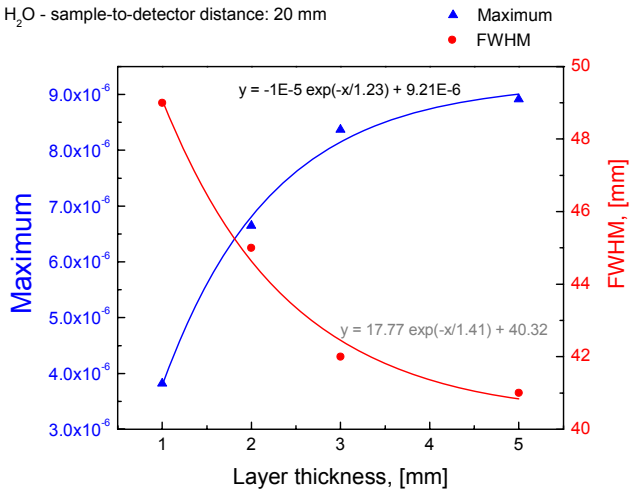


*Fig. 116. Analytical description of the PScF functions by Gauss functions with correspondent maximum and FWHM for a defined sample-to-detector distance.*

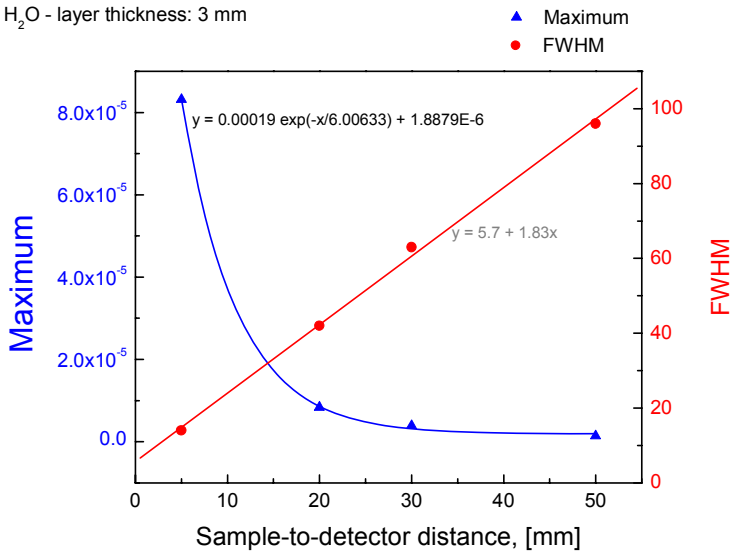


*Fig. 117. Analytical description of the PScF functions by Gauss functions with correspondent maximum and FWHM for a defined layer thickness.*

The obtained behaviours could be fitted analytically by exponential or linear functions as shown in the figures. From these analytical descriptions it was possible to reconstruct the corresponding PScF without simulating it again by Monte Carlo calculations. For this purpose an IDL routine was used which returns the 2D Gauss function by a given FWHM and maximum input parameters, Fig. 118. The so-calculated Gauss functions were used for further corrections.

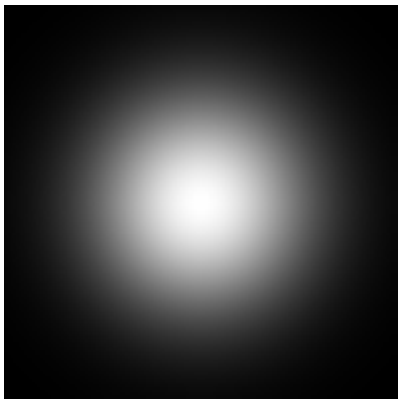

*Fig. 118. Calculated 2D analytical PScF using the parameters listed in the figures above for a water layer with a thickness of 20 mm at a distance of 20 mm from the detector.*

The corrections were performed as a subtraction of the analytical calculated Gauss shaped Point Scattered Function from all the pixels in the sample area. An example for this is shown in Fig. 119 where the result before and after the correction are shown.

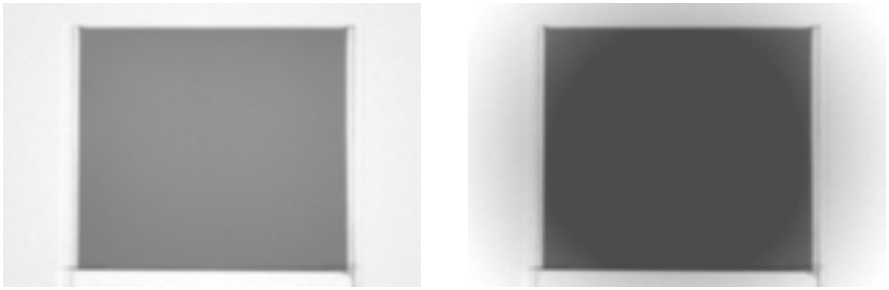

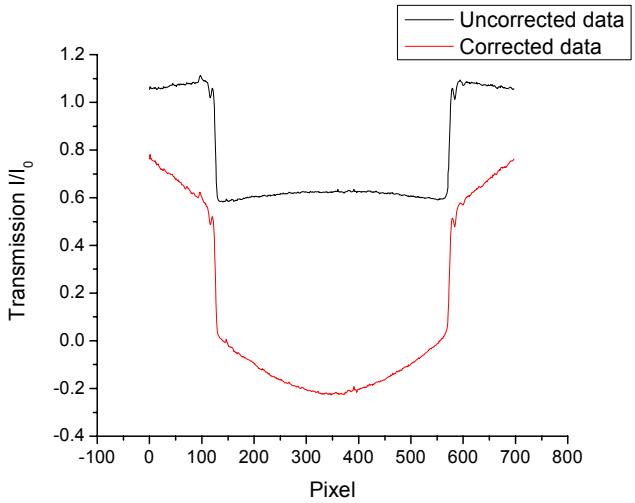


*Fig. 119. Uncorrected (Left) and corrected (Right) radiography images of a 2 mm water layer at a sample-detector distance of 20 mm. (Bottom) The intensity profile is shown below.*

The result presented in Fig. 119 shows that the Gauss-shaped PScF functions are not applicable for corrections of real radiography images. The reason for it is that the subtraction of the constant offset of the PScF for a large number of pixels provides an overestimated correction as shown in Fig. 119.

This was the reason that we decided to describe the analytical function by using some general assumptions of the incoherent scattering process in matter. Comparison between the Gaussian and the $R^2$ function is shown in Fig. 120.

The PSI approach (R. Hassanein) is based on the following relation:

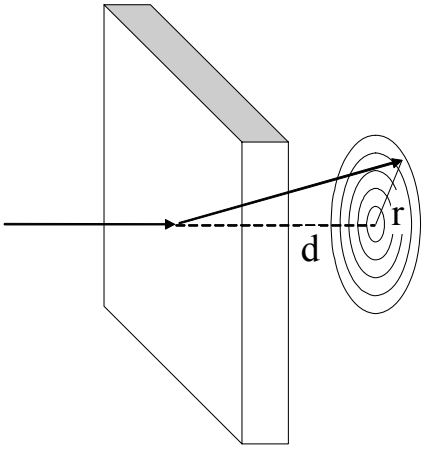


$$\mathrm{PScF}(r) = S_A \cdot \frac{d_A}{4\pi(d_A^2 + r^2)^{3/2}} \cdot \frac{1 - e^{-\Sigma_D \cdot s_D \cdot \sqrt{d_A^2 + r^2}/d_A}}{1 - e^{-\Sigma_D \cdot s_D}} \qquad (2)$$

Beside the material dependent scattering strength, the radial distance r from the forward direction of the beam and the distance from the interaction point in the sample d play the most important role. The second term considers the behaviour of the angular distribution of the scattered neutrons inside the detector with the attenuation coefficient $\Sigma_D$.

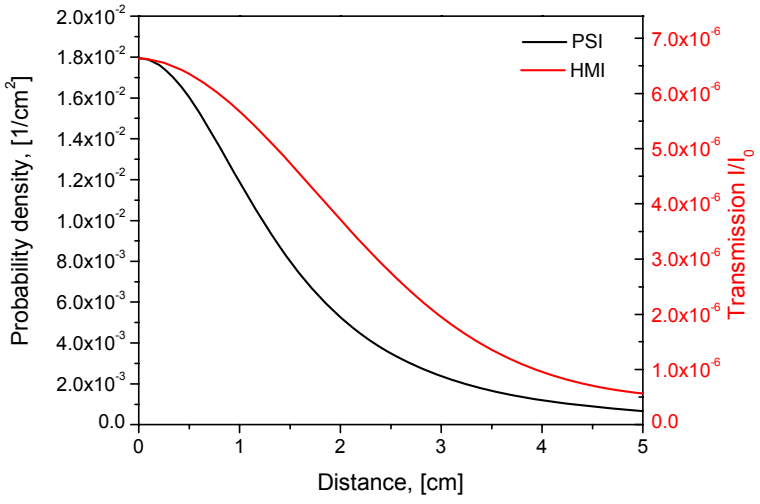


*Fig. 120. Comparison between the analytical description of PScF at HMI (Gaussian) and PSI (Formula (2)) for a 2 mm water layer at a sample-detector distance of 20 mm.*

The used units in Fig. 120 are different due to the different correction algorithms but in general the curves contain the same information and they differ by some normalization

coefficient. The main difference is the shape of the curves which provides different results in the correction procedures. The $R^2$ curve is much steeper and its offset is much lower than the Gaussian curve.

Based on the improved approximation of the PScF, R. Hassanein derived a more global correction algorithm as excerpt of his PhD work. The structure of the QNI software tool is given in the overview of Fig. 121. The method can be applied onto arbitrary imaging tasks with the aim of quantification, when the following conditions are know:

Neutron spectrum

Detector response

Distance detector-sample

Background from the environment

Sample composition

Nuclear data for the material under consideration

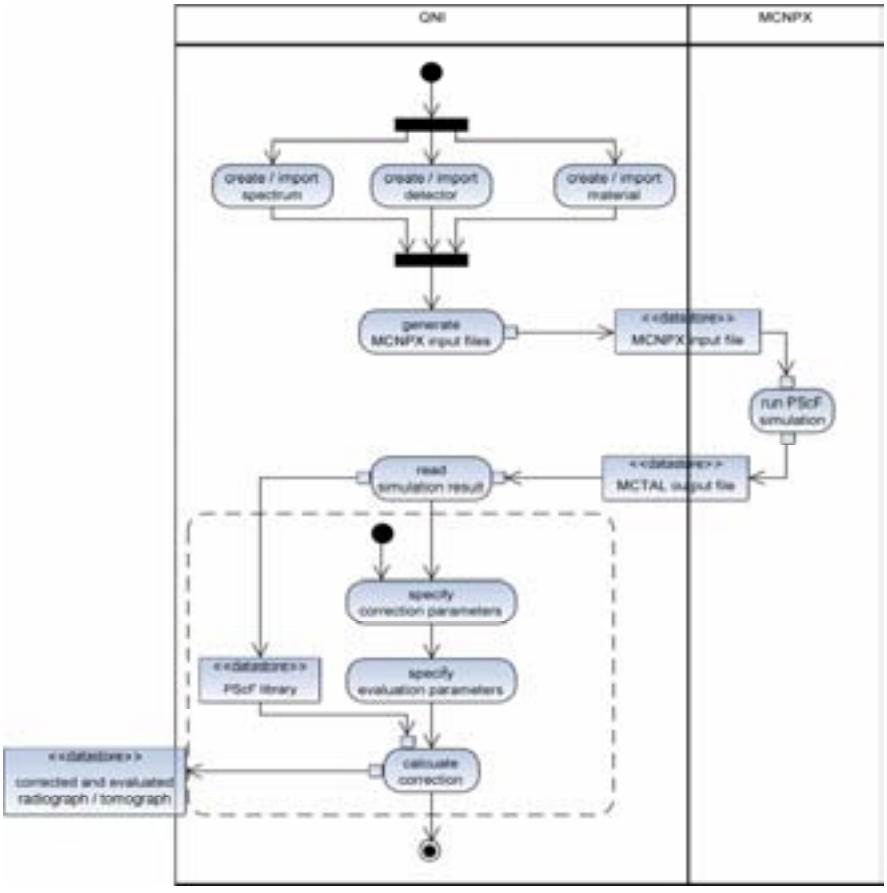


*Fig. 121. Flow map of the QNI software tool for the correction of scattering artefacts in radiography and tomography applications.*

This tool can be made available on request for further applications at different imaging beam lines. The only requirement for using the tool is to mention its origin (Paul Scherrer Institut,

Neutron Imaging & Activation Group, Switzerland). The authors would be glad to get a feedback, how the results fit to the expectations. This might be motivation for further improvements in the future.

### 1.4. Future Improvements for Cold Neutrons

The samples prepared at NECSA – stainless steel (STST) and Al plates with different thickness were investigated at HMI with polychromatic and monochromatic cold neutrons, Fig. 122.

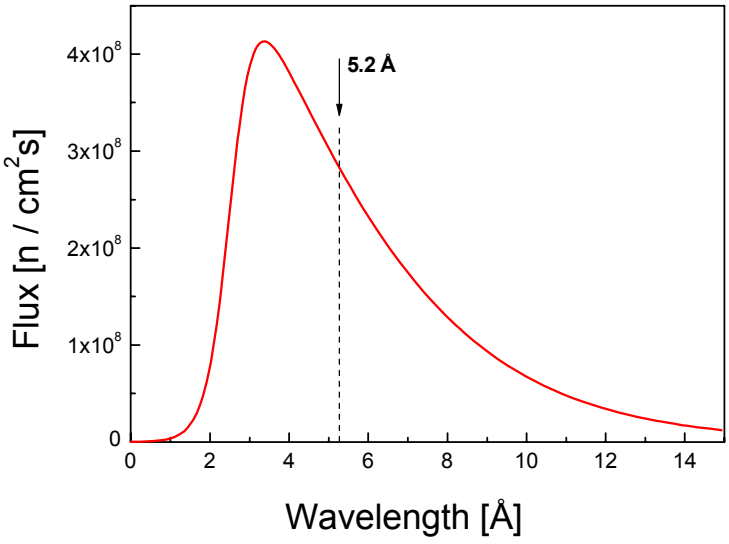


*Fig. 122. Simulated neutron spectrum at neutron guide NL1b (HMI) where the neutron radiography station CONRAD is located. The wavelength of 5.2 Å used for the monochromatic measurements is labeled by an arrow.*

For the experiments with monochromatic neutrons the wavelength tunable option at CONRAD instrument was used [16]. The transmission data at different material thicknesses and distances to the detector were calculated as linear attenuation coefficients and represented in the graphs below (Fig. 123 and Fig. 124).

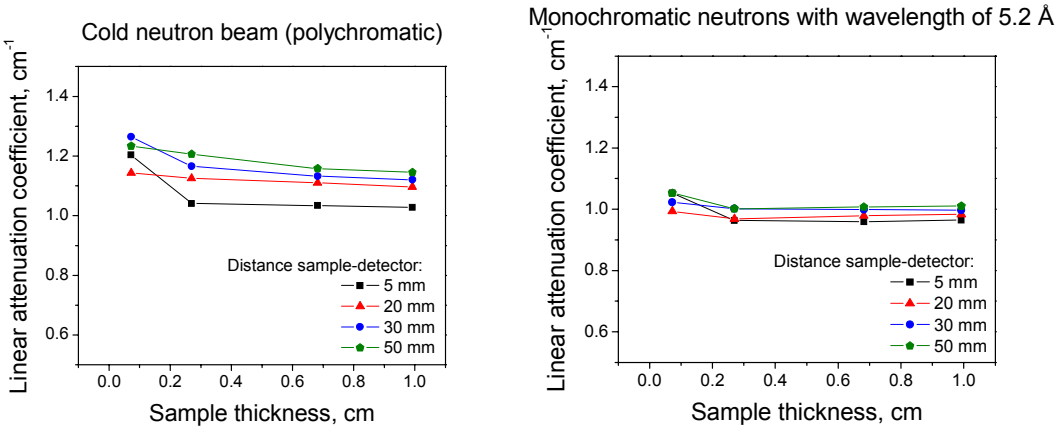


*Fig. 123. Calculated linear attenuation coefficients for STST cubic samples with different thickness and distances to the detector. The samples were measured by polychromatic (left) and monochromatic (right) neutron beam.*

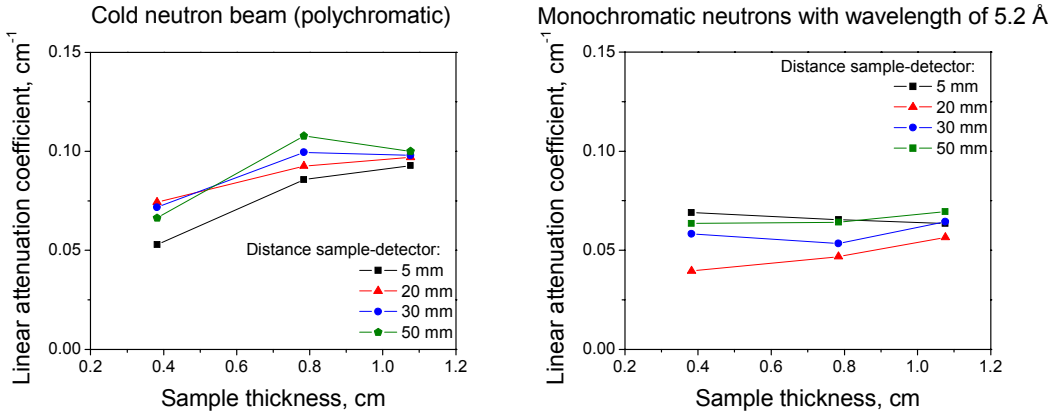


*Fig. 124. Calculated linear attenuation coefficients for Al cubic samples with different thickness and distances to the detector. The samples were measured by polychromatic (left) and monochromatic (right) neutron beam.*

In case of polychromatic cold neutrons the distance between the sample and the detector plays some role. This role is not significant like in the radiography with thermal neutrons if we look at the intensity profiles for a defined steel thickness measured at different distances to the detector, see Fig. 125. The attenuation stays almost constant for distances larger than 5 mm which is fulfilled in most of the cases.

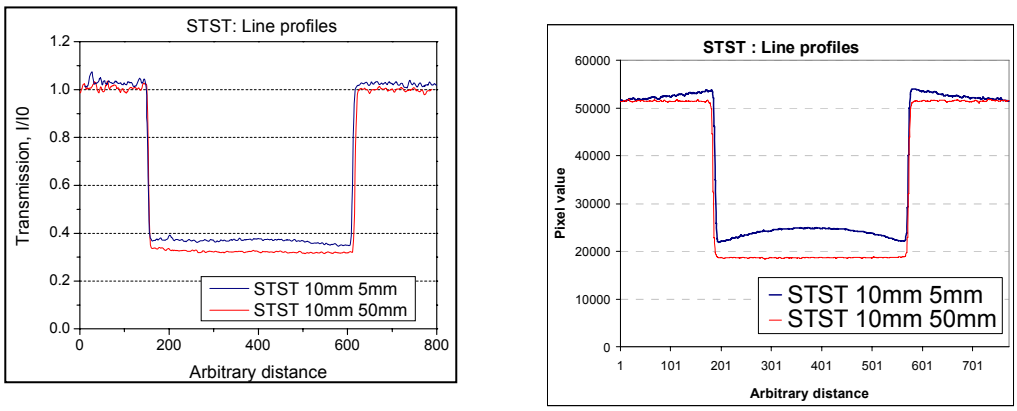


*Fig. 125. Intensity profiles for a STST sample with thickness 6.82 mm at different distances to the detector.*

Explanation for that is the Bragg-cut-off at 4 Å in the steel attenuation spectrum where the Bragg scattering mechanism switches off for larger wavelengths and correspondingly the scattering contribution in the radiography image decreases. In case of monochromatic neutrons with wavelengths above the Brag-cut-off it is seen that the scattering effect plays a minor role in the radiography images, see Fig. 124 (right) and Fig. 125 (right).

## REFERENCES


[1] MURATA, Y., et al., Two-dimensional neutron image excluding the effect of scattered neutrons, Proc. 4th World Conference on Neutron Radiography, San Francisco, 1992, p 583 Published 1994, (Ed. J.P.Barton,) Gordon and Breach Science Publishers.

[2] RAINE, D.A., et al., A scattered effect correction for high resolution neutron radiography and computed tomography, Proc. 5th World Conference on Neutron Radiography, Berlin, 1996, p 91. Published 1997 (Eds.C.O. Fischer, J. Stade, W. Bock) ,Deutsche Gesellschaft fuer Zerstoerungsfreie pruefung E.V..

[3] UNESAKI, H., et al., "Evaluation of scattered neutron component in thermal neutron radiography image – influence of scattered neutrons and unparallelness of incident neutron beam," Proc. 5th World Conference on Neutron Radiography, Berlin, 1996, p 175 Published 1997 (Eds.: C.O. Fischer, J. Stade, W. Bock) , Deutsche Gesellschaft fuer Zerstoerungsfreie pruefung E.V..

[4] KAMALI MAGHADAM, K., et el., Improvement of reconstructed image by elimination of contribution of the scattered neutrons in computed tomography, Proc. 5th World Conference on Neutron Radiography, Berlin, 1996, p191.

[5] PLEINERT, H., LEHMANN, E., Quantitative neutron radiography measurement of hydrogenous distributions, Proc. 5th World Conference on Neutron Radiography, Berlin, 1996, p586 Published 1997 (Eds.: C.O. Fischer, J. Stade, W. Bock) , Deutsche Gesellschaft fuer Zerstoerungsfreie pruefung E.V..

[6] TAKENAKA, H., Application of quantitative measurement method to void fraction of two-phase flow in a rod bundle by neutron radiography, Proc. 6th World Conference on Neutron Radiography, Osaka, p. 531 Published 2001, (Eds.: S. Fujine, H. Kobayashi and K. Kanda) Gordonand Breach Science Publishers.

[7] KARDJILOV, N., LEHMANN, E., VONTOBEL, P., Representation of the image formation in applied neutron radiography in terms of a PSF superposition, Appl. Phys. **A 74** [Suppl.], S228–S230 (2002) Applied Physics A Materials Science & Processing, ITMNR-4: Pennsylvania – SA.

[8] MIDDLETON, M., BEER, F. de, "Calibration of neutron Imagery for petroleum Engineering Applications, Proc. 7th World Conference on Neutron Radiography, Rome, 2002, p. 459 Published 2005, (Eds.: P. Chirco and R. Rosa, ENEA), Italian National Agency for New Technologies, Energy and the Environment .

[9] KARDJILOV, N., BEER, F.de. MIDDLETON,M., LEHMANN E.H., Corrections for scattered neutrons in quantitative neutron radiography , Proc. 7th World Conference on Neutron Radiography, Rome, 2002, p. 521 Published 2005, (Eds.: P. Chirco and R. Rosa, ENEA), Italian National Agency for New Technologies, Energy and the Environment.

[10] KARDJILOV, N., et.al, Scattering Corrections in Neutron Radiography using point scattered functions, Nucl. Instr. & Meth. **A542** (2005) 336-341

[11] HASSANEIN, R., LEHMANN, E.H., VONTOBEL, P., "Methods of Scattering Corrections for quantitative Neutron Radiography", Nucl. Instr. & Meth. **A542** (2005) 353.

[12] HASSANEIN, R., BEER, F. de, KARDJILOV, N., LEHMANN, E.H., "Scattering Correction Algorithm for Neutron Radiography and Tomography Tested at Facilities with Different Beam Characteristics". Physica **B 385-386** (2006) 1194-1196.

[13] HASSANEIN, R., BEER, F. de, KARDJILOV, N., LEHMANN, E.H., "Performance of Scattering Correction Algorithm for Neutron Radiography and Tomography". Proc. 8th World Conference on Neutron Radiography, NIST Gaitherburg, 2006.

[14] LEHMANN, E., VONTOBEL, P., WIENZEL, L., Properties of the Radiography Facility NEUTRA at SINQ and its Potential Use as European Reference Facility, 6th Word Conf. on Neutron Radiography, Osaka, 1999, p. 151 Published 2001, (Eds.: S. Fujine, H. Kobayashi and K. Kanda) Gordonand Breach Science Publishers.

[15] BRIESMEISTER (Ed.), J., MCNP – A General Monte Carlo N-Particle Transport Code, Version 4B, Los Alamos National Lab, Los Alamos, 1996.

[16] CULLEN, D. E., HANSEN, L. F., LENT, E. M., PLECHATY, E. F., Thermal scattering law data: Implementation and testing using the Monte Carlo neutron transport codes COG, MCNP and TART, report of Lawrence Livermore National Laboratory, UCRL-ID-153656, May 17, 2003.

[17] TREIMER, W., et al, Wavelength tunable device for neutron radiography and tomography, Applied Physics Letters, 89, 203504 (2006).

## PUBLICATIONS RESULTING FROM THE CRP


MIKEROV, V.K., ZHITNIK, I.A., BARMAKOV, Ju.N. et al., Prospects for efficient detectors for fast neutron imaging, Applied Radiation and Isotopes, V**.61**, 4, (2004) 529-535.

BARMAKOV, Yu., et al., Detection quantum efficiency and spatial resolution of neutron CCD-detectors, NIM **B213** (2004) 241.

BOGOLUBOV, E., BUGAENKO, O., KUZIN, S., MIKEROV, V., et al., CCD detectors for fast neutron radiography and tomography with a cone beam, NIM **A542** (2005) 187.

BOGOLUBOV, E., MIKEROV, V., SAMOSYUK, V., VERUSHKIN, S., Fast Neutron Imaging with CCD Detectors and Image Plates, to be published in proceedings of International Workshop on Fast Neutron Detection and Applications (FNDA2006), Cape Town, South Africa, April 3-7, 2006.

WHITNEY L. RAAS, et al, "Neutron Resonance Radiography for Explosives Detection: Technical Challenges" Presented at 2005 IEEE NSS/MIC Conference ©IEEE

WHITNEY L. RAAS, etal, "Design and Testing of a High Pressure Gas Target for Fast Neutron Resonance Radiography" Presented at 2005 IEEE NSS/MIC Conference ©IEEE

SCIANI, V., PUGLIESI, F., MAS PEREIRA, PUGLIESI, R., A digital system for track-etch neutron radiography. XXVIII Meeting on Nuclear Physics in Brazil; 07-11/Sep/2005; Guaruja/SP – award – the best paper presented in the Poster section.

PUGLIESI, R., MlG ANDRADE, MAS PEREIRA, PUGLIESI, F., Neutron Induced electron Radiography. 5 International Topical Meeting on Neutron Radiography. Max Planck Institute, 07/2004. Nuc Instruments and Methods – **A 542/1-3** (2005) 81.

PUGLIESI, R., LEHMANN, E., Neutron Induced Electron Radiography using an Image Plate; Applied Radiation and Isotopes 62(2005) 457 – 460. Work in collaboration between IPEN-CNEN/SP and Paul Scherrer Institute (Switzerland) PSI, 2003.

KARDJILOV, N.,et al, "Scattering Corrections in Neutron Radiography using point scattered functions", Conference: ITMNR-5, Munich, Germany 2004, Published: NIM **A, 524** (2005), 336.

HASSANEIN, R., LEHMANN, E., VONTABEL, P., "Methods of Scattering Corrections for quantitative Neutron Radiography", ITMNR-5, Munich, Germany, Published: NIM A, 524 (2005), 353.

HASSANEIN, R., De BEER, F.C., KARDJILOV, N., LEHMANN, E., "Scattering Correction Algorithm for Neutron Radiography and Tomography Tested at Facilities with Different Beam Characteristics". Physica B, 385–386 (2006) 1194.

HASSANEIN, R., KARDJILOV, N., LEHMANN, E.,Performance of Scattering Correction Algorithm for Neutron Radiography and Tomography. WCNR-8, Oct 2006, NIST, USA.

DE BEER, F.C., KARDJILOV, N., LEHMANN, E., "Scattered Neutrons and their effect on Quantitative Neutron Radiography (The Problem)" , WCNR-8, Oct 2006, NIST, USA.

ISLAM, M. N., ALAM, M. K., KHAN, M. K. ZAMAN, M.A, A study of water absorption behaviour of wood and wood plastic composites of Simul using neutron radiography,., Presented in the International Conference on Physics for Understanding and applications, 22-24 February 2004, Dhaka, Bangladesh.

ISLAM, M. N., ALAM, M.K., KHAN, M.K., AHMED, F.U., Determination of defects and water absorption behaviour in jute reinforced polymer composite using neutron radiography technique,. Presented in the Regional Physics Conference, Theme: Physics and Development Synergy, February 11-13, 2006, Dhaka, Bangladesh.

ZIN, M.R.M., MUHAMMAD, A., MOHAMAD, A.A., JAMRO, R. Modification of NUR II neutron Beam Profile of MINT's TRIGA Mark II Research Reactor for Digital Neutron Radiography. Presented at World Conference Neutron radiography – 8 (WCNR-8), October 16-19, 2006, NIST, USA.

ZIN, M.R.M., MUHAMMAD, A., MOHAMAD, A.A., JAMRO, R. Cold thermal neutron radiography experiment by CCD camera at primary flight tube of TRIGA Mark II Research Reactor. Presented at World Conference Neutron radiography – 8 (WCNR-8), October 16-19, 2006, NIST, USA.

MUHAMMAD, A., et al,. Application of Neutron radiography in investigation of Moisture Distribution in Malaysia Wood, Presented at MINT R&D 2004 Seminar, July 12 – 15 July 2004, Selangor, Malaysia.

ZIN, M.R.M., et al., The Comparison of Neutron, Gamma and X-Ray Radiography Images for Materials Evaluation, Presented at the 5th National Seminar on Non-Destructive Testing, October 1-2, 2003, Shah Alam, Malaysia.

SUPRAMANIAM, T., WAGIRAN, H., MUHAMMAD, A., Beam port medium optimization for new neutron radiography collimator design,. Presented at Annual Fundamental Science Seminar, Universiti Teknologi Malaysia, July 4-5, 2005, Johor, Malaysia.

DINCA, M., PAVELESCU, M., Calculation for a Neutron Imaging System Based on a CCD camera, Romanian Journal of Physics, Volume 51, Nos. 3-4, 2006, Bucharest, Romania, pp. 363-370.

DINCA, M., PAVELESCU, M., Detector for neutron and gamma radiography based on CCD cameras, 8th World Conference on Neutron Radiography, October 16-19, 2006, Gaithersburg MD, USA.

## LIST OF PARTICIPANTS


| | |
|---|---|
| Azali Muhammad | Malaysian Nuclear Agency (Nuclear Malaysia),<br>Div. of Industrial Technology,<br>Bangi, 43000 Kajang, Selangor,<br>Malaysia<br>Tel: +60-3-825-0510<br>Fax: +60-3-89250907<br>E-mail: Azali@nuclearmalaysia.gov.my |
| De Beer, F. | NECSA,<br>Building 1500,<br>P.O. Box 582, Pretoria 0001,<br>South Africa<br>Tel: +27123055258/5007<br>Fax: +27123055851<br>E-mail: fdebeer@necsa.co.za |
| Dinca, M. | Institute of Nuclear Research,<br>Str. Campului Nr. 1, Mioveni,<br>P.O. Box 78, Pitesti,<br>Romania<br>Tel: +40 248 213400<br>Fax: +40 248 262449<br>E-mail: dinca@scn.ro |
| Islam Md. Nurul | Bangladesh Atomic Energy Commission,<br>INST, AERE,<br>P.O. Box 3787,<br>Dhaka, Savar1000,<br>Bangladesh<br>Tel: +880 2 770 1829<br>Fax: + 880 2 861 3051<br>E-mail: enrpd@instaere.com<br>mnislam004@yahoo.com |
| Kardjilov, N. | Hahn-Meitner-Institut Berlin,<br>Glienicker Strasse 100,<br>D-14109 Berlin,<br>Germany<br>Tel: +49 30 8062 2298<br>Fax: +49 30 8062 3059<br>E-mail: kardjilov@hmi.de |
| Lanza, R. | Massachusetts Institute of Technology,<br>77 Massachusetts Avenue,<br>Cambridge, MA 02139-4307,<br>United States of America,<br>Tel: 001 617 2532399<br>Fax: 001 617 2532343<br>E-mail: lanza@mit.edu |

| | |
|---|---|
| Lehmann, E. | Paul Scherrer Institute,<br>CH-5232 VILLIGEN PSI,<br>Switzerland<br>Tel:<br>Fax: +41 56 3103131<br>E-mail: eberhard.lehmann@psi.ch |
| Mikerov, V. | All-Russian Research Institue of Atomatics,<br>Lab of Non-destructive Inspection,<br>Shushevskaya 22,<br>127055 Moscow,<br>Russian Federation<br>Tel: ++7-495-1326656<br>Fax: ++7-495-1354061<br>E-mail: vmiker@sci.lebedev.ru |
| Paranjpe, S.K. | IAEA, Scientific Secretary |
| Pugliesi, R. | Comissao Nacional de Energia Nuclear,<br>Inst. de Pesquisas Energeticas e Nucleares,<br>Cidade Universitaria 2242<br>Caixa Postal 11049, BR-05508-000,<br>São Paulo, S.P.,<br>Brazil<br>Tel: +55 11 3816 9178<br>Fax: +55 11 3816 9188<br>E-mail: pugliesi@ipen.br |
| Sinha, A. | High Pressure Physics Division,<br>Bhabha Atomic Research Centre,<br>Trombay, Mumbai 400 085,<br>India<br>Tel: +91 22 255 93679<br>Fax: +91 22 2550 5151<br>E-mail: image@magnum.barc.ernet.in |